



UNIVERSITÀ DEGLI STUDI DI BERGAMO

---

**SOL-GEL SYNTHESIS AND  
HYBRID THIN FILM  
DEPOSITION FOR INNOVATIVE  
TEXTILE FINISHING**

Study, characterization and  
environmental impact evaluation

Claudio Colleoni  
doctoral thesis

© 2012 Dipartimento di Ingegneria Industriale  
Università degli studi di Bergamo  
Tesi di Dottorato in Tecnologie per l'energia e l'ambiente

---

**Claudio Colleoni** SOL-GEL SYNTHESIS AND HYBRID THIN FILM DEPOSITION FOR INNOVATIVE TEXTILE FINISHING  
Study, characterization and environmental impact evaluation

UNIVERSITÀ DEGLI STUDI DI BERGAMO

Facoltà di Ingegneria

Dipartimento di Ingegneria Industriale

DOTTORATO DI RICERCA

IN

TECNOLOGIE PER L'ENERGIA E L'AMBIENTE

XXIV ciclo

anno 2012



**SOL-GEL SYNTHESIS AND HYBRID THIN FILM  
DEPOSITION FOR INNOVATIVE TEXTILE  
FINISHING**

**Study, characterization and environmental impact evaluation**

Doctoral thesis:

Claudio Colleoni

Supervisor:

Prof. Giuseppe Rosace

Dott.ssa Maria Rosaria Massafra (Stazione Sperimentale per la Seta)

Dr. Torsten Textor (DTNW)

© 2012

Dipartimento di Ingegneria Industriale. Università degli studi di Bergamo

ISBN: 978-88-974-13-19-6

Open access copy available at: <http://hdl.handle.net/10446/25392>

Terms of use: <http://aisberg.unibg.it/doc/disclaimer.html>

# Content

<i>Acknowledgements</i>	V
ABSTRACT	VII
PUBLICATIONS	IX
LIST OF ABBREVIATIONS	XIII
INTRODUCTION	XV
CHAPTER 1: SOL-GEL TECHNOLOGY	1
1.1 Sol-gel chemistry	1
1.2 Sol-gel synthesis	5
1.3 Mechanism of hydrolysis	6
1.4 Mechanism of condensation	7
1.5 Mixed alkoxide system	9
1.6 Role of catalyst	11
1.7 Factors over the sol-gel system	12
CHAPTER 2: CHARACTERIZATION TECHNIQUES	15
2.1 Stability sol characterization	15
2.2 Surface characterization	16
2.3 Thermal analysis	17
2.4 Wettability characterization	18
2.5 Optical and photo activity characterization	19
2.6 Textile testing methods	21

CHAPTER 3: FLAME RETARDANT FINISHING	23
3.1 State of the art	23
3.2 Experimental setup	28
3.2.1 Materials	28
- Part A: Phosphorus–doped amino functionalized silica thin film	28
- Part B: Hybrid phosphorous silica film	28
3.2.2 Nanosol preparation and coating process	30
- Part A: Phosphorus–doped amino functionalized silica thin film	30
- Part B: Hybrid phosphorous silica film	31
3.3 Results	33
3.3.1 Part A: Phosphorus–doped amino functionalized silica thin film	33
3.3.1.1 Surface characterization	33
3.3.1.2 Thermal analysis	37
3.3.1.3 Burning behavior	41
3.3.1.4 FT-IR analysis of char residues	42
3.3.1.5 Wash fastness	43
3.3.2 Part B: Hybrid phosphorous silica film	44
3.3.2.1 Surface characterization	44
3.3.2.2 Thermal analysis	48
3.3.2.3 Burning behavior	53
3.4 Conclusion	55
 CHAPTER 4: WATER REPELLENT FINISHING	 57
4.1 State of the art	57
4.2 Experimental setup	66
4.2.1 Materials	66
4.2.2 Nanosol preparation and coating process	67
4.3 Results	69
4.3.1 Surface characterization	69
4.3.2 Water-repellent properties	70
4.4 Conclusion	81

CHAPTER 5: SELF CLEANING FINISHING	83
5.1 State of the art	83
5.2 Experimental setup	87
5.2.1 Materials	87
- Part A: Study of sol stability	87
- Part B: Optical and photo-activity characterization	89
5.2.2 Nanosol preparation and coating process	89
- Part A: Study of sol stability	89
- Part B: Optical and photo activity characterization	93
5.3 Results	95
5.3.1 Part A: Study of sol stability	95
5.3.1.1 FT-IR characterization	95
5.3.1.2 DLS measurement	105
5.3.1.3 Turbidity measurement	110
- Single-step procedure	110
- Two-step procedure	111
5.3.1.4 Viscosity measurement	124
5.3.2. Part B: Optical and photo-activity characterization	128
5.3.2.1 Surface characterization	128
5.3.2.2 Optical characterization	130
5.3.2.3 Photodegradation of dyestuff	138
5.3.2.4 Mechanical properties	142
5.4 Conclusion	143
CONCLUSION	145
APPENDIX	151
LIST OF FIGURES	159
LIST OF TABLES	165
REFERENCE	167



## Acknowledgements

*First of all, I would like to express my gratitude to Prof. Giuseppe Rosace, for providing me the opportunity to work in the research field of sol-gel technology for textile applications, for his expert guidance and assistance in every aspects of this work.*

*I am grateful to Dr. Maria Rosaria Massafra of Stazione Sperimentale per la Seta (Milano) for her support to my research activity and for giving me the opportunity to increase my scientific skills.*

*I am indebted to Dr. Torsten Textor of Deutsches Textilforschungszentrum Nord-West e.V. (DTNW, Krefeld, Germany) for the precious advices, suggestions, the stimulating discussions and the confidence placed in me.*

*I wish to thank Stazione Sperimentale per la Seta for giving me the opportunities to do the PhD.*

*I also extend my thanks to my friends and colleagues prof. Giovanna Barigozzi, Dr. Giovanna Brancatelli, Dr. Emanuela Guido, prof. Veronica Migani and Dr. Nicholas Paris for the precious advices, suggestions and practical help they gave me.*

*I would like to thank the entire DTNW institute for given me the opportunities to develop a part of my thesis in its laboratories.*

*I also wish to thank Prof. Marco Marengo and his research group and Dr. Carlo Antonini in particular for the contact angle measurement and useful advice.*

*I am grateful to Mr. Alessandro Gigli for his expertise and technical advice.*

*Special Thanks to DTNW research group and Leonie Derksen and Frauke Sachse in particular for the help they provided in collecting the data for my work.*

*I wish to thank all those who helped me. Without them, I could not have completed my research activity.*

*Last but not the least, I would like to thank Veronica and my family who supported me throughout my life.*





## ABSTRACT

The aim of the present work was to study and to characterize a new approach to finish textile fabrics. This new approach is based on the production of a thin film on the textile surface containing a metal-organic precursor. For these reasons, organic-inorganic hybrid thin films based on silica or titania sols were developed by sol-gel process for flame retardant, hydro-repellent and self cleaning fabrics. The proposed hybrid compounds for textile finishing are expected to help the development of new finishes, constituting a valid alternative to the well established commercially available treatments of textile. In fact, traditional treatments could have several disadvantages: they could be hazardous materials for the workers during the production, application as well as for the end-user who wears the treated cloths. Moreover, they are responsible for water pollution and for high energy consumption during the industrial application.

Halogen free flame retardants hybrid films were realized to enhance the thermal and fire stability of cotton. To this aim specific combination of silica precursors (3-aminopropyltriethoxysilane (APTES) and diethylphosphatoethyltriethoxysilane (DPTES)), phosphorus donors (diethylphosphite (DEP) and DPTES) and nitrogen donors (APTES and melamine-derivative resin (MF)) were tested. FT-IR spectroscopy was exploited for assessing the formation of the silica skeleton on the cotton surface and for evaluating the interactions between the cellulosic fibres and the doped film. The effect of the concurrent presence of Si, P and N on cotton was investigated by thermogravimetric analyses; the flammability behavior was instead assessed by vertical flammability tests. The sol-gel treatments in the presence of phosphorus and nitrogen turned out to play a protective role on the degradation of the cotton fibres, hindering the formation of volatile species that fuel the further degradation, thus promoting the formation of a carbonaceous structure.

Free fluorocarbon water repellent hybrid films were also realized onto cotton and PES fabrics using octyl triethoxysilane (OTES) as precursor and MF as cross-linker. Three different MF concentrations and four MF:OTES molar ratios were evaluated. ATR FT-IR spectroscopy was used to evaluate the chemical structure of the coating while repellent behavior of the treated cotton samples was investigated by contact angle, water uptake, drop and Du Pont test and compared to untreated

sample data. Generally, high repellency was observed with the increase of both the melamine concentration and molar ratio: the best results was obtained using the sols prepared with 100g/L of resin and 1:4 molar ratio (MF:precursor).

Finally, a self cleaning study was developed following two main research approaches. In the first one, stable aqueous titania sols were synthesized at suitable pH for the industrial application without the addition of alcohols, glycol or acetyl acetone. Different synthesis parameters such as acetate buffer ( $\text{CH}_3\text{COOH}$  and  $\text{CH}_3\text{COONa}$ ) and precursor concentrations, synthesis temperature, route of sol preparation, etc. were studied to evaluate possible effect on the sol stabilization with or without chitosan used as stabilizer. The stability of sols was investigated using FT-IR, dynamic light scattering analysis, turbidity and rheological measurements. Sol stability depends on the interaction occurring between  $\text{TiO}_2$ , acetate buffer and chitosan in the sol. Stable sols were only obtained when titania precursor was initially dissolved in pure acetic acid at pH 4. The stability improved by adding chitosan. In the second approach,  $\text{TiO}_2$  thin film coatings were realized on cotton fabrics by sol-gel technique using titanium iso-propoxide. The effect of different starting acidic solutions (nitric, hydrochloric and acetic acids) as well as the addition of polyethylene glycol (PEG) onto two different (0.25M and 0.025M) concentrations of  $\text{TiO}_2$  were deeply investigated. Both XRD and optical characterization showed a deposition of thin films without crystalline structure whose band gaps were between 3.3 to 3.5 eV. The photocatalytic activity, evaluated by degradation of Procion red PX4B dyestuff, was carried out under visible and UV (365 nm) sources. The bleaching rate of the undoped  $\text{TiO}_2$  films showed an interesting linear correlation with pKa of the acid used which also depends on the concentration. The addition of PEG into the mineral sol-gel solution dramatically increased the rate of dye degradation under UV exposure, whilst the degradation was less evident under light exposure. The effect of titanium on the fabric properties was also addressed: an expected decrease in the mechanical properties (lower than 15%) was observed after 100 hours under both visible and UV light exposure.

The developed textile treatments allowed to improve the fabric properties in the meanwhile maintaining the substrate mechanical properties. Moreover, water and energy consumptions are reduced due to the use of sol-gel technique, resulting in more sustainable processes.

## PUBLICATIONS

### Papers

1. J. Alongi, C. Colleoni, G. Malucelli, G. Rosace "Thermal and fire stability of cotton fabrics coated with hybrid phosphorus-doped silica films" *Journal of Thermal Analysis and Calorimetry*, DOI 10.1007/s 10973-011-2142-0.
2. G. Brancatelli, C. Colleoni, M.R. Massafra, G. Rosace "Effect of hybrid phosphorus-doped silica thin films produced by sol-gel method on the thermal behavior of cotton fabrics" *Polymer Degradation and Stability* 96 (2011) 483-490.
3. V. Migani, H. Weiss, M.R. Massafra, A. Merlo, C. Colleoni, G. Rosace "Polydimethylsiloxane derivatives side chains effect on sytan functionalized" *Applied surface Science*, 257 (2011) 3904-3912.
4. C. Colleoni, M.R. Massafra, V. Migani, G. Rosace "Dendrimer Finishing Influence on CO/PET blended Fabrics Colour Assessment" *Journal of Applied Polymer Science*, 120 (2011) 2122-2129.
5. G. Rosace, R. Canton, C. Colleoni "Plasma enhanced CVD of SiO<sub>x</sub>CyHz thin film on different textile fabrics: influence of exposure time on the abrasion resistance and mechanical properties" *Applied Surface Science*, 256 (8) (2010) 2509-2516.

### Chapter of books

1. G. Rosace, V. Migani, C. Colleoni, MR. Massafra, E. Sancaktaroglu "Nanoparticle Finishes Influence on Color Matching of Cotton Fabrics" *Chemistry and Chemical Engineering Research Progress* (2010) Nova Science Publishers, Inc. ISBN: 978-1-61668-502-7.

### Conference proceedings

1. C. Colleoni, G. Rosace, T. Textor "Increased stability of aqueous TiO<sub>2</sub> sols prepared without stabilizing alcohol" 5th Aachen-Dresden International Textile Conference – Germany, Aachen, 24-25 Nov 11. ISBN 1867-6405.

2. G. Brancatelli, C. Colleoni, M.R. Massafra, G. Rosace "Characterization and thermal behaviour of cotton fabric treated by phosphorus-doped silica thin film" International Workshop: Characterization of Safe Nanostructured Polymeric Materials - Pozzuoli (Naples) Italy, 3-4 March 2011 ISBN 978-973-702-826-6.
3. G. Brancatelli, C. Colleoni, A. Gigli, M.R. Massafra, N. Paris, G. Rosace "Hybrid organic-inorganic finishing for multifunctional textiles" 22nd International IFATCC congress – Italia, Stresa, 5-7 Mag 10. ISBN 9788896679005.
4. J. Alongi, J. Tata, F. Carosio, A. Frache, G. Malucelli, G. Rosace, C. Colleoni, G. Brancatelli, D. Losio, G. Fusi, A. Andretta, A. Scalvedi, C. Pilenga "Nanoparticles as promising flame retardant additives for textile fabrics" 22nd International IFATCC congress – Italia, Stresa, 5-7 Mag 10. ISBN 9788896679005.
5. G. Brancatelli, C. Colleoni, A. Gigli, M.R. Massafra, N. Paris, G. Rosace "Hydrophobic hybrid nanocomposite coating by a sol-gel process" 22nd International IFATCC congress – Italia, Stresa, 5-7 Mag 10. ISBN 9788896679005.
6. G. Brancatelli, C. Colleoni, A. Gigli, M.R. Massafra, N. Paris, G. Rosace "Phosphorous doped SiO<sub>2</sub> coatings for flame retardant fabrics" 22nd International IFATCC congress – Italia, Stresa, 5-7 Mag 10. ISBN 9788896679005.
7. G. Brancatelli, C. Colleoni, A. Gigli, M.R. Massafra, N. Paris, G. Rosace "Hybrid silica coatings for wear-resistant textiles" 22nd International IFATCC congress – Italia, Stresa, 5-7 Mag 10. ISBN 9788896679005.
8. V. Migani, H. Weiss, M.R. Massafra, A. Merlo, C. Colleoni, G. Rosace "Influence of silicone side chains on textile finishing of polyamide intended for sportwear" 22nd International IFATCC congress – Italia, Stresa, 5-7 Mag 10. ISBN 9788896679005.
9. F. Isella, S. Bisignano, C. Colleoni, L. Esposito, G. Rosace, G. Freddi "Laccase-aided bleaching treatments onto cellulosic fibers" 22nd International IFATCC congress – Italia, Stresa, 5-7 Mag 10. ISBN 9788896679005.
10. J. Alongi, J. Tata, F. Carosio, A. Frache, G. Malucelli, G. Rosace, C. Colleoni, G. Brancatelli, D. Losio, G. Fusi, A. Andretta, A. Scalvedi, C. Pilenga "Nanoparticles as promising flame retardant additives for textile fabrics" NanolTatTex 2009 – Italia, Sesto San Giovanni (MI), 10-11 Nov 09.

11. J. Alongi, A. Andretta, G. Brancatelli, C. Colleoni, A. Frache, G. Fusi, A. Gigli, C. Pilenga, G. Rosace, A. Scalvedi, J. Tata “Comparison of different cross-linkers for the application of flame retardant nanoparticle additives on textile fabrics in finishing process” NanolItalTex (2009) – Italia, Sesto San Giovanni (MI), 10-11 Nov 09.
12. G. Rosace, V. Migani, C. Colleoni, M.R. Massafra, E. Sancaktaroglu “Nanoparticle Finishes Influence on Color Matching of Cotton Fabrics” ITEC2009 Proceeding 1st International and 7<sup>th</sup> national Iranian Textile Engineering conference – Iran, Rasht, 27-29 Oct 09.
13. C. Colleoni, M.R. Massafra, G. Rosace, “Effect of Nanoparticle Finishing onto Color Matching of Textile Fabrics” 5<sup>th</sup> National Color Group Conference – Italia, Palermo, 7-9 Oct 09, pag. 203-213. ISBN: 978-88-96225-24-0.
14. C. Colleoni, I. Donelli, G. Freddi, F. Isella, N. Paris, G. Rosace, “Effect of various pectinolytic enzymes mixing ratio in cotton scouring” 6th International Conference on Textile and Polymer Biotechnology – Belgium, Belgium, 23-25 Sept 09, pag 325-326. ISBN: 978-90-81392-41-9.

**Software (SIAE):**

1. ACHEO (Analysis of Textile Chemistry Processes Cost).



## LIST OF ABBREVIATIONS

APTES	3-Aminopropyltriethoxysilane
ATR	Attenuated Total Reflection
CA	Contact Angle
CH	Chitosan
DEP	Diethylphosphite
DPTES	Diethylphosphatoethyltriethoxysilane
DLS	Dynamic Light Scattering
DSC	Differential Scanning Calorimetry
EDX	Energy Dispersive X-ray spectroscopy
FT-IR	Fourier-Transform Infrared Spectroscopy
HOIMs	Hybrid Organic Inorganic Materials
KM	Kubelka Munk
MF	Melamine derivative resin
OTES	Octyltriethoxysilane
PEG	Polyethylene Glycol
PFOA	Perfluorooctanoate
PFOS	Perfluorooctane Sulfonate
PR	Procion Red PX4B
SEM	Scanning Electron Microscope
TBT	Titanium (IV) Butoxide
TGA	Thermo Gravimetric Analysis
TTIP	Titanium Tetraisopropoxide
WAXD	Wide Angle X-ray Diffraction
XRD	X-Ray Diffraction





## INTRODUCTION

Textile processing can be realized through three stages: pretreatment (or preparation to dyeing), coloration (both dyeing and printing operations) and finishing. Finishing is the final step in the fabric manufacturing process, to provide the properties and performances that customers will value, and to give special functional properties. Most finishes are applied to fabrics such as wovens, knitwear or nonwovens. But there are also other finishing processes, such as yarn finishing, for example sewing yarn with silicones and garment finishing. Textile finishing can be subdivided into two distinctly different areas:

- chemical finishing (wet finishing), that involves the application of chemicals to textiles to achieve a desired result;
- mechanical finishing (dry finishing), that uses mainly physical means to change fabric properties and usually alters the fabric appearance as well. This finishing also encompasses thermal processes such as heat setting.

The proper formulation of chemical finishes requires consideration of several important factors: the type of textile being treated (fibre and construction); the performance requirements of the finish (extent of effect and durability); the cost to benefit ratio; restrictions imposed on the process by availability of machinery, procedure requirements, environmental considerations; and compatibility of different formula components as well as the interaction of the finishing effects. To bring all these parameters to an acceptable compromise is not easy, even for a single purpose finish. But usually several types of finishes are combined for economical reasons mostly in one bath (only one application and drying process). This is often the hardest challenge of chemical finishing. First, all components of the finish bath must be compatible. Precipitations of anionic with cationic products have to be avoided. The emulsion stability of different products may be reduced by product interactions. More difficult is often the second hurdle, the compatibility of the effects of the different types of finishes that are being combined:

- some effects are similar or assist each other, for example silicone elastomers cause water repellency, softeners bring about antistatic effects and antistatic finishes can be softening;

- some effects are obviously contradictory, for example hydrophobic finishes and hydrophilic antistatic finishes, or stiffening and elastomeric finishes, or stiffening and softening finishes;
- other types of finishes typically reduce the main effect of a finish type, for example the flame retardant effect is decreased by nearly all other types of chemical finishes as they add flammable components to the fabric;
- fortunately true antagonistic effects are rare, but true synergistic effects are also rare, where the resulting effect of a combination is greater than the sum of the single effects of the combined products. Examples of both cases are different types of flame retardants.

Chemical finishing has always been an important component of textile processing, but in recent years the trend to "high tech" products has increased the interest and use of chemical finishes. As the use of high performance textiles has grown, the need for chemical finishes to provide the fabric properties required in these special applications has grown accordingly [1].

Nanotechnology is increasingly attracting worldwide attention because it is widely perceived as offering huge potential in a wide range of end uses. The unique and new properties of nanomaterials have attracted not only scientists and researchers but also businesses, due to their huge economical potential. The concept of nanotechnology is not new: it is defined as the utilization of structures with at least one dimension of nanometer size for the construction of materials, devices or systems with novel or significantly improved properties due to their nano-size. Nanotechnology can best be described as activities at the level of atoms and molecules that have applications in the real world. Nano-particles commonly used in commercial products are in the range of 1 to 100 nm. Nanotechnology also has real interesting application for the textile industry. This is mainly due to the fact that conventional methods used to impart different properties to fabrics often do not lead to permanent effects, and will lose their functions after laundering or wearing. Nanotechnology can provide high durability for fabrics, because nano-particles have a large surface area-to-volume ratio and high surface energy, thus presenting better affinity for fabrics and leading to an increase in durability of the function. Moreover nano sized chemicals can have different properties compared to the larger sized versions. This can offer opportunities for manufacturing new products such as

technical textile. In fact, the evolution of textiles didn't stop with the setting up of the so called "functional textiles"; recent development in materials engineering, information and biology have conferred a new role to textiles, so that they have become potentially available to be used with new technologies based on the integration of these disciplines. In this way the change is substantial: textile fabrics used not only for wear, but also for furnishings, building industry, medicine, sensing.

The purpose of the present work is to study and to characterize a new approach to finish textile fabrics based on the production of a thin film on their surface by metal-organic precursor designed from the nanoscale. The final aim is to develop protection systems with improved hydro repellency, flame retardant and self-cleaning properties on textile fabrics and a low environmental impact in the application of chemicals. In particular, multifunctional silane hybrid molecules were used to design sol-gel treatments and to modify the surface structure of organic polymers. In the experimental part of this thesis different mixture of hybrid silicon alkoxides with organic molecules were applied onto textile fabrics and cured for the development of effective and environmentally friendly protection systems: flame retardant, hydro repellency and self cleaning. Most significant factors and conditions were investigated in order to obtain high quality textile fabrics finished via sol-gel route. Chemical and morphological characterization of the treated textile surface have shown their good properties compared to untreated samples for both natural and synthetic fabrics.



# Chapter 1

## Sol-Gel Technology

### 1.1 Sol-gel chemistry

Sol-gel processing is a common chemical approach to produce high purity materials shaped as powders, thin film coatings, fibres, monoliths and self-supported bulk structures [2].

Sol-gel materials continue to attract attention for a variety of applications; this most likely is due to the versatility of their processing and the ease with which their properties may be tailored to fit a particular application. The sol-gel technologies owe their origin to Ebelman [3] who has developed in 1845 a technology for obtaining a solid material by slow hydrolysis of esters of silicic acid. Afterwards, that method is developed and approved by Geffcken and Berger [4] for deposition of oxide films over glass. The sol-gel method became popular in the ceramics industry around the mid-1970s, and various types of inorganic glass were manufactured based on this approach [5]. Philipp and Schmidt [6] and Wilkes et al.

[7] carried out pioneer works on the preparation of organically modified silicate (Ormosil or CERAMER) using various types of alkoxysilane via the sol– gel process.

The sol-gel process is a versatile wet chemical process to make ceramic and glass materials. It is a chemical synthesis method, mainly based on inorganic polymerization reactions, initially used for the preparation of inorganic materials such as glasses and ceramics. This technique offers many advantages among them the low process temperature, the ability to control the composition on molecular scale and the porosity to obtain high surface area materials, the homogeneity of the final product up to atomic scale. Moreover, it is possible to synthesize complex composition materials, to form higher purity products through the use of high purity reagents, and to provide coatings over complex geometries.

Inorganic sol-gel-derived materials had been investigated and commercialized a few decades ago and due to the profound understanding of the underlying chemical and technical processes are still present as important examples of large-scale applications of the sol-gel technology [8,9,10]. The synthesis technique involves the transition of a system from a colloidal liquid, named sol, into a solid gel phase.

The sol-gel technology allows to prepare ceramic or glass materials in a wide variety of forms: ultra-fine or spherical shaped powders, thin film coatings, ceramic fibres, microporous inorganic membranes, monolithics, or extremely porous aerogels. An overview of the sol-gel process is illustrated in Figure 1.

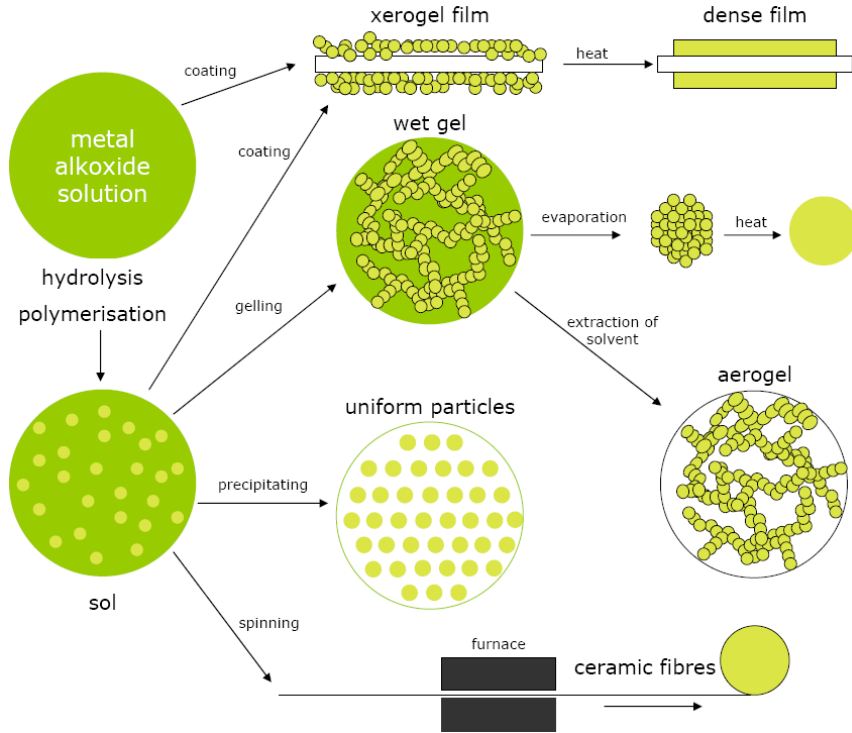


Figure 1. Sol-gel process.

When the sol is cast into a mould, a wet gel will form. By drying and heat-treatment, the gel is converted into dense ceramic or glass materials. If the liquid in a wet gel is removed under a supercritical condition, a highly porous and extremely low density aerogel material is obtained. As the viscosity of a sol is adjusted into a suitable viscosity range, ceramic fibres can be drawn from the sol. Ultra-fine and uniform ceramic powders are formed by precipitation, spray pyrolysis, or emulsion techniques. The network obtained by sol-gel technique can be divided into four basic groups (Figure 2):

- 1) **Type 1:** Inorganic network formers, Tetramethoxysilane  $\text{Si}(\text{OCH}_3)_4$  Tetraethoxysilane  $\text{Si}(\text{OC}_2\text{H}_5)_4$  and Ti-isobutylate, etc. In addition, other authors [11] have investigated the availability for deposition of protective coatings on steel sheets of asymmetric silanes from the type  $\text{R}_1\text{-Si}(\text{OR}_2)_3$  as:  $\text{CH}_3\text{-Si}(\text{OCH}_3)_3$ ,  $\text{CH}_3\text{-Si}(\text{OC}_2\text{H}_5)_3$ ,  $\text{CH}_3\text{-Si}(\text{OC}_4\text{H}_9)_3$ . The possibilities for application of the sol-gel route for development of glasses and glass-ceramic materials is analyzed in detail by Helmut Dislich [12].



- 2) **Type 2:** Inorganic network formers with organic non-reactive modification. Due to the hydrolytic stability of Si-C bond, a wide variety of organic groups are available for the modification of the inorganic networks. The obtaining of nano-particles from ionic carboxylates, as aluminum isopropylate  $\text{Al}(\text{C}_2\text{H}_5\text{COO})_3$ , zirconium oxy-dicarboxylate  $\text{ZrO}(\text{COO})_2$  is also described as an example for the application of the sol-gel method for the obtaining of organic-modified silicates and ceramics [13].
- 3) **Type 3:** they form inorganic networks with reactive organic groups which are available modification for crosslinking/polymerization reactions, or organic monomers/polymers with silylated and groups for crosslinking/co-condensation via inorganic Si-O-Si bonds. These substances are the key element for the obtaining of hybrid polymers. The uniting feature of that kind of systems is the bonding between the organic network and the inorganic matrix, which allows the creation of entirely new generation of advanced materials, ORMOSIL-materials (Organically modified silanes), which were renamed as "ORMOCER" - Organically Modified Ceramics. The properties of materials obtained could be drawn from high hardness and brittleness to high plasticity and mildness, corresponding to the relation between the contents of the inorganic and organic quote.
- 4) **Type 4:** Organic monomers which react via chemical crosslinking or polymerization reactions. Typical examples for this group are the gels obtained by Pechini. In 1967, Pechini [14] developed a process for the preparation of the precursor polymeric resin. First, a mixture of cations is formed in an organic complexing agent, (citric acid or ethylenediaminetetraacetic acid, EDTA) and ethylene glycol solution. Second, the cations become a chelate and the polymeric resin forms. Finally this polymer decomposes at 573K. This method could be modified via the number of the active moieties (functional groups) of the corresponding precursors. The polymerization process could be terminated by addition of mono-functional substance - by that manner the average length could be controlled. As consequence, the plasticity of the obtained product could be controlled as well.

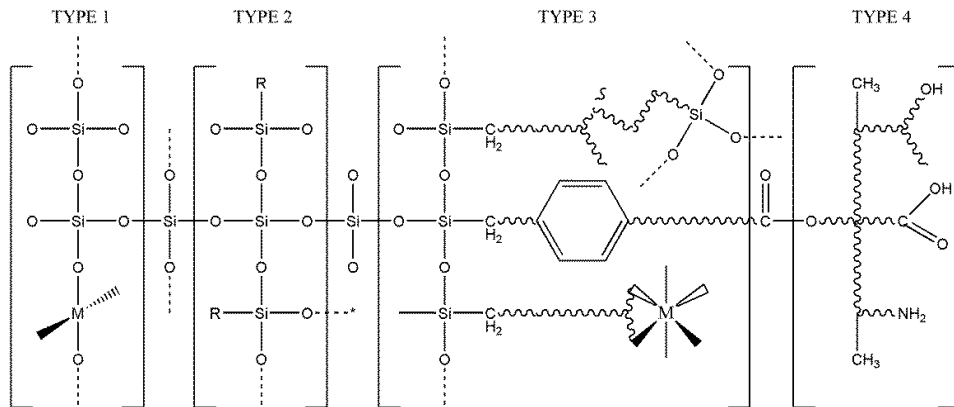


Figure 2. Different kind of network.

## 1.2 Sol-gel synthesis

The sol-gel process involves two steps: hydrolysis of metal alkoxides to produce hydroxyl groups and residual alkoxy groups, followed by heat treatment which induces polymerization (polycondensation), to form a three-dimensional network. In general, transition metals have low electronegativities and their oxidation state is frequently lower than their coordination number in an oxide network. Commonly, the most preferred starting reagents (called “precursors”) are alkoxides with general formula:  $M_x(OR)_y$ , where M is an element with valence y and R = alkoxy group.

These alkoxides must exhibit useful properties to control the chemical synthesis of oxides:

1. *easy to purify*, a lot of alkoxides can be distilled in order to obtain highly pure products;
2. *wide variety*, it is possible to choose R among a large number of alkylic groups in order to obtain the required reactivity;
3. *possible control*, of the alkoxides hydrolysis and the polycondensation of hydrolysed species;
4. *mixed alkoxides*, as a further control means of the stoichiometry and homogeneity of the final products.

Coordination expansion occurs spontaneously upon reaction with water or other nucleophilic reagents to achieve their preferred coordination. Metal alkoxides are in general very reactive due to the presence of highly electronegative OR groups (hard-p donors) that stabilize the metal in its highest oxidation state and render it very susceptible to nucleophilic attack. The lower electronegativity of transition metals causes them to be more electrophilic and thus less stable toward hydrolysis, condensation and other nucleophilic reactions. Controlling the conditions can be difficult but successful control of the reaction conditions has the potential to produce materials of consistent size, shape and structure. The lower electronegativity of transition metals causes them to be more electrophilic and thus less stable toward hydrolysis, condensation and other nucleophilic reactions.

### 1.3 Mechanism of hydrolysis

As stated previously the sol-gel reaction involves hydrolysis of the metal alkoxide followed by condensation. Hydrolysis of alkoxides occurs through a nucleophilic substitution (SN) reaction. When a nucleophile, such as water is introduced to alkoxide a rapid exothermic reaction proceeds. The nucleophilic addition (AN) of water involves a proton from the attacking nucleophile (water) being transferred to the alkoxide group. The protonated species is then removed as either alcohol or water (Figure 3).

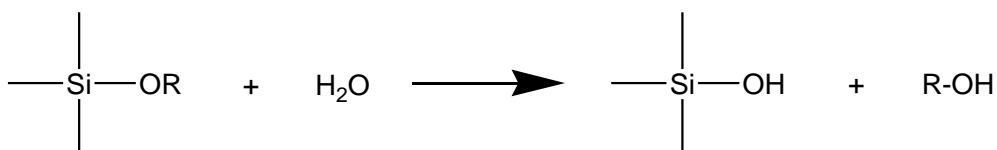


Figure 3. Hydrolysis reaction.

The nucleophilic substitution reaction that occurs during hydrolysis can be described as follows:

- 1) nucleophilic addition of the H<sub>2</sub>O onto the positively charged metal atom;
- 2) proton transfer, within the transition state from the entering molecule to the leaving alkoxy group.

The hydrolysis step generate low molecular weight (alcohol and water) that must be removed from the system, and such removal would lead, in the limit, to a tetrahedral SiO<sub>2</sub> network if the species were silicon. The removal of these byproducts also contribute to the high shrinkage that occurs during the classical sol-gel process. For non-silicate metal alkoxides, generally no catalyst is needed for hydrolysis and condensation because they are very reactive. In the case of silicon based metal alkoxides, the hydrolysis and condensation reactions typically proceed with either an acid or base as catalyst.

### 1.4 Mechanism of condensation

Condensation reactions complete the sol-gel process. Condensation can proceed through either alcoxolation or through oxolation. In both processes an oxo bridge is formed between the metals (M–O–M) but the leaving group differs. During alcoxolation, two partially hydrolysed metal alkoxide molecules combine and an oxo bridge is formed between the two metals with alcohol departing as the leaving group (Figure 4).

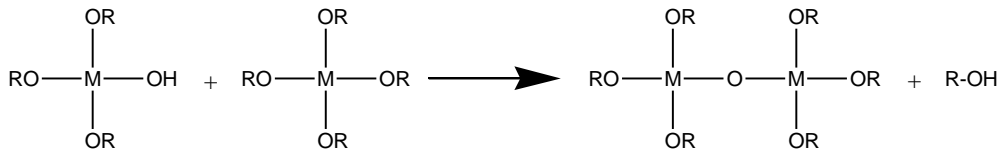


Figure 4. Alcoxolation reaction.

In oxolation (Figure 5) two partially hydrolysed metal alkides combine to form an oxo bridge between the metal centres but water is the leaving group.

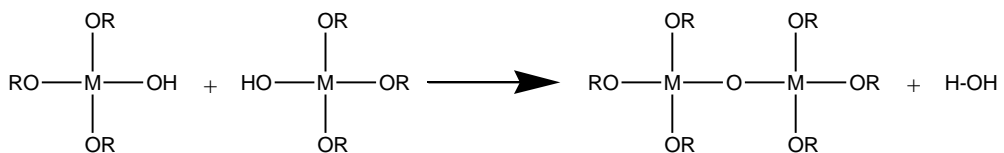


Figure 5. Oxolation reaction.

Condensation reactions can proceed to form large chains of molecules through polymerisation. The electrophilicity of the metal, the strength of the entering nucleophile and the stability of the leaving group all have an influence over the thermodynamics of the hydrolysis and condensation reactions. Another major factor regarding sol-gel reaction kinetics is the extent of oligomerisation (molecular complexity) of the metal alkoxide. Molecular complexity varies depending on the nature of the metal atom. An increase in atomic size causes an increase in molecular complexity. The alkoxide ligand also influences molecular complexity. As an example,  $\text{Ti}(\text{OEt})_4$  is an oligomer, but  $\text{Ti}(\text{OPr})_4$  is monomeric.  $\text{Ti}(\text{OPr})_4$  is more susceptible to hydrolysis than  $\text{Ti}(\text{OEt})_4$  because terminal OR ligands are more reactive towards proton transfer than bridging ligands. Employing a solvent may also influence the reaction kinetics as if a suitable solvent is chosen; it may be preferentially hydrolysed over the alkoxide ligands. This allows for greater control over the reaction kinetics through the correct use of solvent. The structure and morphology of the resulting network strongly depend on the nature of the catalyst, in particular, the pH of the reaction. In the case of the common silicon alkoxides, since the hydrolysis rate is high under an acidic environment relative to that of condensation, acid catalysis promotes the development of more linear or polymer-like molecules in the initial stages. For a pure metal alkoxide system, this will result in the formation of high-density, low fractal dimension structures. On the other hand, base catalysis results in a higher condensation rate. Therefore, this environment tends to produce more of a dense-cluster growth leading to dense, colloidal particulate structures. In addition to the pH of the reaction, the size of the alkoxy group can also influence the hydrolysis and condensation reactions through a steric or leaving group stability effect. For example, species such as tetramethoxysilane (TMOS) tends to be more reactive than tetraethoxysilane (TEOS). Controlling the conditions can be difficult but successful control of the reaction conditions has the potential to produce materials of consistent size, shape and structure.

## 1.5 Mixed alkoxide system

Mixed-metal alkoxide systems are also of great interest because of the potential properties and applications they provide. In the case of different metal alkoxide combinations, the structure and morphology of the resulting network depend not only on the nature of catalyst but also on the relative chemical reactivity of metal alkoxides. The great difference in their reactivity can often cause phase separation. Therefore, the control of the reactivity of metal alkoxides is necessary in order to be able to tailor the structure of the resulting materials. The hydrolysis and condensation reactions in the sol-gel process generally start with the nucleophilic addition of hydroxylated groups onto the electrophilic metal atoms which results in an increase of the coordination number of the metal atom in the transition state. As described by Sanchez and Ribot [15], the degree of reactivity of a given metal or semi-metal atom of an alkoxide is not due only to the electrophilic nature but rather is more a function of degree of unsaturation. The extent of unsaturation is given as  $(N - Z)$ , where  $N$  is the coordination number of the atom in the stable oxide network and  $Z$  is the oxidation state. Table 1 lists the electronegativity and the degree of metal unsaturation for a few metal alkoxides. It is noted that silicon has a low electrophilicity and zero degree of unsaturation. Therefore, silicon alkoxides are less reactive. On the other hand, non-silicate metal alkoxides, including elements such as Ti, Zr, Al, and B with higher unsaturation, all have much higher reactivity than silicon. They are so sensitive to moisture, even in the absence of a catalyst, that precipitation of the oxide will generally occur as soon as water is present. For example, the hydrolysis and condensation rates of titanium butoxide are much faster than that of tetraethoxysilane (TEOS). As a result, titanium butoxide generally reacts rapidly with water and precipitates out of the reaction mixture before it can core act with the TEOS into a network. The sequence of reactivity is expressed as follows:

**Table 1.** Electronegativity ( $\chi$ ), Coordination Number (N), and Degree of Unsaturation (N-Z) for some Metals.

Alkoxides	$\chi$	N	Z	N-Z
Al(OR) <sub>3</sub>	1.61	6	3	3
Ce(OR) <sub>4</sub>	1.12	8	4	4
Si(OR) <sub>4</sub>	1.90	4	4	0
Sn(OR) <sub>4</sub>	1.96	6	4	2
Ti(OR) <sub>4</sub>	1.54	6	4	2
Zr(OR) <sub>4</sub>	1.33	7	4	3

There are several ways to control the core activity of two or more metal alkoxide species to avoid unnecessary phase separation. Chemical additives, such as glycols, organic acids (acetic acid) have often been used as chelating ligands to slow the hydrolysis and condensation reactions of non-silicate metal alkoxides. After forming a complex with the chelating ligand, the species between metal and chelating agent is less easy to hydrolyze. However, the chelating ligand will normally remain which alters the structure of the final network. Chemically controlled condensation (CCC), a procedure proposed by Schmidt and Seiferling, has also been used to control the difference in reactivity of various metal alkoxides. Specifically, hydrolysis of a fast-reacting alkoxide species is slowly initiated by the controlled release of water from the esterification of an organic acid with an alcohol. Once the fast-reacting alkoxide has been partially hydrolyzed and condensed, water is added to complete the overall reaction and to incorporate the slower reacting alkoxide. Another useful method was used by Parkhurst et al. to incorporate titanium butoxide into TEOS-based silica gel. In this procedure, the TEOS species is allowed to partially hydrolyze and condense in the presence of an acid catalyst and water. Then, fast-reacting titanium butoxide is added. Once introduced, it quickly hydrolyzes and at least partially condenses into the preexisting immature TEOS-based network rather than precipitating as titania [16].

## 1.6 Role of the catalyst

Acid and base catalysts can have a strong influence over hydrolysis and condensation rates as well as the structural properties of the final product. The addition of an acid will result in the preferential protonation of the negatively charged alkoxide group (Figure 6). Protonation of the alkoxide group produces good leaving groups which enhance the reaction kinetics, eliminating any proton transfer that occurs in the transition state and thus allowing hydrolysis to go to completion upon the addition of water.

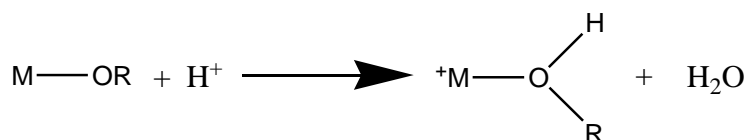


Figure 6. Acid catalyst reaction.

The condensation pathway can be influenced by the ease of protonation of the different alkoxide ligands (Figure 7).

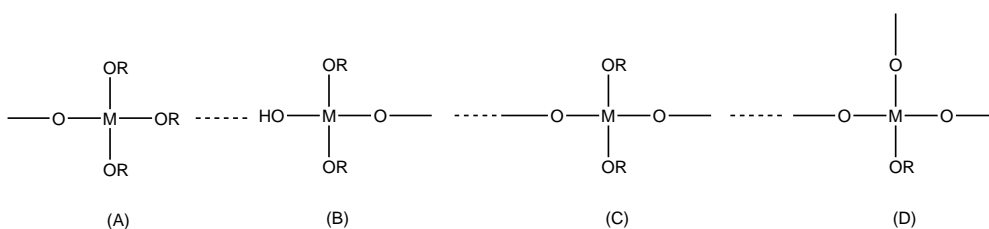
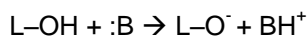


Figure 7. Partially hydrolysed polymer.

The ease of protonation decreases following,  $A > B > C > D$ , this reflects the electron providing power of the ligands, which decreases as alkoxy < hydroxo < oxo. Because of this, acid catalysed condensation occurs at the end of chains rather than the middle, resulting in longer polymer chains with little branching. A combination of acid catalysts with low  $r$  values (water:metal ratio in alkoxide) result in monolithic gels or sols [17]. The kinetics of the condensation reactions are severely retarded



with high acid concentrations ( $H+/Ti = 1$ ) [18]. In alkaline conditions, hydroxo ligands are deprotonated, producing strong nucleophiles:



where  $L = M$  or  $H$  and  $B = OH^-$  or  $NH_3$ . The hydrolysis rate of  $Ti(OBu)_4$  was less in basic conditions than in acidic or neutral conditions. It was postulated that the nucleophilic addition of  $OH^-$  may reduce the partial charge of the titanium metal centre ( $\delta(Ti)$ ), making the hydrolysis reaction less favourable. While hydrolysis kinetics are retarded in basic conditions, the condensation kinetics of metal alkoxides are enhanced. Calculated partial charge values of  $\delta(Ti)$  calculated for model sites A – D (Figure 7) show a decrease in the order of reactivity toward nucleophilic attack in the order  $D > C > B > A$ . Therefore, base-catalysed condensation (and hydrolysis) should be directed toward the middle rather than the end of chains, resulting in the formation of compact, highly branched species.

## 1.7 Factors over the sol-gel systems

As well as in all of the rest of chemical technologies, the synthesis conditions influence the structure and the properties of the products. Some of the most important parameter in sol gel synthesis are following reported:

- 1) **Composition and nature of precursors:** The precursor have to be soluble in the liquid medium and to posses reactivity in the system. It is obvious that the properties of the obtained gel depends generally on the kind of precursor used, its concentration, and the nature of the reactions that occurs in the sol. Also, the alkyl radicals are very important for composition, structure and properties of the sol and consequently for the film realized, as well as the metal ion in the corresponding alkoxides used. Hasegawa and Sakka [19] have investigated four different tetraalkyl silanes as follows: Tetramethoxysilane (TMOS), Tetraethoxysilane (TEOS), Tetrapropylloxysilane (TPOS), and Tetrabutylloxysilane (TBOS). By application of in-situ chromatographic methods, they have established that the

gel-forming system of each tetraalkoxysilane has its individual distribution of concentration of chains with different rate of polymerization, at the same conditions. Comparative research were realized by other authors [20]. They used  $C_3H_7-Si(OCH_3)_3$  "C3";  $C_8H_{17}-Si(OCH_3)_3$ , "C8";  $C_{18}H_{37}-Si(OCH_3)_3$ , "C18", and  $(CH_3O)_3Si-C_2H_4-Si(OCH_3)_3$  to realize a protective coating. The authors have established that the length of the aliphatic chain strongly influence over the durability and protective ability of the coatings, obtained from these sols. The length of the alkyl chain and the kind of functional group influence the properties of the films as well as the intermolecular interactions among the corresponding organic chains. For example, the literature [21] reports the synthesis of materials composed by metal alkoxide (TEOS) and crosslinking substance 3-glycidoxypropyl trimethoxysilane (GPTMS), for obtaining of boehmite ( $\gamma-AlO(OH)$ ), also could be found from the literature. Modifications of that System are used for obtaining of corrosion protective coatings [22,23].

- 2) **Solvent.** The liquid medium of the reacting systems is usually represented by mixture of alcohols, water, and catalysts. The hydrolysis is usually catalyzed in acid condition, but the literature reports also sol synthesized by alkali catalyst [24]. The control of the intensity of the evaporation plays an important role on the structure of the gel products. If the evaporation rate is too fast, the corresponding products (xerogel, powder, etc.) will shown fractures, disruptions, cracks, and difference in the density distribution. Moreover, the rate of evaporation influences the intensity of particle agglomeration and condensation processes.
- 3) **Influence of pH of the medium.** The pH of the sol solution influence the rate of hydrolysis that depends also on the kind of precursor, length of alkyl chain as well as over the content of not reacted monomer residuals in the sol. Two different acids could promote different hydrolysis rate even when they are added at the same molar quantity. That phenomenon is originated from the difference of the oxidation activity of the corresponding anions. As well known the synthesis of silica sol carries out in alkali condition bringing to the formation of yield highly branched cluster (e.i. spherical nanoparticles). While, in acid condition, the synthesis bring to yield primarily linear or randomly branched polymer. Izumi et al. [11] have investigated the

differences of the hydrolysis rate of methyl-triethoxy-silane ( $\text{CH}_3\text{Si}(\text{C}_3\text{H}_5\text{O})_3$ ) and phenyl-triethoxy-silane ( $\text{C}_6\text{H}_5\text{Si}(\text{C}_3\text{H}_5\text{O})_3$ ) in acidic (HCl) and alkaline ( $\text{NH}_4\text{OH}$ ) media. As results, even if the medium, used to hydrolyze the precursor, has the same characteristic, the hydrolysis rate depends on the kind of precursor. In acid condition, the  $\text{CH}_3\text{Si}(\text{C}_3\text{H}_5\text{O})_3$  precursor has already hydrolyzed (100%) at the first hour while for the  $(\text{C}_6\text{H}_5\text{Si}(\text{C}_3\text{H}_5\text{O})_3)$  precursor the complete hydrolysis is observed after the fourth hour. The hydrolysis reaction in alkaly medium is slower than the hydrolysis catalyzed by HCl. The  $(\text{C}_6\text{H}_5\text{Si}(\text{C}_3\text{H}_5\text{O})_3)$  precursor is hydrolyzed at the second hour, but the first one - after five hours. The addition of salts also has its influence over pH of the medium. The use of buffer (weak acid and its salt) should shift the dissociation equilibrium of the acid towards the neutral point. The salts could serve as modifiers of different organic hydroxyl-derivatives. The influence of salts depends from their chemical nature and quantity as well as the moment of their addition. [25]. The cations of different complex-formers as salts of ethylene-diamine-tetraacetic acid (EDTA) could form "knots" between the polymeric chains [26].

- 4) **Temperature.** As well as in all rest kinds of synthesis, the temperature has significant influence over the on the properties of the sol synthesized. The temperature influences the rate, mechanism and interaction of hydrolysis and condensation reactions. Obviously, it has direct influence on the kinetics of the chemical reactions. The synthesis temperature are also important because influence also the evaporation of the solvent and consequently the concentration of the substances in the sols. [27].
- 5) **Surfactants.** Surfactant acts on the solubility of the precursor in the solvent. In the same time they provoke a flocculation and thus they could be less available in solution. The mechanism of the surfactant action is based on the forming of cover on the particle surface. So, due to the presence of these films a separation between the particle, and the liquid medium is represented. The surfactants act changing the surface tension between the components in the system. So, they could act as stabilizer of the particle in the sol, strongly depressing the process of the sedimentation. In this way, it's possible realize homogenues film and modify the porosity and the flexibility of the film realized on the surface.

# Chapter 2

## Characterization Techniques

### 2.1 Stability sol characterization

The nanosol stability was studied by measuring of the variation of the turbidity solution. In according with ISO 7027 nephelometric method, the turbidity measurement were performed using a Hach Ratio XR turbidimeter manufactured by Hach Co. The sample was placed in a vessel (diameter of 25 mm and height of 50 mm) and the measurements were taken in the range of 0–4000 nephelometric turbidity units. Formazin solution was used as a primary standard to calibrate the turbidimeter.

The changes in the average particle size of detached TiO<sub>2</sub> was measured by dynamic light scattering (DLS) with a Malvern Instruments Zetasizer Nano-S system. Samples in water solution, at a temperature of 25°C, were irradiated with red light (HeNe laser, wavelength  $\lambda = 632.8$  nm) and the intensity fluctuations of the scattered light (detected at a backscattering angle of 173°) analyzed to obtain an autocorrelation function. The angular intensity of the scattered light was measured by a series of photosensitive detectors whose number and positioning have been

optimized to achieve maximum resolution across a broad range of sizes, using the cumulants analysis and a size distribution using a regularization scheme by intensity, volume, and number. The map of scattering intensity versus angle was used to calculate the particle sizes. Data were acquired in automatic mode, ensuring enough photons were accumulated for the result to be statistically relevant.

The stability of the sols was also studied through the change of sol viscosity. Rheological properties of the nanoparticle suspension were determined at constant temperature (25°C) using a strain-controlled concentric viscometer (VT550, Gebruder HAAKE GmbH, Germany) equipped with a cone-cup geometry sensor system (MV-DIN 53019, HAAKE, Germany). These measurements were performed at constant shear rate ( $\dot{\gamma}$ ), with fixed intervals between measurements depending on the shear-rate range; every 10 s<sup>-1</sup> over 10–100 s<sup>-1</sup> and every 100 s<sup>-1</sup> over 100–1000 s<sup>-1</sup>. Rheological properties were always measured 20 s after the viscometer reaching the desired shear rate. The suspensions typically reached an equilibrium stress in less than 10 s, this duration is hence sufficient to ensure that the sampled rheological properties were taken under steady-state conditions.

## 2.2 Surface characterization

In order to explore the deposition of thin films, a morphological analysis of the textile fabric surfaces was carried out by means of a scanning electron microscope (SEM), using a Jeol JSM-6300 (Jeol USA Inc., Peabody, USA) equipped with energy dispersive X-ray spectroscopy (EDX) for surface elemental analysis. Each EDX measurement was performed twice, once for the uncoated substrate and the second for the same substrate coated with film.

The crystalline phase of the TiO<sub>2</sub> thin films on cotton fabric was investigated by XRD analysis. Wide angle X-ray diffraction (WAXD) spectra were obtained at 20°C using a Siemens D-500 diffractometer equipped with a Siemens FK 60-10 2000W tube (Cu Ka radiation,  $\lambda = 0.154$  nm). The operating voltage and current were 40 kV and 40 mA, respectively. The data were collected from 24 to 70 2 $\theta^\circ$  at 0.02 2 $\theta^\circ$  intervals.

FT-IR transmittance spectra were recorded at room temperature in the range from 4000 to 650  $\text{cm}^{-1}$  with 64 scans and a resolution of 4  $\text{cm}^{-1}$  using a Thermo Avatar 370 spectrophotometer, equipped with attenuated total reflection (ATR) accessory and ZnSe or diamond crystals.

## 2.3 Thermal analysis

Thermogravimetric analyses (TGA) of the samples (Part A: Phosphorus-doped amino functionalized silica thin film) were carried out on a TA Instruments Model TGA Q500, operating under nitrogen and air atmosphere using a platinum pan containing samples of approximately 4 mg ( $\pm 0.0001$ ). The runs were performed over a temperature range between 30 and 600°C at 10 °C/min heating rate and 60 ml/min flow. The thermal stability of the fabrics (Part B: Hybrid phosphorous silica film) was evaluated by thermogravimetric (TGA) analyses from 50 to 800°C with a heating rate of 10 °C/min. A Pyris1TGAQ500 analyzer was used, placing the samples in open alumina pans (ca. 10 mg), in air atmosphere (60 ml/min).

Differential scanning calorimeter (DSC) measurements were performed on an MDSC apparatus TA Instruments at a heating rate of 10 °C/min under nitrogen atmosphere (50 ml/min). The runs were carried out over a temperature range between 25 and 500°C.

Burning behavior of the samples (Part A: Phosphorus-doped amino functionalized silica thin film) was studied using the Flammability Tester Model 7633E by United States Testing Company, inc., according to ASTM D 1230-94 standard method [28]. In these tests the sample is mounted in a frame and held in a special apparatus at an angle of 45°. A standardized flame is applied to the surface from the bottom; the ignition time was set at 5 seconds. Five samples for each textile fabric were processed and an average of the data was taken for interpretation.

The flame retardancy properties of the prepared samples (Part B: Hybrid phosphorous silica) film were measured using a vertical fabric flammability test, applying a propane flame for 5 seconds at the centre of a fabric specimen (50 mm x 100 mm) and repeating the application for at least two times: this configuration allows to test the fabrics in the most drastic way. The test was repeated 5 times for

each formulation in order to get reproducible data, measuring burning time, rate and the final residue.

## 2.4 Wettability characterization

Different kind of tests were used to study the hydrophilic/hydrophobic behaviour of the textiles. Even if the contact angle is usually recognized as scientific method to evaluate the hydrophobicity also empirical tests were performed to have a complete view of phenomena. Textile surfaces are not often completely homogenous/smooth and this condition could lead to wrong measurements. Moreover, the fabric construction, the dimension of warp, dyes, other finishing agents, and the like, can also influence fabric absorbency. The presence of smaller single fibers on the fabric surface that are present intrinsically in the structure can modify the water drop shape and, consequently, to distort the contact angle measurement.

Contact angle and hysteresis: The wettability of the films was evaluated by measuring the contact angle (CA) of a 10 mg water droplet placed on the film surface using the contact angle meter equipped with a CCD camera at a ambient temperature. The hysteresis was calculated as difference between advancing contact angle and receding contact angle.

Drop test absorbency: drops of water are placed on the fabric surface (horizontal surface), and the time it takes for the drops to be absorbed into the fabric is measured. The Absorbency Rating is calculated by obtaining five values, deleting the high and low values, and averaging the remaining three values. If the drop has not been absorbed in 30 seconds the test have to considerer end, stop the timer and record 30 seconds as the value. Absorption has occurred when the drop has penetrated into the fabric.

DuPont test [29]: a drops of each standard test liquids, consisting of a selected series of water/alcohol solutions with varying surface tensions (Table 2), are placed on the fabric surface and observe wetting, wicking and contact angle. Afterwards it is noted whether the different mixtures do not wet the fabric for at least 10 seconds. The aqueous repellency grade is the highest numbered test liquid

which does not wet the fabric surface. The scale ranges from one to eight, with a rating of eight signifying the most repellent surface.

**Table 2.** Different water/isopropanol mixtures used for DuPont test.

Grading	Ratio water/isopropanol [v/v]
1	98:2
2	95:5
3	90:10
4	80:20
5	70:30
6	60:40
7	50:50
8	40:60

Water uptake: the test measures the percentage of water absorbed after the immersion of sample in a water solution (A, wt%). The water absorbed percentage was calculated as average of three samples according to the Equation 1:

$$A = \frac{W_f - W_i}{W_i} 100 \quad (\text{Equation 1})$$

The sample was first weighed ( $W_i$ ) and after that put in a becker containing 300 ml of water. It was let there for 30 seconds and then weighed again ( $W_f$ ).

## 2.5 Optical and photo activity characterization

UV-vis reflectance spectroscopy was used to characterize the optical absorption properties and the photocatalytic efficiency of  $\text{TiO}_2$  films. Diffuse reflectance spectra of the samples were recorded on a double beam UV-vis



scanning spectrophotometer (Lambda 950 Perkin Elmer), equipped with a diffuse reflectance accessory (RSA-PE-150 Labsphere). The reflectance of each sample was measured in the wavelengths range from 250-800 nm at room temperature.

The optical energy band gap of thin films was calculated using the Tauc relation [30]. The fundamental absorption, which corresponds to electron excitation from the valence band to conduction band, can be used to determine the nature and value of the optical band gap,  $E_g$ . The relation between the absorption coefficient,  $\alpha$ , and the incident photon energy,  $h\nu$ , can be written as Equation 2 [31].

$$\alpha h\nu = B_i(h\nu - E_g)^n \quad (\text{Equation 2})$$

where  $h$  is the Planck' s constant (J s),  $B_i$  is the absorption constant,  $\nu$  is the frequency of the light ( $s^{-1}$ ) and  $n$  is an index that characterizes the optical absorption process and is theoretically equal to 1/2, 3/2, 2 and 3 for direct allowed, direct forbidden, indirect allowed and indirect forbidden transitions, respectively.

For solid samples the absorption coefficient ( $\alpha$ ) can be replaced by the diffuse absorption coefficient,  $F(R_\infty)$ , by approximation of the reflectance data in according to the Kubelka-Munk equation (Equation 3) [32,33]:

$$KM = F(R_\infty) = \frac{k}{s} = \frac{(1 - R_\infty)^2}{2R_\infty} \quad (\text{Equation 3})$$

where  $F(R_\infty)$  is the remission function or the Kubelka-Munk function,  $R_\infty$  is the absolute reflectance of an effectively infinitely thick layer,  $k$  is its molar absorption coefficient, and  $s$  is the scattering coefficient. Moreover,  $k/s$  is proportional to the absorption coefficient and, thus, to the concentration of the  $TiO_2$ : it offers a correlation between reflective measurement and concentration of specimen to evaluate. Therefore, the band gap energy was deduced plotting the modified Kubelka–Munk function  $[(F(R_\infty)h\nu)^{1/2}]$  against  $h\nu$ : the intercept among linear Tauc plot's region and the photo energy axis is the value of  $E_g$  [34].

The photocatalytic activity of  $TiO_2$  thin films was assessed by monitoring the dyestuff degradation after exposure of the dyed fabric to UV ( $\lambda_{max} = 365$  nm) or visible (day light lamp; L15W/10, Osram) sources. The experiment was carried out in

a Helios Italquartz photochemical reactor equipped with 10 lamps. Each sample (60 mm x 37 mm) was dyed as follow: first, the fabric was wetted by 0.30 ml of EtOH to improve the wettability and, then, left for 2 minutes at room temperature to remove the excess of solvent. Subsequently, the cotton fabric was dyed using 0.67 ml of dye solution (0.075 g/L), dried at 37°C for 10 minutes in a oven and stored for 24 hours. The realized samples were put in the samples holder and placed in the exposure chamber in vertical position at a distance of 10 cm from the light source and irradiated at thermostat temperature (303K) and constant humidity for several exposure cycles.

The photocatalytic degradation was assessed from the changing of the absorption intensity at the lambda max of dyestuff. It was calculated starting from the Kubelka-Munk equation (Equation 4), as follow:

$$dyestuff\ degradation\ \% = \frac{\left[ \left( \frac{K}{S} \right)_i - \left( \frac{K}{S} \right)_{UD} \right]}{\left[ \left( \frac{K}{S} \right)_0 - \left( \frac{K}{S} \right)_{UD} \right]} * 100 \quad (\text{Equation 4})$$

Where  $\left( \frac{K}{S} \right)_{UD}$  is the KM value of the undyed sample,  $\left( \frac{K}{S} \right)_0$  is the KM value of the dyed sample before exposure to the light source and  $\left( \frac{K}{S} \right)_i$  is the KM value of the sample after exposure to different times.

## 2.6 Textile testing methods

Mechanical analysis of fabric samples were realized at  $20 \pm 2^\circ\text{C}$  and  $65 \pm 4\%$  RH, according to standard ISO 139:2005 [35]. The textile fabric's tensile strength was measured according to ASTM D5035 [36], using an Instron Tensile Tester. Ten yarn specimens for each fabrics were prepared for testing, ten for warp direction and the other ten for weft direction. Pretension  $0.5 \pm 0.1\text{ cN tex}^{-1}$ , load cell of 1000 cN were used. To investigate the presence of changes in the mechanical properties after 100 hours of light irradiation (UV or visible), the tensile strength of coated and uncoated samples was evaluated in Helios Italquartz photochemical reactor, previously used for the photo activity measurements.

To evaluate washing resistance treated and untreated textiles were washed according to the international standard EN ISO 6330:2000 with the selected procedure 6A in Wascator FOM71 CLS washing machine [37].

# Chapter 3

## Flame Retardant Finishing

### 3.1 State of the art

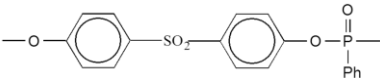
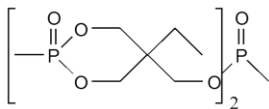
At the beginning of the twenty-first century, the population of the Earth, 6,300,000,000 inhabitants, annually experience a reported 7,000,000–8,000,000 fires with 70,000–80,000 fire deaths and 500,000–800,000 fire injuries [38]. Domestic fire safety is an area of concern, since almost 30% of the worldwide fires take place in dwellings, resulting in an astonishing 80% of fire deaths. Although sometimes it is hard to distinguish whether a fire is the consequence of human behaviour or technical failure, usually statistics demonstrate that the former factor is more relevant than the latter. In particular, cigarettes, small flames such as candles and cooking accidents turn out to be the most common source of ignition in combination with the presence of upholstered furniture and textiles. In particular, fires involving residential upholstered furniture (as the first ignited item) represent the leading reason for fire deaths in U.S. households, annually claiming 300 lives,

leading to 500 serious burn injuries and resulting in 1.6 billion dollars damages, according to the U.S. Consumer Product Safety Commission [39]. Incident evaluations have shown that people are confronted with smoke and its effects during evacuation [40]; these give rise to slowing down of the ability to react and escape and eventual unconsciousness followed by death by carbon monoxide poisoning as a major risk [41]. For all the above reasons, most of the scientific community efforts have been addressed to investigate the flammability of textiles, fibres and fabrics [42,43,44,45,46,47]. Million of meter of textiles are product every year for the furniture, clothing, interiors, and technical textiles including curtains. Flame retardant textiles can be obtained by chemical after-treatment of the flammable fibres, or using fibres which have been flame retarded during production, or inherently flame retardant fibres (LOI index upper than 30). Moreover, a combination of these methods can be realized.

Wool is regarded as a naturally flame-resistant fibre for many applications and it is treated to improve flame retardant properties by zirconium and titanium complexes. Specific agents used for this purpose are potassium hexafluoro zirconate,  $K_2ZrF_6$  and potassium hexafluoro titanate,  $K_2TiF_6$ .

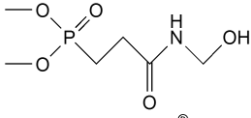
Polyester fibres may be flame retarded by incorporating a co-monomeric phosphinic acid unit into the PET polymeric chains. Various additives and co-monomeric modifications are available as shown in Table 3.

Table 3. Currently available flame retardants for polyester.

Generic type	Nature	Structure
Phosphine acid derivative (Trevira® CS)	Co-monomer	$\begin{array}{c} \text{O} \\ \parallel \\ \text{HO}-\text{P}-\text{Y}-\text{COOH} \\   \\ \text{X} \end{array}$ <p>X = H or alkyl Y = alkylene</p>
Bisphenol S (Toyobo® GH)	Additive	
Cyclic phosphonate (Amgard® 1045)	Dimeric additive	

For cotton, the most important commercial flame retardants can be classified into three categories [48]: flame retardants based on phosphorus (condensed phase mechanism) and halogens (gas phase mechanism), synergistic systems containing flame retardant enhancers (nitrogen-phosphorus and antimony-halogens) and flame retardants with physical effects (alumina, borate). Some of these treatments have serious drawbacks: for instance the use of halogens as flame retardants is restricted because of the toxicity of their combustion gases, whereas although inorganic salts can provide excellent flame retardant properties for cellulose, they have very poor laundering durability. In particular, the research activity are focused both to replace halogen formulations which are being increasingly questioned regarding their environmental sustainability and to increase the durability of flame retardant finishing. The current industrial flame retardant finishes treatments for cotton are shown Table 4.

**Table 4.** Currently available flame retardants for cotton.

Type	Durability	Structure/formula
<b>Salts</b>	Non-durable or semi-durable, depending on N	$\text{HO} \left[ \begin{array}{c} \text{O} \\    \\ \text{P} - \text{O} \\   \\ \text{O} \text{NH}_4^+ \end{array} \right]_n \text{H}$
	Non-durable	$(\text{NH}_4)_2\text{HPO}_4$
	Non-durable	Aluminium and boron
<b>Organo phosphorous</b>	Durable to more than 50 launderings	 , e.g. Pyrovatex® CP
	Durable to more than 50 launderings	THPC-urea-NH <sub>3</sub> condensate, e.g. Proban® CC
<b>(Back) Coatings</b>	Semi-durable to fully durable	Sb <sub>2</sub> O <sub>3</sub> + DeBDE (or HBCD) + acrylic resin, e.g. Myflam® (Mydrin)
	Semi-durable	$\text{C}_n\text{H}_{2n+2m}\text{Cl}_m$

Studies on cellulose pyrolysis explained that at high temperatures phosphorus compounds are able to phosphorylate the C(6) of the glucose monomer, preventing the source of fuel formation as levoglucosan and promoting the dehydration process, competitive route to the depolymerization (Figure 8) [49].

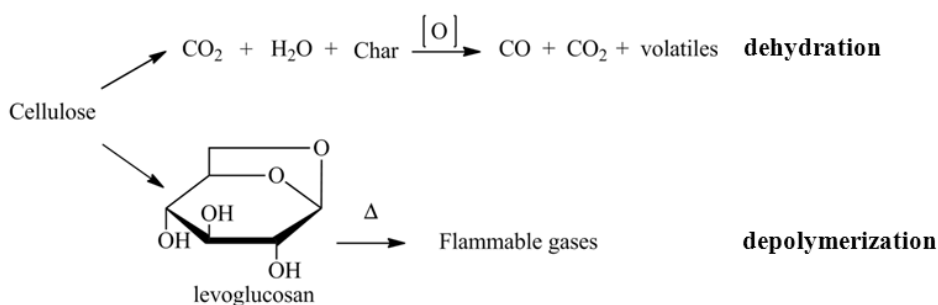


**Figure 8.** General products for cellulose pyrolysis.

In the flame retardant systems based on phosphorus-nitrogen compounds the organic nitrogen may be converted to phosphorus acid amides that also catalyze the dehydration and carbonization of cellulose. In this way, decreasing the amount of combustible gases at reduced temperatures, the formation of a carbonaceous replica of the original textile fiber is improved. Several studies demonstrated that the most effective flame retardant treatments are those which support the transformation of the flammable polymer material to a carbonaceous char [50]. The charred residue not only reduces the production of flammable volatiles but also realizes a flame and heat barrier between the ignition source and the fabric inner layers [51]. Many recent papers deal with the enhancing char forming properties achievable not only by conventional intumescent systems but also by increasing thermal barrier properties through nanoparticles [52].

The treatment of cellulosic materials with hydrolyzed metal alkoxide solutions is an excellent tool to convey new properties to polymer surfaces, particularly if organic components are incorporated into the formulation. In this composition the hybrid organic/inorganic materials (HOIMs) [53] show the properties of both phases or even new. The interactions giving cohesion to the composite can be weak (hydrogen, van der Waals or ionic bonds) or strong (covalent or ionic-covalent bonds). Their synthesis can be performed through the sol-gel method [54]: by the hydrolysis and condensation of a metal-organic precursor such as an

alkoxide,  $M(OR)_n$ , a porous three-dimensional inorganic network able to embed active species can be achieved. Therefore, the thermal stability at high temperatures proper of inorganic constituents can be combined with the flame retardancy of organic intumescent phosphorus based compounds. Some papers have already reported about the improved flame retardancy of polyacrylonitrile and cotton fabrics induced by hybrid coatings consisting of a  $SiO_2$  matrix and  $H_3PO_4$  [55]. The flame retardant study was developed in two main research approaches.

In the first activity (part A [56]) three new halogen-free hybrids finishes from the sol-gel precursor organically-modified 3-aminopropyltriethoxysilane (APTES) were synthesized and used in order to develop flame retardant cotton fabrics. More specifically a first sol (Si) containing APTES was prepared with the aim of studying the effect of the thin film consisting of precursor on the flame retardancy of cotton fabrics. Further Si sol was used as basis for the synthesis of the two other sol treatments. The second sol (Si-P), obtained by addition of the diethylphosphite (DEP) to the first one, was produced with the aim of exploiting the effectiveness of the P-N synergism in this system. Finally, the melamine derivative resin (MF) was added in the third sol (Si-P-C) in order to enhance the covering of textile fabric and also to increase the flame retardant power of the thin film since the melamine, known as an intumescent agent, brings a remarkable nitrogen amount [57].

The second approach (part B [58]) was focused on the preparation of silica based thin films through the sol-gel technique, in the presence of co-reactants containing Phosphorus and Nitrogen elements, aiming to assess their effect on the thermal stability and flammability of cotton fabrics. To this aim, 3-aminopropyltriethoxysilane (APTES) and melamine derivative resin were reacted with diethylphosphatoethyltriethoxysilane (DPTES). The choice of hybrid phosphorus precursor is due to the presence of covalent bond between phosphorus functionality and the inorganic group in order to increase the laundering durability.

FT-IR and SEM-EDX study of xerogels applied on glass slides and/or textile treated fabric was carried out in order to investigate the chemical and morphological structure of the produced thin films onto cotton surface. TGA and/or DSC analyses were carried out on the treated fabrics for thermal characterizations. Finally the untreated and treated flammability was measured by the burning test.



## 3.2 Experimental setup

### 3.2.1 Materials

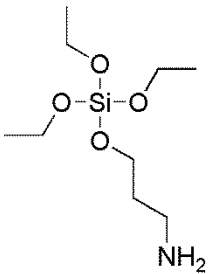
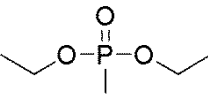
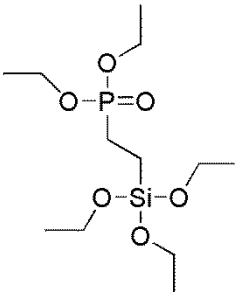
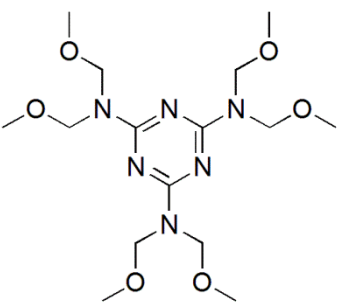
#### **- Part A: Phosphorus-doped amino-functionalized silica thin film**

Scoured and bleached 100% plain-weave cotton fabric (weight 237 g/m<sup>2</sup>) was used in this research. The fabrics were washed in 2% non-ionic detergent at pH 7 and 40°C for 20 min, and then rinsed several times with de-ionized water, dried and put into drier for storage. The cleaned samples were conditioned under standard atmospheric pressure at 65 ± 4% relative humidity and 20 ± 2°C for at least 24 hours prior to all the experiments [59]. The sol-gel precursor 3-aminopropyltriethoxysilane (APTES, purity grade 98%) and the diethylphosphite (DEP, purity grade 94%) were purchased by Sigma-Aldrich. The melamine based crosslinking agent (MF in aqueous solution, purity grade 50%), commonly used in textile finishing processes, was kindly provided by Europizzi S.p.A. (Italy). The chemical structures of the used compounds are shown in Table 5. All the chemicals and reagents were directly used without further purification.

#### **- Part B: Hybrid Phosphorus silica film**

Scoured and bleached 100% plain-weave cotton fabric (mass 237 g/m<sup>2</sup>) was supplied by Mascioni Spa, Cuvio (Va), Italy. The fabrics were washed in 2% non-ionic detergent at 40°C for 20 min, and then rinsed several times with deionized water, dried and put into drier for storage. The cleaned samples were conditioned under standard atmospheric pressure at 65 ± 4% relative humidity and 20 ± 2°C for at least 24 h before all the experiments. APTES (sol-gel precursor) and DPTES were purchased from Sigma Aldrich and Gelest, respectively. N,N,N',N',N'',N''-hexakis-methoxymethyl-[1,3,5] triazine- 2,4,6-triamine (MF) in aqueous solution (50 %w/v) is commonly used in textile finishing processes, was kindly provided by Europizzi S.p.A. (Italy). All chemicals were used without any further purification. Their structures are schematized in Table 5.

**Table 5.** Name, code and chemical structures of the sol-gel precursors, the organo-phosphorus compound and the cross-linker.

Name	Code	Chemical formula
3-aminopropyltriethoxysilane	APTES	
Diethylphosphite	DEP	
Diethylphosphatoethyltriethoxysilane	DPTES	
N,N,N',N',N'',N''-Hexakis-methoxymethyl-[1,3,5] triazine-2,4,6-triamine	MF	

### 3.2.2 Nanosol preparation and coating process

#### **Part A: Phosphorus–doped amino-functionalized silica thin film**

The sol solutions for the cotton fabrics impregnation as well as for the production of the xerogels were synthesized according to the molar ratios shown in Table 6. 23.39 mL (0.1 mol) of APTES were hydrolyzed with 8 mL (0.0008 mol) of HCl (0.1 N) in 168.61 mL of deionized water under vigorous stirring for 12 h at room temperature, obtaining the **Si** sol. The resulting pH value was 4.5. For the **Si-P** sol 23.39 mL (0.1 mol) of APTES and 8 mL (0.0008 mol) of HCl (0.1 N) and 13.70 mL (0.1 mol) of DEP were used. The **(Si-P-C)** sol containing the M cross-linker was prepared by adding 13.01 g (0.017 mol) of resin and 2.60 g of dimethylbenzene sulphonic acid catalyst (20% on cross-linker weight). The molar ratios of APTES:HCl:H<sub>2</sub>O were 1:0.008:94, 1:0.008:86 and 1:0.008:91 for the Si, Si-P and Si-P-C sols, respectively.

In order to produce the xerogels and investigate their chemical structure little amounts of each sol were applied on glass slides, the solvent was removed at 80°C for 2 h and the thin films were subjected to a thermal treatment at 120°C (Si, Si-P) or at 150°C (Si-P-C) for 1 h.

The cotton fabrics (20 cm X 30 cm) were impregnated with the hybrid sols and afterward were passed through a two-roll laboratory padder (Werner Mathis, Zurich, Switzerland) at nip pressure of 1.5 bar with 70% ofwet pick-up. After drying (80°C for 2h) the fabrics were cured (at 120°C, 5 min for Si and Si-P and at 150°C, 2 min for Si-P-C sol treated fabrics) in an electric laboratory oven Table 6.

The curing temperature for the fabric treated with the Si-P-C hybrid sol was enhanced to 150°C in order to assure an efficient crosslinking of the resin, according to the related technical sheet. The amount (wt% owf) of material deposited on the samples was determined and reported in Table 6. Each sample was weighed before ( $W_i$ ) and after the padding and thermal treatment ( $W_f$ ), using Mettler balance ( $\pm 10^{-4}$  g) to determine amount of material charged (A) as following (Equation 5):

$$A = \frac{W_f - W_i}{W_i} 100 \quad (\text{Equation 5})$$

Table 6. Molar ratios of hybrid sols.

Code	Chemicals	Molar Ratio	Drying		Curing		Amount (wt % owf)
			T (°C)	t (h)	T (°C)	t (min)	
Si	APTES		80	2	120	5	12.47
Si-P	APTES, DEP	1:1	80	2	120	5	19.03
Si-P-C	APTES, DEP, M	1:1:0.17	80	2	150	2	30.63

### - Part B: Hybrid Phosphorus silica film

The sol solutions for the cotton fabrics impregnation as well as for the production of the xerogels were synthesized according to the molar ratios shown in Table 7. 2.93 mL (0.0125 mol) of APTES and 3.98 mL (0.0125 mol) of DPTES were hydrolyzed, separately, with 2 mL (0.0002 mol) of HCl (0.1 N) in 45.07 mL of deionized water under vigorous stirring for 12 h at room temperature to obtain the silica sols. Three different solutions containing the MF (cross-linker) were prepared by adding 1.5 g (0.002 mol), 3 g (0.004 mol) and 4.5 g (0.006 mol) of MF and dimethylbenzene sulphonic acid (20% on crosslinker mass) in deionized water up to 50 mL of total volume. For the APTES-DPTES05, APTES-DPTES1 and APTES-DPTES2 sols (50 mL of total volume), the molar ratios of APTES (0.06, 0.12 and 0.25 M) and DPTES (0.25 M) were 1:4, 1:2 and 2:2, respectively. DPTES sols (0.25 M) containing MF were prepared by adding 3.98 mL (0.0125 mol) of DPTES in three different solutions with, respectively, 1.5 g (0.002 mol), 3 g (0.004 mol) and 4.5 g (0.006 mol) of resin and dimethylbenzene sulphonic acid (20% on cross-linker mass); subsequently, distilled water was added for achieving a final volume of 50 mL. The cotton fabrics (20 cm X 30 cm) were impregnated with the sols and afterwards were passed through a two-roll laboratory padder (Werner Mathis, Zurich, Switzerland) with 70% of wet pick-up. After drying (80°C for 2 h) the fabrics were cured (at 150°C for 2 min) in a laboratory oven. The total dry solids add-on on cotton samples (A, wt%) was determined by massing each sample before ( $W_i$ ) and after the impregnation with the sol solution and the subsequent thermal treatment ( $W_f$ ), using a Mettler balance ( $\pm 10^{-4}$  g).

The upload, collected in Table 7 was calculated according to the following equation (Equation 6):

$$A = \frac{W_f - W_i}{W_i} 100 \quad (\text{Equation 6})$$

Table 7. Investigated formulations.

Sample	[APTES]	[DPTES]	[MF]	A*
	[M]	[M]	[g/L]	[wt.-%]
APTES	0.25	-	-	10.4
DPTES	-	0.25	-	22.1
MF30	-	-	30	1.9
MF60	-	-	60	3.9
MF90	-	-	90	6.0

## Molar Ratio (mol:mol)

	[APTES]	[DPTES]	[MF]	
APTES-DPTES05**	0.5	2	-	20.7
APTES-DPTES1**	1	2	-	24.8
APTES-DPTES2**	2	2	-	31.6
MF-DPTES1**	-	1	1	30.1
MF-DPTES2**	-	2	1	49.2
MF-DPTES3**	-	3	1	70.5

\* amount of material charged on the cotton samples. \*\* DPTES = 0.25 M

### 3.3 Results

#### 3.3.1 Part A: Phosphorus-doped amino-functionalized silica thin film

##### 3.3.1.1 Surface characterization

Since infrared absorption bands characteristics of the hybrid thin film applied onto the fabric surface are covered by the strong vibrational peaks of the cellulosic substrate, the pure xerogels have been prepared in order to conduct analytical measurements.

The ATR FT-IR spectra of the Si, Si-P and Si-P-C xerogels applied and annealed on glass slides and the frequencies of major absorption bands are shown in Figure 9 and Table 8, respectively.

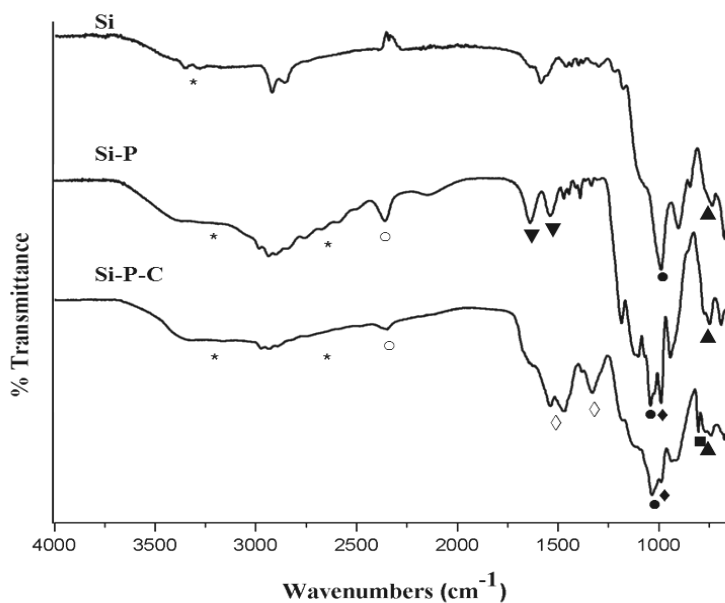


Figure 9. ATR FT-IR of the synthesized hybrid organic-inorganic xerogel.

In the Si xerogel spectrum the bands at 3300, 1001, 749-786  $\text{cm}^{-1}$  are due to the  $\text{NH}_2$  and Si-O-Si stretching, and Si-O-Si bending modes [60]. These vibrational bands confirm the formation of the inorganic  $\text{SiO}_2$  matrix. In the spectrum of the hybrid Si-P xerogel these absorption bands show some changes due to the

interactions between the organically modified silica matrix and the phosphorus compound. In this condition the NH<sub>2</sub> group results protonated as evidenced by the multiple bands between 3400 and 2500 cm<sup>-1</sup> ascribed to N-H stretching modes characteristic of amino-protonated species [61].

**Table 8.** Major vibrational frequencies of the Si, Si-P and Si-P-C xerogels.

Frequencies (cm <sup>-1</sup> )			Vibrational modes	Absorption band ID
Si	Si-P	Si-P-C		
3300	3300-2500	3300-2500	v (NH <sub>2</sub> )	*
	2355	2355	v (P-H)	○
1001	1043	1041	v (Si-O-Si)	●
	1638; 1540		δ (N-H)	▼
		1544; 1479; 1336	v (C=N) triazine	◇
	991	991	v (P-O)	◆
		812	δ (C=N) triazine	■
749-786	749-786	749-786	δ (Si-O-Si)	▲

Accordingly the symmetric and asymmetric N-H bending modes appear at 1638 and 1540 cm<sup>-1</sup>. The disappearance of the typical DEP P=O stretching band at 1250 cm<sup>-1</sup> [62] suggests a coordination of all the phosphoryl oxygens to amino-protonated nitrogen via hydrogen bonding (Figure 10). The P-O stretching modes are shifted to 991 cm<sup>-1</sup> because of an electronic delocalization [63] probably due to the hydrolysis reaction on P-OEt moiety favored by process conditions (pH and temperature) as reported in the open literature in the case of P-OMe bond cleavage [64].

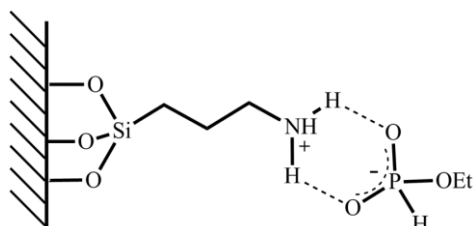


**Figure 10.** Proposed interaction between the hydrolyzed APTES and DEP.

The infrared spectrum of Si-P-C xerogel is very similar to that of the Si-P one except for the bands characteristics of the MF cross-linker: the broad bands at 1546, 1479 and 1335  $\text{cm}^{-1}$  are ascribed to the triazine ring and exogenous C-N stretching vibrations, whereas that at 813  $\text{cm}^{-1}$  is due to the triazine ring out-of-plane bending [65]. During the condensation and annealing process probable cross-linking reactions occur between the MF resin and the APTES sol according to the proposed mechanism displayed in Figure 11.

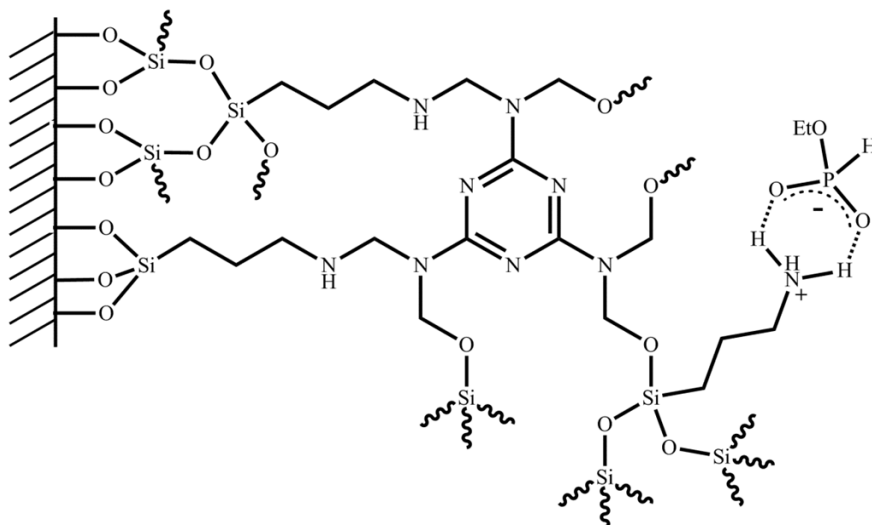


**Figure 11.** Proposed interactions after condensation and annealing process for Si-P-C xerogel.

The FT-IR spectra of the untreated and treated cotton fabrics are shown in Figure 12. Generally the spectra are very similar to that of the untreated one. In the treated samples spectra an overall slight decrease in the intensities at 3500-3000  $\text{cm}^{-1}$  characteristic of cellulose hydrogen bonded O-H stretching vibrations was observed, indicating the presence of the thin film on the surface of cotton fabric [66].



The presence of the  $\text{SiO}_2$  matrix is also confirmed by the small Si-O-Si bending mode absorption at  $795\text{ cm}^{-1}$  in all the spectra except for that of the Si-P-C sol treated fabric, where this weak band is overlapped by the triazine ring out-of-plane bending, observed at  $813\text{ cm}^{-1}$ .

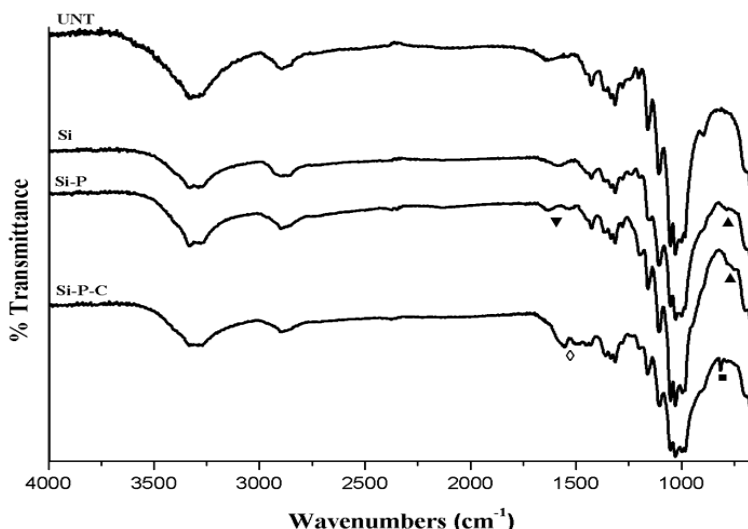


**Figure 12.** ATR FT-IR ATR spectra of untreated and treated cotton fabrics.

In order to find evidence of any relevant change in the fabric surface due to the treatment with the hybrid sols, analysis by scanning electron microscopy (SEM) was performed and images for treated and untreated cotton fabrics are shown in Figure 13. The surface of fabrics covered with pure Si sol (Figure 13b) is slightly rougher than that of the untreated one (Figure 13a), indicating the existence of  $\text{SiO}_2$  matrix distributed uniformly onto the textile fibers. In the magnification of the sample treated with the Si-P sol (Figure 13c) aggregations of the hybrid coating material cover clearly the fiber surface. The presence of MF cross-linker in the Si-P-C sol makes the organic-inorganic thin film more homogeneously distributed on the fiber surface (Figure 13d). Composition of the films was determined by energy dispersive X-ray analysis (EDX). For treated cotton fabric surfaces, silicon and phosphorus were the only detected elements in addition to fabric reference (Figure 13).

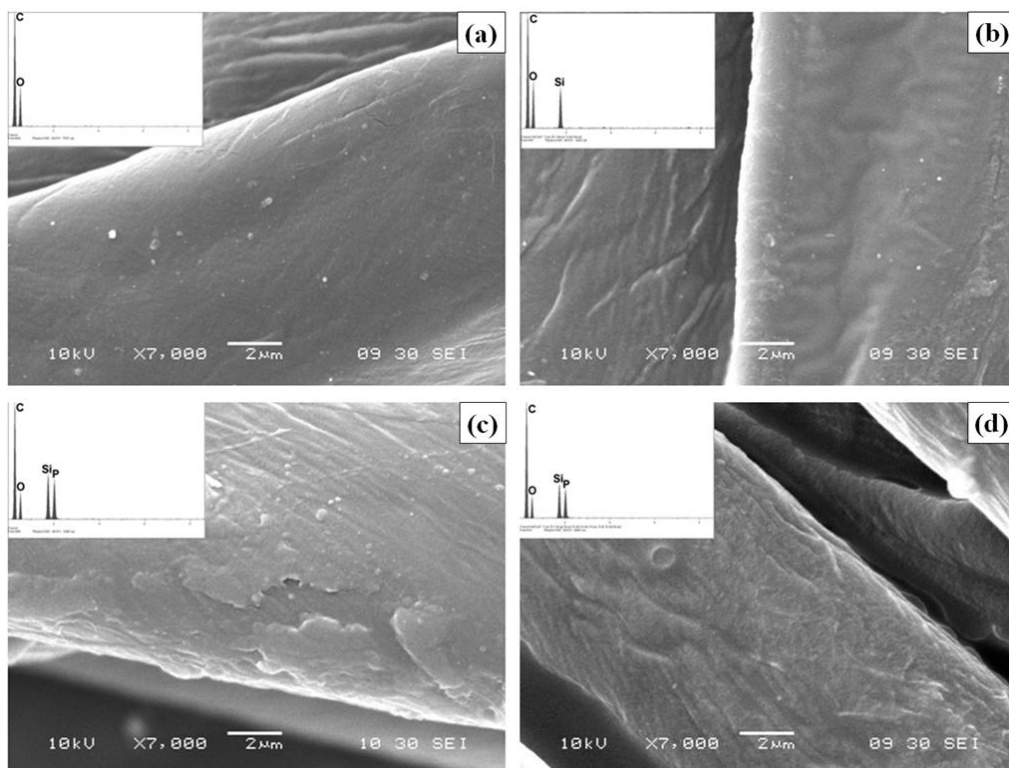


**Figure 13.** SEM micrographs and EDX spectra of cotton fabrics untreated (a), and treated with Si (b), Si-P (c) and Si-P-C (d) sols.

### 5.3.1.2. Thermal analysis

Studies on the thermal decomposition of the treated fabrics were carried out by TGA-DTG and DSC analyses both under nitrogen and air atmosphere. TG analysis of pure cotton sample in nitrogen (Figure 14a) shows the onset temperature of degradation at about 300°C, exhibiting its maximum of weight loss rate at about 378°C (Figure 14b) due to depolymerization by trans-glycosylation reactions [67]. The cotton fabric treated with Si sol shows a lower decomposition temperature, reaching the maximum of weight loss rate at 361°C. The fabrics treated with Si-P and Si-P-C sols show a similar trend with a degradation temperature significantly lower than that of the untreated fabric, and with the weight loss rate maximum around 320°C.

Besides the main degradation at 358°C in the TGA curve of untreated cotton fabric in air atmosphere (Figure 14c), an additional weight loss takes place around

500°C due to oxidation of the charred residue [67], not leaving significant residue. Instead the fabric treated with Si sol shows the same decomposition temperature of the untreated sample, but the silica thin film inhibits the oxidation of the cellulose material and accordingly provides a greater amount of carbonaceous residue at 600°C. The samples treated with the Si-P and Si-P-C sols show similar thermal stability in air with maximum of weight loss rate at 316°C and 319°C, respectively (Figure 14d).

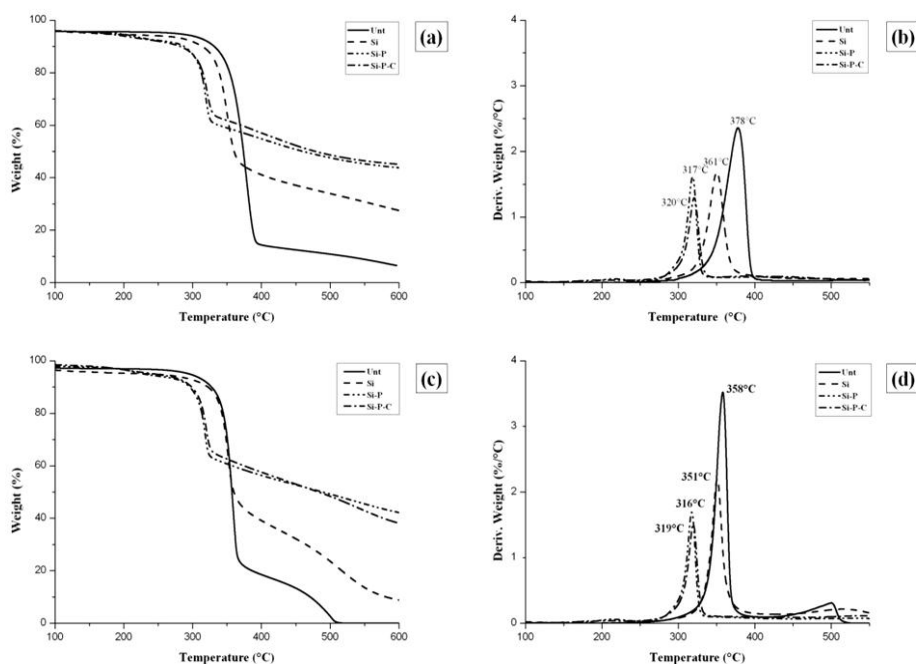


**Figure 14.** TGA and DTG curves of cotton fabrics in nitrogen (a, b) and air (c, d) atmosphere.

In Table 9 the char yield, that is the amount of material which was neither combustible nor volatile at temperatures below 600°C, is listed for all the samples both in nitrogen and in air. The % weight loss at 600°C in nitrogen atmosphere is reduced from 93% (untreated cotton) to about 73% (Si treatment), 56% (Si-P treatment) or 55% (Si-P-C treatment). The % weight loss is greater in air due to the oxidation of char. As well known the char yield denotes the flame retardancy of polymers [50,51,68]. Therefore from these results it comes out that the pure silica Si sol stabilizes the char toward the oxidation process, producing a higher amount of

char when compared to the untreated cotton sample, as observed in nano-composite cellulose fibers and polymer materials, where the role of silica is described as a heat barrier [69]. Instead, for the samples treated with the hybrid Si-P and Si-P-C sols, the decrease of initial decomposition temperature and the remarkable char yield are due to the catalytic dehydration of cellulose promoted by the phosphorus compound.

For this reason the decreasing of the onset degradation temperature facilitates the carbonaceous residue formation giving a lower percentage of flammable volatile products [70]. Although the MF cross-linker is known as an intumescent char-forming agent [57], it seems not to significantly affect the thermal behavior of the treated cotton fabrics, since the Si-P and Si-P-C sol treatments have a similar effectiveness of char formation, both in nitrogen and in air.

**Table 9.** Temperature maximum of weight loss rate and char yields at 600°C of cotton fabrics in nitrogen atmosphere.

Treatment	Nitrogen		Air		
	T <sub>dec</sub> [°C]	Char Yield [%]	T <sup>1</sup> <sub>dec</sub> [°C]	T <sup>2</sup> <sub>dec</sub> [°C]	Char Yield [%]
Unt	377,74	6,54	358,44	499,95	0,01
Si	361,23	27,50	351,07	515,16	8,85
Si-P	317,31	43,80	316,35	-	42,18
Si-P-C	320,12	45,19	319,00	-	38,11

DSC analyses shown in Figure 15 corroborate the TGA experiments: in nitrogen the untreated cotton sample DSC curve (Figure 15a) shows a strong endotherm at 370°C due to the depolymerization of cellulose with formation of levoglucosan and its evaporation [71]. For the sample treated with the Si sol the endotherm is broader and shifted at lower temperatures, around 300°C, and is followed by an exotherm at 353°C probably due to cross-linking reactions at high temperatures leading to final carbonaceous char [72]. The same exotherm appears at lower temperatures and becomes sharper and more intense for the fabrics treated with the hybrid Si-P and Si-P-C sols. Since the relative magnitudes of these

exotherms are also related to the amounts of char formed, a correspondence between DSC and TGA analyses is observed because the sols containing phosphorus promote more intensely the cross-linking processes during thermal decomposition leading to a larger final amount of carbonaceous residue.

The pattern of DSC curves obtained in air (Figure 15b) is different from that observed in nitrogen (Figure 15a). The DSC curve of untreated cotton sample shows an exotherm at 374°C due to simultaneous formation and volatilization of levoglucosan and other volatile products and chemisorption of oxygen on the char. A second exotherm starting over 420°C results from the combustion of the char at higher temperatures [67,73]. This peak corresponds to the weight loss observed around 500°C in thermogravimetry (Figure 14d) which might indicate self-ignition of the char [71]. For the sample treated with Si sol the exotherm associated with the pyrolysis and char formation is broad and shows a maximum at 372°C. The exothermic decomposition peaks occur at lower temperatures, 302°C and 308°C for the fabrics treated with Si-P and Si-P-C sols, respectively.

As observed in the TGA curves, the hybrid Si-P and Si-P-C thin films promote the cotton degradation at a lower temperature so that the decomposition speed is slowed down.

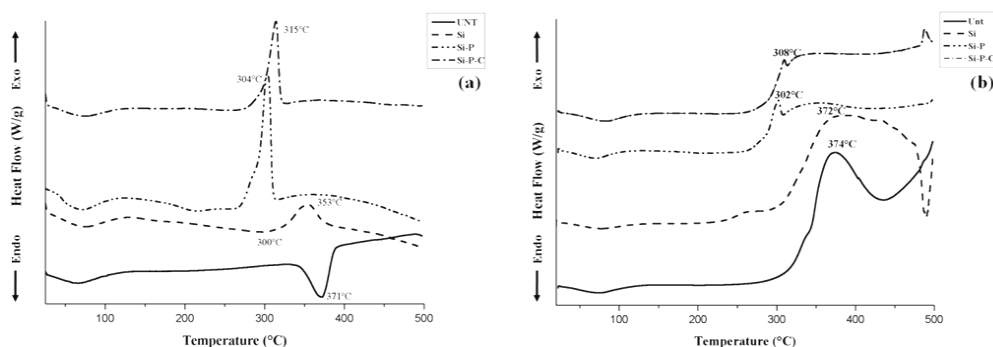


**Figure 15.** DSC curves of cotton fabrics in nitrogen (a) and air (b) atmosphere.

### 3.3.1.3. Burning behavior

Differences in the burning behavior of the untreated and treated cotton fabrics can be observed in the images taken at the end of the ASTM flammability test (Figure 16). In these experiments the time of exposure to flame was set at 5 s. The combustion times, taken after the flame spreading, are reported in Table 10. After removing the ignition source, the untreated cotton fabric burns very rapidly in 27 s leaving a very poor residue. For the cotton fabric treated with Si sol, the flame spreads after removing the ignition source until it reaches the top end of the fabric sample. The flame extinguished in a total of 60 s affording a slightly shrunken charred fabric. Although in the deposited silica thin film there are  $\text{-NH}_2$  groups, nitrogen when present alone has very limited flame retardant properties. Nevertheless, the combustion proceeds without after glowing and, differently from the untreated fabric, at the end a remarkable carbonaceous residue very similar to the original fabric structure is produced as observed in Figure 16.

On the contrary, the samples treated with Si-P and Si-P-C sols exhibit non-flammability properties: the flame immediately extinguishes upon removing the ignition source, leaving behind a small charred area. It is noteworthy that the same level of non flammability has been raised by treating the cotton fabric with the hybrid Si-P sol without the MF cross-linker contribution: being a nitrogen provider APTES enhances the phosphorus performance (synergism phosphorus-nitrogen). Although the role of nitrogen in P-N synergistic flame retardants is not well understood, evidence exists that cellulose phosphorylation and thus char production are enhanced by formation at high temperatures of polymeric species containing P-N bonds [74].

**Table 10.** Combustion times of cotton fabrics (weft direction) after exposing to flame for 5 seconds.

Sample	Combustion Time (s)
Unt	27,2
Si	60
Si-P	Not flammable
Si-P-C	Not flammable

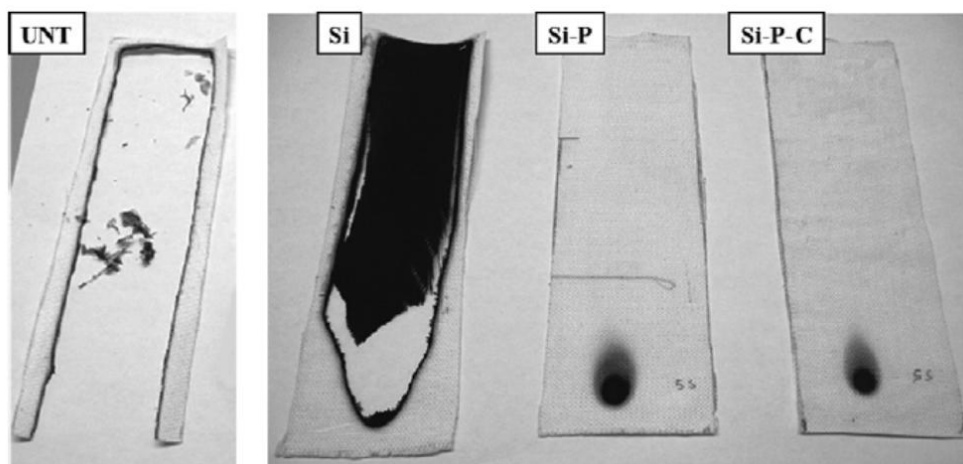


**Figure 16.** Samples subjected to flammability test after exposure to flame for 5 seconds.

#### **3.3.1.4. FT-IR analysis of char residues**

The residues left after TGA experiments were collected and subjected to FT-IR analysis. The spectra of the treated cotton samples pyrolyzed at 600°C are displayed in Figure 17. The residues of the fabrics treated with Si, Si-P and Si-P-C sols show characteristic peaks at 3436, 2942, and around 1600  $\text{cm}^{-1}$  which can be assigned to O-H, C-H and C=C stretching modes, respectively. The formation of species with double bonds is due to dehydration and loss of hydroxyl groups. The residue of the fabric treated with Si sol displays a peak at 1078  $\text{cm}^{-1}$  ascribed to the Si-O-Si stretching mode; the band at 805  $\text{cm}^{-1}$  due to the Si-O-Si bending vibration confirms the presence of the inorganic  $\text{SiO}_2$  matrix in all the charred residues. The decreasing intensity of the C-H and O-H bond stretching vibrations in the treated samples from Si to Si-P-C indicates more efficient dehydration and cross-linking reactions. In the spectrum of the residue of the fabric treated with Si-P sol the peaks at 1100  $\text{cm}^{-1}$  can be ascribed to the P=O stretching vibration [75]. The presence of P-N species can be highlighted by the peak at 1004  $\text{cm}^{-1}$ , but the exact interpretation of the absorption bands in this region is made difficult by several overlaps. In the spectrum of the pyrolyzed fabric treated with Si-P-C sol the C=C stretching is shifted at 1594  $\text{cm}^{-1}$ .

This phenomenon can be due to the more extended conjugation of C=C bonds and formation of C=N bonds. Further, the broad bands between 1115 and 989  $\text{cm}^{-1}$  are due to the formation of C-N bonds [57]. The FT-IR spectra of the charred residues confirm the more pronounced tendency of the Si-P and Si-P-C hybrid thin films to promote the cross-linking reactions in cellulose substrates at high temperatures as compared with the Si sol effectiveness.

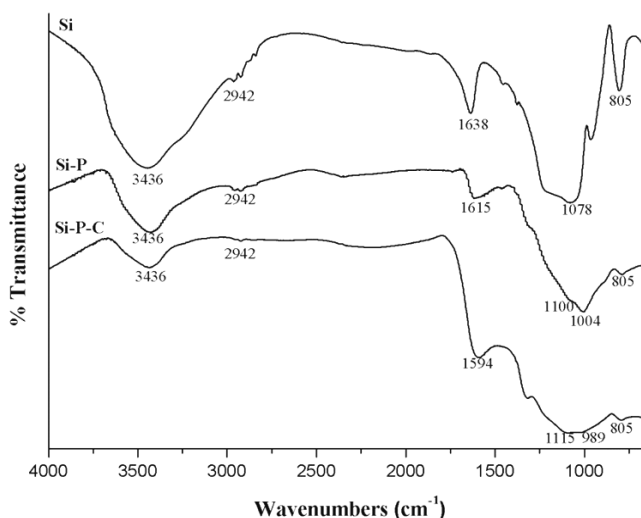


**Figure 17.** ATR FT-IR spectra of cotton fabrics treated with **Si**, **Si-P** and **Si-P-C** sols pyrolyzed at 600°C.

### 3.3.1.5 Wash fastness

All the treated samples exhibited almost the same behaviour of Si sample even after 5 washing cycles. In fact, in the EDX spectra of Si-P and Si-P-C samples, the absorption peaks referable to the phosphorus were no more present. That means that the phosphorus compound present in the hybrid Si-P and Si-P-C deposited film was removed from the textile surface, probably due to the ionic interaction between the hydrolyzed DEP and the organically modified  $\text{SiO}_2$  matrix, shown in Figure 10 and Figure 11.



### 3.3.2 Part B: Hybrid Phosphorus silica film

#### 3.3.2.1 Surface characterization

Figure 18 shows the absorption bands related to the vibrational modes of the functionalities present on the cotton fabrics treated with the hydrolyzed pure precursor sol (DPTES or APTES) and MF. In addition, the FT-IR spectra of the hybrid thin films, obtained mixing DPTES with MF or APTES, applied and annealed on the textile samples are shown in Figure 19 and Figure 20, respectively.

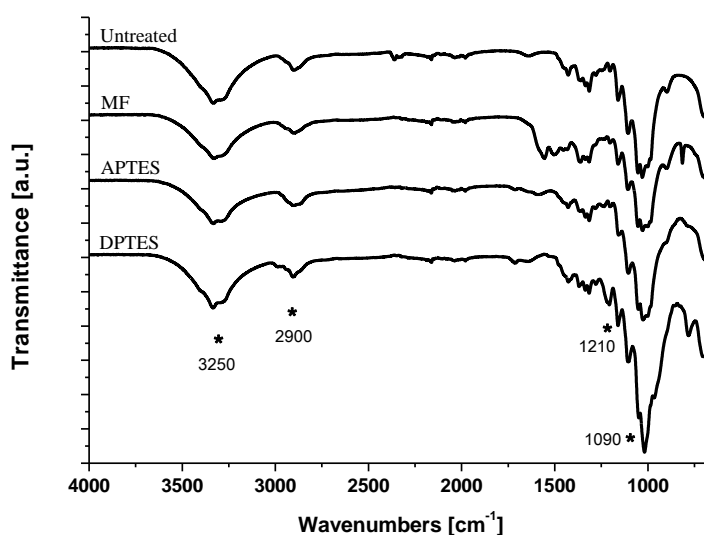


Figure 18. FT-IR spectra of untreated, APTES, DPTES and MF treated cotton fabrics.

The frequencies of the main absorption bands are shown in Table 11. All the spectra show a broad absorption band over  $3500\text{--}3000\text{ cm}^{-1}$  (hydrogen bonded O–H stretching) and a large peak at around  $2900\text{ cm}^{-1}$  (C–H stretching of a long alkyl chain), both attributable to infrared absorption frequencies of untreated cotton [76]. The spectra of the sol–gel treated samples show a slight decrease in the intensity of the OH stretching band, indicating the presence of the hybrid film on the cotton surface. In all the treated samples, a Si–O–Si basic skeleton can be foreseen by the presence of signals at  $1090\text{ cm}^{-1}$  (Si–O stretching) and  $800\text{ cm}^{-1}$  (Si–O bending). As far as the DPTES spectrum is concerned, the strongest intensity of the absorption band (Si–O bending) can be attributed to the overlapping with P–O vibration. In the

same spectrum, the P=O absorption band (located at 1241  $\text{cm}^{-1}$  for pure DPTES) appears at 1210  $\text{cm}^{-1}$  in xerogel spectra, e.g. shifted towards low frequency range. Such a shift is an indication of the involvement of phosphonyl groups in the formation of hydrogen bonds.

**Table 11.** Main vibration modes of DPTES, APTES and MF thin film.

DPTES [ $\text{cm}^{-1}$ ]	APTES [ $\text{cm}^{-1}$ ]	MF [ $\text{cm}^{-1}$ ]	Literature [ $\text{cm}^{-1}$ ]	Peak characteristic
1020	1000		1061; 1001; 1043; 1053	$\nu$ (Si-O-Si) stretching
1019; 770	770		749	$\delta$ (Si-O-Si) bending
854	856		860 ; 687	$\delta$ (Si-C)
	1577; 1482		1580 ; 1477	$\delta$ (N-H)
			3300	$\nu$ (NH <sub>2</sub> )
2800-3000	2800-3000		2800-3000	$\nu$ (C-H)
780-784			784	$\nu$ (P-O)
1230			1241	$\nu$ (P=O)
		1556; 1504; 1361	1544 ; 1479	$\nu$ (C=N) triazine
		814	812	$\delta$ (C=N) triazine

Furthermore, amino groups that literature reports at about 3300 and 1638  $\text{cm}^{-1}$  are not observed because they are covered by the characteristic peaks of cellulose. In Figure 19 the spectra of the cotton sample treated with DPTES and MF at several molar ratios are compared with the pure cotton. The treated samples show an overall slight decrease in the intensities at 3500 and 3000  $\text{cm}^{-1}$  (cellulose hydrogen bonded O–H stretching), thus indicating the presence of the hybrid film on the cotton surface. The characteristic band of MF at 1556  $\text{cm}^{-1}$  is ascribed to the stretching of triazine ring, whereas that at 814  $\text{cm}^{-1}$  is due to triazine ring out of plane bending. The band at 780  $\text{cm}^{-1}$  is ascribed to the presence of siloxane bonds or P–O stretching vibrations that increase by increasing DPTES:APTES molar ratio.

The enhancement of the intensity of this band causes the partial covering of the triazine ring signal at  $814\text{ cm}^{-1}$ .

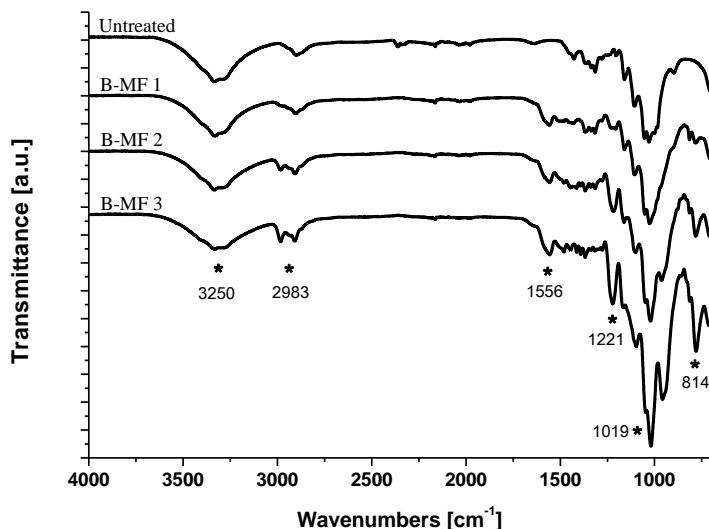


**Figure 19.** FT-IR spectra of untreated and DPTES:MF (B-MF) treated cotton fabrics. Molar ratio 1:1 (B-MF 1), 2:1 (B-MF 2), 3:1 (B-MF 3).

The presence of the silica phases is confirmed by a strong Si–O–Si band at  $1019\text{ cm}^{-1}$  that increases with the precursor concentration; at the same time, the bands at  $1221$  and  $2983\text{ cm}^{-1}$  (P=O and CH stretching, respectively) refer to the used DPTES:APTES molar ratios (Figure 20). The presence of the silica matrix is confirmed by the Si–O–Si band at  $1027\text{ cm}^{-1}$ ; an absorption band at  $784\text{ cm}^{-1}$  is also observable, the intensity of which can be partially ascribed to the P–O vibration. Finally, the effect of the phosphonyl group on the formation of hydrogen bonds is confirmed by the presence of the band at  $1210\text{ cm}^{-1}$ .

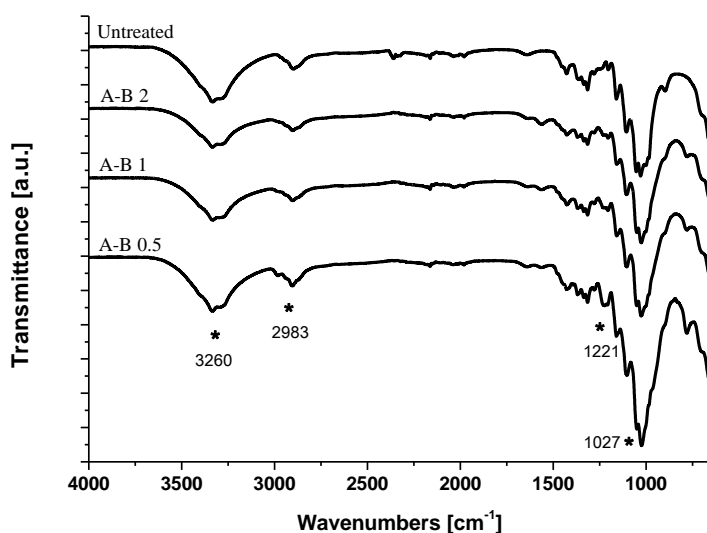


**Figure 20.** FT-IR spectra of untreated and APTES:DPTES (a-b) treated cotton fabrics. Molar ratio 0.5:2 (a-b 0.5), 1:2 (a-b 1), 2:2 (a-b 2).

Some possible schemes of cellulose/silica crosslinking interaction are shown in Figure 21.

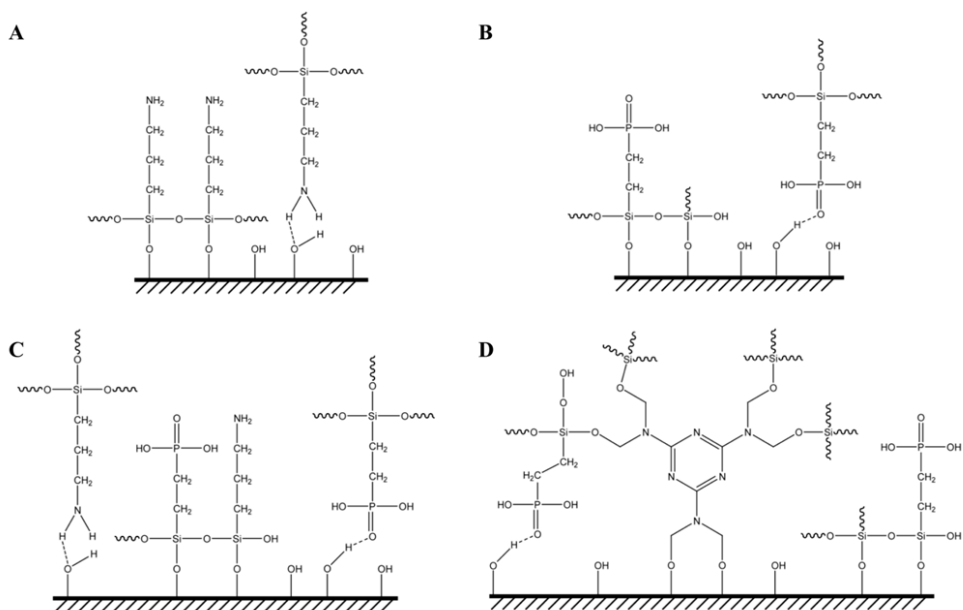


**Figure 21.** Schematic representation of possible orientations of APTES (a), DPTES (b), APTES-DPTES (c) and DPTES-MF (d) on the cotton fabric surface.

Some typical SEM magnifications of the sol-gel treated cotton fabrics are reported in Figure 22. All the formulations containing phosphorus, silica and nitrogen show similar morphologies: a homogeneous and compact film located at the fibre interconnections (warp and weft) and partially covering their walls is observed. Furthermore, the type of precursor used in the sol-gel process affects the homogeneity of distribution of the hybrid coating. Although the elemental mapping is qualitative, it is noteworthy that the fabrics treated with MF-DPTES3 show a wide distribution of Si and P elements on the fibres unlike the formulation containing both APTES and DPTES (i.e. APTES-DPTES2) or only DPTES.

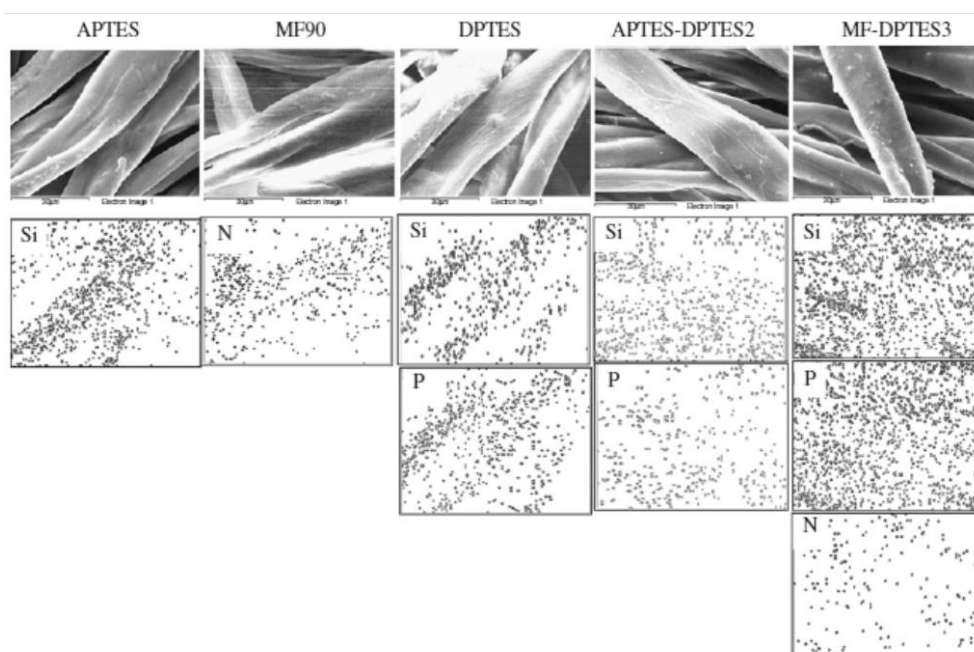
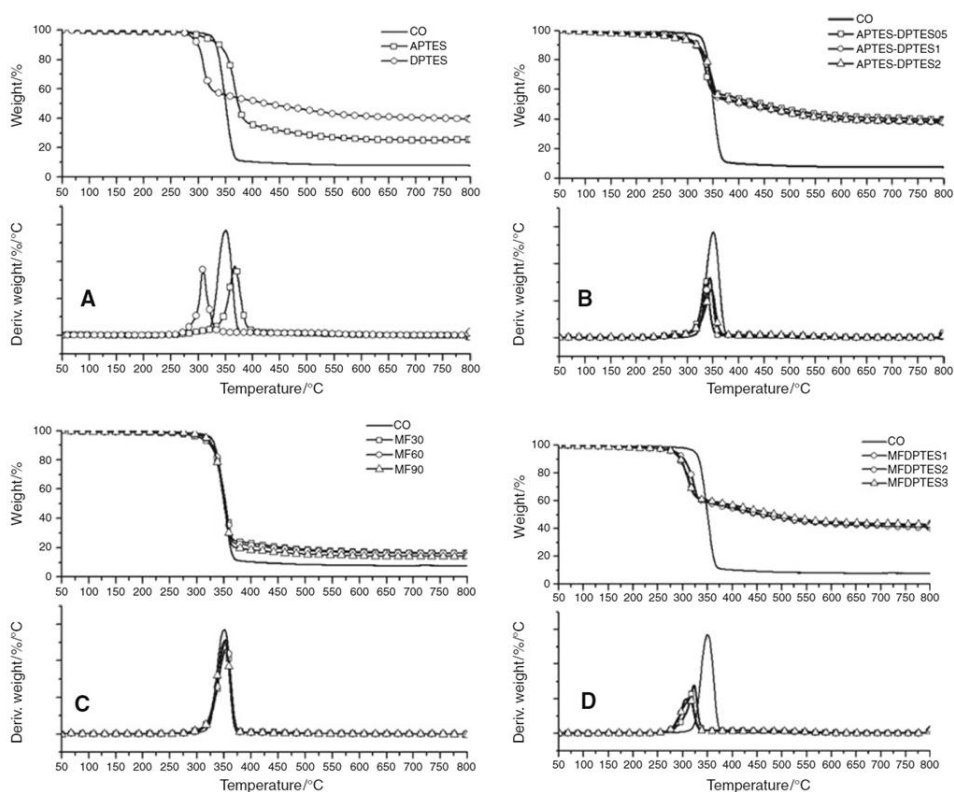


Figure 22. SEM magnifications of some formulations under study.

### 3.3.2.2 Thermal analysis

The thermal and thermo-oxidative stability of the samples was investigated by means of TG analysis: the typical curves are plotted in Figure 23a, b and the data are collected in Table 12 (for nitrogen) and Table 13 (for air). As well described in the literature, cotton shows a peculiar thermal degradation in both the atmospheres [77]. Usually, cotton pyrolyses in nitrogen according to two alternative pathways: (i)

the decomposition of the glycosyl units to char at lower temperature and (ii) the depolymerization of such units to volatile products containing levoglucosan at higher temperature.



**Figure 23.** TG and dTG curves of untreated and treated cotton fabrics in nitrogen.

Figure 23a shows that the cotton under study degrades thermally by only one step due to the decomposition of the glycosyl units to a multilamellar carbonaceous structure (known as char) with a maximum of mass loss rate at 350°C (Table 12). If the cotton is treated only with APTES or DPTES, its thermal stability increases, as indicated by the shifting of  $T_{max}$  values towards higher temperatures and by the final residue at 750°C (Table 12). By combining APTES and DPTES in different molar ratios (Figure 23b), it is possible to observe a joint effect amongst the sol-gel derived silica and P and N elements present in the hybrid film. As it is well described in the literature, silica is able to act as a physical barrier to the thermal and thermo-oxidation of cotton, blocking the heat and oxygen transfer towards the

fabric. The concurrent presence of Si, P and N in the hybrid coating turns out to further hinder the formation of volatile products during the first step of cellulose degradation and, at the same time, to favour the formation of the char. This hypothesis was confirmed by the high residues found at 360, 500 and 750°C. In order to further investigate the behaviour of the hybrid coatings containing Si, P and N species, MF was used in different concentrations and combined with DPTES as an alternative of APTES. When cotton was treated with only MF (Figure 23c), the mechanism and kinetics, through which the fabric degrades, did not change in remarkable way, with the exception of the final residue at 750°C. Similar results were found when a combination of MF and DPTES was employed. In spite of a significant anticipation of the degradation that starts at lower temperatures with respect to untreated cotton (Figure 23d), these films are able to protect the cellulose from its degradation, as already observed with APTES–DPTES-based formulations; furthermore, they show the highest residues at 750°C (41, 42 and 43 vs. 8% for MF–DPTES1, MF–DPTES2, MF–DPTES3 and cotton, respectively).

**Table 12.** TGA data of neat cotton and treated fabrics in nitrogen.

Sample	T <sub>max1</sub> * [°C]	Residue at 360°C [%]	Residue at 500°C [%]	Residue at 750°C [%]
<b>CO</b>	350	49	9	8
<b>APTES</b>	369	85	29	25
<b>DPTES</b>	310	56	46	40
<b>APTES-DPTES05</b>	336	58	47	41
<b>APTES-DPTES1</b>	343	59	44	39
<b>APTES-DPTES2</b>	346	63	44	39
<b>MF30</b>	354	56	21	17
<b>MF60</b>	354	58	18	16
<b>MF90</b>	351	50	16	14
<b>MF-DPTES1</b>	323	59	47	41
<b>MF-DPTES2</b>	315	60	48	42
<b>MF-DPTES3</b>	311	60	49	43

\* from derivative curves.

In air, cotton exhibits a three step degradation process, as described by Price et al. [77,29]: (i) production of the aliphatic char and volatile products (in the range 300–400°C), (ii) conversion of some aliphatic char to an aromatic form, yielding CO and CO<sub>2</sub> as a consequence of simultaneous carbonization and char oxidation (between 400 and 800°C) and (iii) further oxidation of char (and any remaining hydrocarbon species) mainly to CO and CO<sub>2</sub> (at ca. 800°C).

**Table 13.** TGA data of untreated cotton and treated fabrics in air.

Sample	T <sub>max1</sub> * [°C]	T <sub>max2</sub> * [°C]	Residue at 360°C [%]	Residue at 500°C [%]	Residue at 750°C [%]	Residue at 1100°C in oven [%]
CO	341	467	14	2	2	<1
APTES	342	498	41	27	8	5
DPTES	306	514	53	45	23	6
APTES- DPTES05	328	-	56	49	27	10
APTES- DPTES1	333	-	57	42	22	9
APTES- DPTES2	339	-	60	45	21	12
MF30	335	500	39	23	3	<1
MF60	334	500	37	22	5	<1
MF90	334	498	31	19	4	<1
MF-DPTES1	319	-	60	43	20	9
MF-DPTES2	315	-	60	49	29	15
MF-DPTES3	310	-	60	50	33	18

\* from derivative curves.

In the systems under investigation, two decomposition peaks of cotton in air are observable in between 340 and 470°C (Figure 24a; Table 13). Figure 24a, c show TGA curves of pure cotton and fabrics treated with APTES, DPTES and MF, in



air. With the exception of a slight anticipation in the T onset for the APTES-based formulation, the first degradation peak (T<sub>max1</sub>) turns out to be affected by the presence of each single species (Table 13). On the contrary, in presence of both APTES and DPTES, regardless of the used molar ratio, the degradation profile of cotton strongly changes (Figure 24b): indeed, the char formation is favoured, whereas the second step disappears (Table 13). This behaviour can be attributed to the thermal insulation exerted by silica, which favours the char formation and thus causes the second step to disappear: indeed, the residues at 360, 500 and 750°C are higher than that of pure cotton (Table 13). Analogously to what observed for the degradation in nitrogen, these hybrid phosphorus-doped silica films are able to protect cotton from its degradation in air in a more efficient way than each single component and their action is still present over 1000°C. Indeed, in order to check the thermal stability of the treated fabrics at high temperature in air, some tests were performed treating the samples in an oven at 1100°C for 1 h: the obtained data, collected in Table 13 (last column), agree with the TGA results and further confirm an increase of the thermal stability of cotton in air probably due to the higher carbonaceous char content. This conclusion does not indicate the occurrence of a synergistic effect due to the presence of the different elements within the hybrid coating, even though it seems quite evident that the combination of these species is capable to further improve the thermo-oxidative stability of the fabric. As far as MF is concerned, its combination with DPTES shows performances comparable with APTES. An increased thermal stability of cotton in air is achieved for all the compositions under study (Figure 24d). These results are very important since cotton flame retardancy should increase as a consequence of its increased thermal stability in air (see next section).

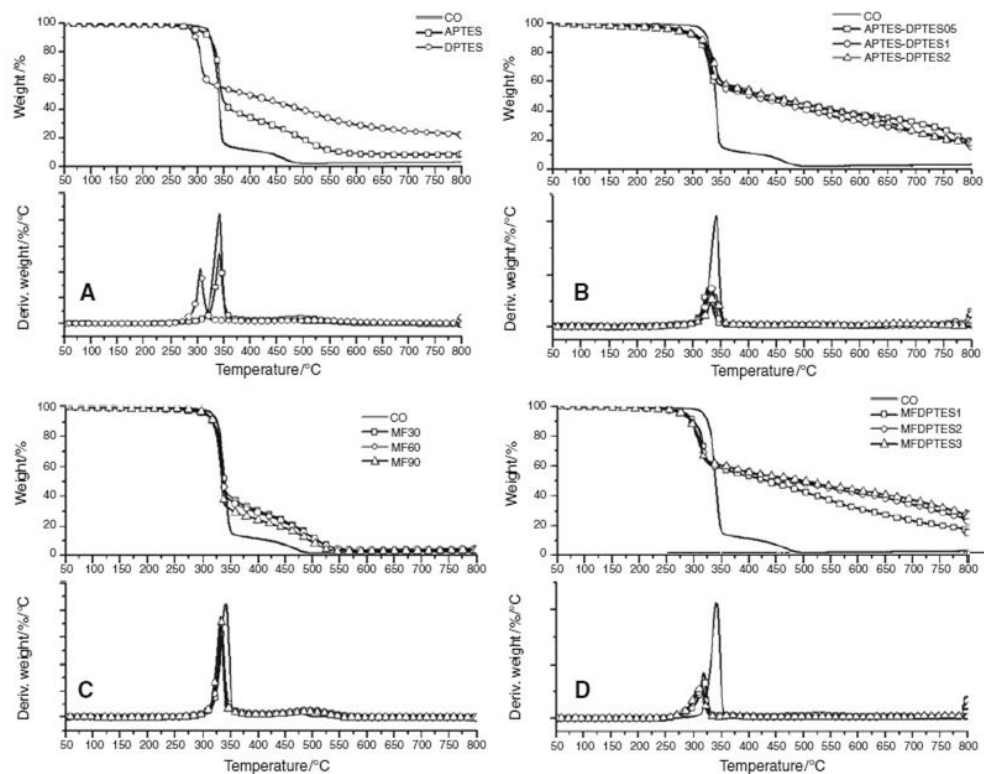


Figure 24. TG and dTG curves of untreated and treated cotton fabrics in air.

### 3.3.2.3 Burning behavior

The flame retardant properties of the treated fabrics were evaluated in terms of flammability: the prepared formulations were ignited directly by a flame (in vertical configuration) and the response of the material was measured in terms of total burning time and final residue. The flammability data, collected in Table 14, show that the formulations containing either APTES–DPTES or MF–DPTES are able to significantly reduce the total burning time and rate of cotton and to protect the treated fabric from flame. This behaviour is attributable to the protective role of the films deposited on the cotton surface that favour the char formation instead of the production of volatile species that could promote a further combustion.

The most important result is the formation of high residues at the end of the test in comparison with pure cotton or cotton separately treated with APTES, DPTES or MF, as shown in Figure 25.

**Table 14.** Collected data of pure cotton and treated fabrics by flammability tests.

Sample	Total burning time [s]	Rate [mm/s]	Residue [%]
CO	33	10	27
APTES	24	7	33
DPTES	35	6	37
APTES-DPTES05	21	10	60
APTES-DPTES1	20	9	48
APTES-DPTES2	24	8	53
MF30	150	10	27
MF60	51	12	19
MF90	28	8	20
MF-DPTES1	17	10	79
MF-DPTES2	19	8	68
MF-DPTES3	23	7	66

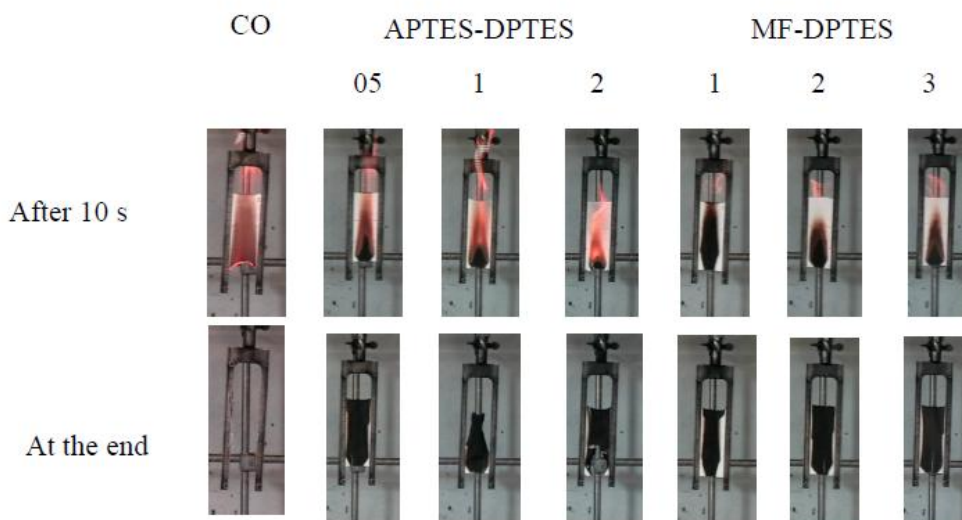


**Figure 25.** Residues of untreated and treated cotton fabrics at the end of the flammability test.

### 3.4 Conclusion

Organic-inorganic hybrid thin films based on silica sols were developed by sol-gel process for flame retardant cotton fabrics. The proposed hybrid compounds for textile finishing may be helpful for the development of new halogen free flame retardants, constituting a valid alternative to the well established commercially available treatments for cotton, based on ammonia chemistry that is required to ensure curing reactions.

The flame retardant study was developed using two main research approaches.

In the first one (part A), FT-IR studies were useful to clarify the chemical structure of the synthesized HOIMs: while in the Si xerogel the SiO<sub>2</sub> matrix showed free NH<sub>2</sub> groups, in the Si-P one the nitrogen atom of NH<sub>2</sub> moiety resulted protonated and involved in a hydrogen bonding interaction with the partially hydrolyzed diethylphosphite. Beside the ionic interaction in the Si-P-C xerogel covalent bonds linked the silica matrix and the M cross-linker. TGA and DSC analyses of the treated cotton samples revealed that these sol-gel treatments are efficient flame retardant finishings for cellulose fabrics: indeed, the fabric covered by the Si thin film was able to produce a greater amount of char as compared to the untreated fabric both in nitrogen and in air atmosphere. This effect was enhanced for the fabrics treated with Si-P and S-P-C sols due to the decrease of degradation temperature. The burning tests demonstrated that although the cotton sample treated with the pure silica sol burned, it left a residue replica of the original fabric structure. The high levels of flame retardancy induced by the hybrid Si-P and Si-P-C thin films were explained by the remarkable char production promoted by the synergism phosphorus-nitrogen and also by the high cross-linking degree resulted in the FT-IR spectra of the samples pyrolyzed at 600°C. Unfortunately the proposed finishes did not show a high washing fastness but the relevance of this poor durability depends on the fabric end use, i.e. for clothing or non-conventional applications. Further investigations are necessary to ensure the functional coatings have high long-term and wash stability.

In the second approach (part B), sol-gel processes were exploited for assessing the effects derived from the concurrent presence of two silica hybrid precursor containing nitrogen (APTES) or phosphorus (DPTES) on cotton's thermal

and fire stability, in which the organic functionality is strongly bonded by covalent bonds to the silica precursor in order to increase the laundering durability. To this aim, a specific combination of a phosphorus silica precursor (DPTES) and N donors (3-aminopropyltriethoxysilane and melamine derivative resin, respectively) was chosen and exploited for obtaining hybrid phosphorus doped silica films on the cotton surface. FT-IR analysis revealed the formation of Si-O-Si bonds of inorganic network the formation of hydrogen bonds due to the interactions of the phosphonyl groups and for the APTES-MF treated samples also the covalent bonds linked the silica matrix and the MF cross-linker. Such sol-gel treatments showed significant enhancements of the thermal and thermo-oxidative stability of cotton, thanks to the protective role of the hybrid films that were found to promote the char formation, limiting, at the same time, the production of volatile species. All samples treated showed a reduced burning rate, unfortunately they burned with a formation of a residue replica of the original structure of the fabric.

# Chapter 4

## Water Repellent Finishing

### 4.1 State of the art

Wettability of a solid surface is an important property because controlling the surface wettability is crucial in many applications. In fact, repellency is desirable for many industrial and biological fields such as antifouling paints for boats, antisticking of snow for antennas and windows, self cleaning, buildings materials and metal refining. Water-repellent coatings have important applications for automobile glass. They improve a driver's ability to see clearly and drive more safely by reduction of glare in the rain at night, since a highly hydrophobic surface brings the beading up and rolling off of raindrops. Nevertheless, probably, one of the first uses of repellent material has regarded the textiles to the protection of man against weather, for example, against rain and snow. Currently, hydrophobic properties are of high interest for textiles with water, oil or soil repellent properties, e.g. for special clothes, home textiles like carpets or upholstered furniture and some

outdoor textiles. Such textile materials are often advertised as easy-to-clean or easy-to-care. Besides the above mentioned materials used in the household the repellence of many technical textiles is also of great importance. The intervals in which filters have to be cleaned or exchanged strongly depend on its repellence properties. If a material has to be cleaned less frequently its product life time increases. At the same time, medical applications require repellent bandages or plasters for wound treatment that are less adhesive to healing wound. Repellent textiles are also used for food industry such as conveyor belts. The food products are often a mix of aqueous and oil based ingredients that must not stick to the conveyor surface in order to meet hygiene standards.

The wettability of a surface is usually expressed by contact angle (CA)  $\theta$  of a water droplet, which is given by Young's equation (Equation 7):

$$\cos \theta = \frac{(\gamma_{SV} - \gamma_{SL})}{\gamma_{LV}} \quad (\text{Equation 7})$$

Where  $\gamma_{SV}$ ,  $\gamma_{SL}$  and  $\gamma_{LV}$  refer to interfacial surface tensions with S, L, and V as solid, liquid and gaseous, respectively. Young's angle is a result of thermodynamic equilibrium of free energy at the solid-liquid-vapor interphase.

Depending on the value of the contact angle, surface properties are determined as hydrophilic (CA < 90°) or hydrophobic (CA > 90°). Two types of contact angle values are used: static and dynamic contact angles. For a flat surface, equilibrium contact angle is given by Young's equation (Equation 7). Dynamic contact angles are non-equilibrium CAs. Static CAs are obtained by sessile drop measurements, where a drop is deposited on the surface and the value is obtained by a goniometer. Dynamic contact angles are measured e.g. during the growth (advancing CA,  $\theta_a$ ) and shrinkage (receding CA,  $\theta_r$ ) of a water droplet. The difference between  $\theta_a$  and  $\theta_r$  is defined as contact angle hysteresis ( $\Delta\theta$ ).

Surfaces with water contact angle higher than 150° are called superhydrophobic or ultraphobic (with very little CA hysteresis). This very high CA is normally called apparent CA since this value does not represent the "real" CA value of the corresponding flat surfaces.

Surface energy and surface roughness are the main factors influencing water repellency. The functional group  $-CF_3$  on top of a surface has the lowest surface energy. The surface energy for a surface with a substitution of fluorine atoms is in the following order:  $-CF_3 < -CF_2H < -CF_2 < -CH_3 < -CH_2$  [78]. However, even a surface covered with regularly oriented  $-CF_3$  groups, the highest water contact angle can be only  $119^\circ$  when the surface is flat [79]. Thus, enhancement of surface roughness is an undoubted requirement of a superhydrophobic surface.

In fact, the superhydrophobic surfaces are usually covered with micro- or nanoscale asperities (rough). The behavior a water droplet on a rough surface is schematically shown in Figure 26. Water can either penetrate the asperities or suspend above the asperities. In either case, much higher contact angles are observed than that obtained for the corresponding flat surface. These two situations are named the Wenzel state (penetration) and the Cassie–Baxter state (suspension) after the corresponding theoretical models: the Wenzel [80] and Cassie–Baxter [81] (CB) models. These two models form the basic guidelines for the study of superhydrophobic surfaces [82].

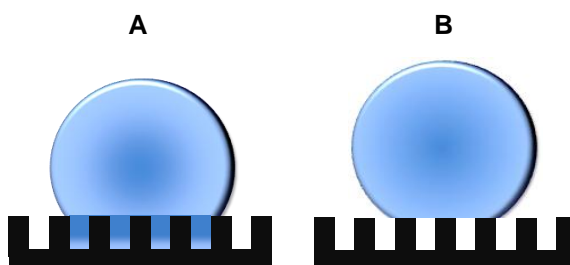


**Figure 26.** Schematic description of wetting states of a drop placed on a surface. A. Wenzel state, B. Cassie-Baxter state.

The basic assumption in Wenzel's theory is that the liquid follows the roughness of the surface as shown in Figure 26 (A). At thermodynamic equilibrium, there is a linear relationship between the apparent contact angle of the surface and the roughness factor of the given surface (Equation 8):

$$\cos \theta^w = r \cos \theta \quad (2) \quad \text{(Equation 8)}$$



where  $\theta^w$  corresponds to the apparent contact angle,  $r$  is the surface roughness defined as the ratio of actual area of liquid-solid contact to the projected area ( $r > 1$ ), and  $\theta$  is the equilibrium contact angle on flat surface (Young's angle).

Following Wenzel's model for a hydrophobic surface  $\theta^w > \theta > 90^\circ$  and for a hydrophilic surface  $\theta^w < \theta < 90^\circ$ . Roughness enhances both hydrophobicity or hydrophilicity depending on the nature of the corresponding flat surface [83]. In the Wenzel's regime, the contact angle and its hysteresis increases as the roughness factor increases for a hydrophobic surface. Nevertheless, it has been demonstrated that the contact angle increases gradually with the roughness factor until it exceeds 1.7 then contrary to the Wenzel's model the contact angle hysteresis starts to decrease [84,85]. The decrease in the contact angle hysteresis is ascribed to the switching from the Wenzel to the Cassie–Baxter state because of the increased air fraction leading to the suspension of water droplet on top of the asperities as shown in Figure 26B. The suspension of water droplet is also described as a composite state. As a result of the suspension of the water droplet on the asperities, in the Cassie–Baxter (CB) model [81], the apparent contact angle is the sum of all the contributions of the different phases as described as follow (Equation 9):

$$\cos \theta^c = f_1 \cos \theta_1 + f_2 \cos \theta_2 \quad (\text{Equation 9})$$

where  $\theta^c$  is the apparent CA,  $f_1$  and  $f_2$  are the surface fraction of phase 1 and 2, respectively;  $\theta_1$  and  $\theta_2$  CA are the of phase 1 and phase 2, respectively.

Generally, the chemical nature of fibers influence the wettability properties of materials. As well known, natural fibre materials such as cotton or other cellulosic materials are hydrophilic, whereas the most of the synthetic fibres, such as polyester, polyethylene or polypropylene are comparatively hydrophobic. Nevertheless, the polyamides and polyacrylic fibres are relatively hydrophilic. In Table 15 the surface energies of some textile materials are reported.

**Table 15.** Surface energies of selected polymers and inorganic oxides [86].

Materials	Critical surface tension [mN/m]
Polytetrafluoroethylene	18.5
Polypropylene	31.0
Polyethylene	33.0
Poly(styrene)	34
Polyvinylchloride	39
Polyester	43
Polyamide 6.6	46
Glass	47
Silica, fused	78
TiO <sub>2</sub> (anatase)	91

There are different methods for imparting water repellency to textiles:

- Mechanical incorporation of water repellent products in or on the fiber and fabric surface, in the fiber pores and in the spaces between the fibers and the yarns. An example are paraffin emulsions.
- Chemical reaction of the repellent material with the fibre surface, for example fatty acid resins, i.e. the formation of a repellent film or coating on the fibre surface like silicone and fluorocarbons products.

Up to now the repellent chemicals used in this field are paraffin repellents, stearic acid-melamine repellents, silicone water repellents and fluorocarbon-based repellents.

The paraffin repellents are emulsions containing aluminium or zirconium salts of fatty acids (Figure 27). These materials form polar-non-polar junctions increasing the finish's adhesion to polar fibre surfaces. The paraffinic portion of the repellent mixture is attracted to the hydrophobic regions, while the polar ends of the fatty acid are attracted to the metal salts at the fiber surface. Such finishing can be applied by exhaustion and padding but they increase flammability. The advantages

of paraffin repellents are low cost and their uniform waterproof effect, but the inconveniences are the lack of durability to laundering and dry cleaning and their low air and vapor permeability.

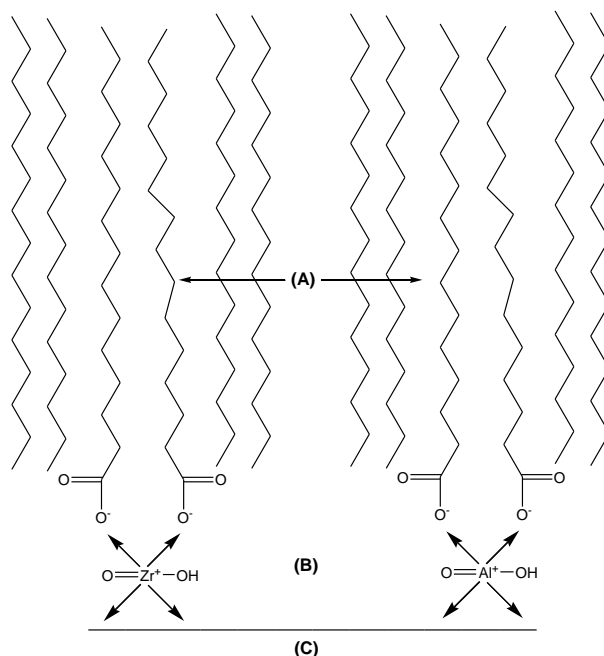


**Figure 27.** Fatty acid metal salts. A) hydrophobic interactions; B) polar interactions; C) fibre surface.

The stearic acid-melamine repellents are formed by reacting stearic acid with melamine-based resin (Figure 28). The water repellency is provided by the hydrophobic character of the stearic acid groups and the N-methylol groups react with cellulose or with each other (crosslinking) to generate permanent effects. The advantages of the use of stearic acid melamine repellents are the increase of durability to laundering and a full hand imparted to treated fabrics. The disadvantages are the tendency to exhibit finish mark-off, decreased fabric tear strength and wear resistance.

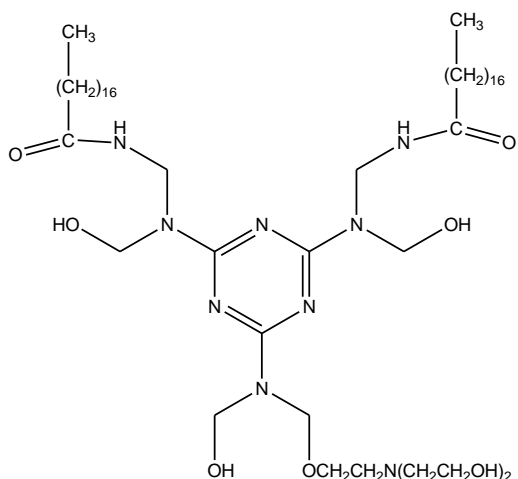


Figure 28. Stearic acid and melamine derivative.

Another kind of repellent finishes for textile application are silicones. Silicones represent important auxiliaries in the textile industry for processing and finishing. The structure of the polydimethylsiloxanes enables it to form hydrogen bonds with fibres and to have an hydrophobic outer surface. In order to gain durability silicones used for water repellent treatments, consist of three components, a silanol, a silane and a catalyst. The last one enables moderate condensation conditions and promotes the orientation of the silicone film. The oriented methyl groups generate the water repellency. The advantages of the use of silicones repellents are high degree of water repellency at relatively low add-on. To improve shape retention, they give a very soft fabric hand and good wash fastness. Unfortunately they suffer a deterioration in the fastness to light and rubbing, an increased pilling, a reduced repellency if excessive amounts are applied and mostly no oil and soil repellence. Moreover, due to their hydrophobic nature they attract hydrophobic dirt.

The largest group of textile impregnating agents are nowadays perfluorocarbon resins produced from the copolymerization of fluorine-containing esters of acrylic/methacrylic acid with fluorine free monomers or mixtures of different polymers. An important quality for optimal repellency is the orientation of the perfluoro side chains to almost crystalline structures achieved with heat treatments. This orientation can be decreased by washing but it can be regenerated

by a new heat treatment like ironing. Fluorocarbons have some advantages like a higher resistance to washing and dry cleaning, a more rapid drying of treated fabrics, a good breathability, wearer comfort and they are oil-repellent. The disadvantages of using fluorocarbons could be divided in:

- Disadvantages application: they can't be applied by exhaustion and they need for special treatment of waste water
- Disadvantages in use: high costs, graying during laundering, potentially hazardous.

Currently prefluorooctanoate (PFOA) and perfluorooctane sulfonate (PFOS), belonging to the family of perfluorinated surfactants (PFSs), are used for water and oil repellency and for other applications like cosmetics production and insecticide formulations (Figure 29).



Figure 29. Structure of PFOA and PFOS.

They have several advantages like good solubility, low volatility and stability under environmental conditions. The presence of strong C-F bonds makes them chemically and thermally very stable and resistant to hydrolysis and photolysis. Thanks to these properties, these substances have been used to create liquids with low surface tension.

**Table 16.** POFA and POFS properties.

	POFA <sup>1)</sup>	POFS <sup>2)</sup>
<b>Molecular weight, g/mol</b>	414.07	538.2
<b>Vapour pressure at 25°C, Pa</b>	4.2	3.31 x10 <sup>-4</sup>
<b>Solubility in pure water at 25°C, mg/L</b>	9500 <sup>3)</sup>	680
<b>Melting point, °C</b>	45-50	> 400
<b>Boiling point, °C</b>	189-192	not measurable
<b>pKa</b>	2-3	- 3.27 (calculated)

<sup>1)</sup> free (Prevendouros at al, 2006; Boit,1975)

<sup>2)</sup> potassium salt (OECD, 2002, Environment Agency,2004)

<sup>3)</sup> solubility of the perfluorooctanoate

The Scientific Committee on Health and Environmental Risks (SCHER) classified PFOS as dangerous substances [87]. PFOA and PFOS have been reported to enter the environment during the production and manufacturing, processing and dispersing of fluoropolymers. Also industrial waste waters have been suggested as likely sources. To emphasize this problem, the scientists have found high concentration of PFOS in some animals like eagles, seals and bears. Moreover, PFOA and PFOS seemed to be persistent in the environment, bioaccumulative and toxic. A mortality study performed on workers employed in jobs posing high exposure risk showed an increased number of deaths from bladder cancer.

In the recent years hydrophobic and water-repellent coatings on sol-gel basis have been investigated as alternative to traditional repellent finishing because of their high commercial and industrial importance [88, 89]. Modified inorganic sols seem to be very promising for applications on different types of materials, also for organic materials like textile. Further, compared to commercially available organic coating agents such inorganic, hydrophobic coatings are expected to exhibit an increased stability at higher temperature around 180°C.

The aim of this study is to prepare water repellent textiles via sol-gel technique using non-fluorinated additives both for cotton and polyester fabrics. Water-repellent films on the fabric surfaces were made using mixtures of octyltriethoxysilane (OTES) and melamine derivative resin. The water repellency is

provided by the hydrophobic character of the silica precursor while MF resin was used in order to increase the adhesion of xerogel on the fabric realizing. Three different melamine concentrations and four MF:OTES molar ratios were evaluated. Contact angle, water uptake, drop test and DuPont test were performed to investigate change in the wettability.

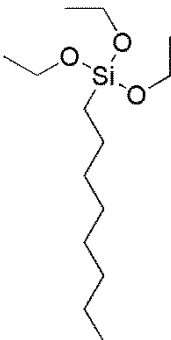
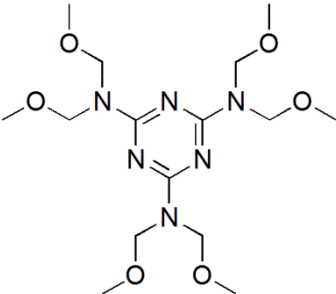
## 4.2 Experimental setup

### 4.2.1 Materials

Octyltriethoxysilane (OTES, purity grade 98%) was purchased from Sigma-Aldrich. The melamine based crosslinking agent (N,N,N',N',N'',N''-hexakis-methoxymethyl-[1,3,5] triazine-2,4,6-triamine: MF in aqueous solution, purity grade 50w/v %), commonly used in textile finishing processes, and dimethylbenzene sulphonic acid were kindly provided by Europizzi S.p.A. (Italy). The chemical structures of the used compounds are shown in Table 17. All the chemicals and reagents were directly used without any further purification.

Scoured and bleached 100% plain-weave cotton fabric (weight 237 g/m<sup>2</sup>) and 100% PET were supplied by Mascioni Spa, Cuvio (Va), Italy. The fabrics were washed in 2% non-ionic detergent at pH 7 and 40°C for 20 min, and then rinsed several times with de-ionized water, dried and put into drier for storage. The cleaned samples were conditioned under standard atmospheric pressure at 65 ± 4% relative humidity and 20 ± 2°C for at least 24 h prior to all the experiments [90].

**Table 17.** Name, code and chemical structures of the sol-gel precursors and the cross-linker.

Name	Code	Chemical formula
Octyltriethoxysilane	OTES	
N,N,N',N',N'',N''-Hexakis-methoxymethyl-[1,3,5] triazine-2,4,6-triamine	MF	

#### 4.2.2 Nanosol preparation and coating process

Silica sols were prepared mixing a octyltriethoxysilane sol and MF in a water solution using hydrochloric acid as catalyst to a final volume of 50 mL. The molar ratio of H<sub>2</sub>O:HCl was 1:0.008. The melamine based resins concentrations in the solutions were fixed at 20 g/L, 60 g/L and 100 g/L in which the MF:OTES molar ratio were 1:1, 1:2, 1:3 and 1:4, respectively. The obtained transparent sol was left under magnetic stirring for 1h, then dimethylbenzene sulphonic acid was added in the sol and stirred for 30 minutes. The fabrics (cotton or polyester, A4 size) were treated with the sols by pad-curing procedure. The fabrics were impregnated in the sols, then they were passed through a two-roll laboratory padder (Werner Mathis, Zurich, Switzerland) for three times to a finally 70% of wet pick-up. After drying (80°C for 10 minutes) the fabrics were cured at 120°C for 5 minutes and 150°C for 1 min in a oven.



The samples have been coded as a function of kind of substrate, melamine and precursor concentrations used. they are summarized in Table 18.

**Table 18.** Investigated formulations.

<b>Sample</b>	<b>MF [g/L]</b>	<b>molar ratio MF:OTES</b>
UnCotton	-	-
UnPET	-	-
OMF1	20	-
OMF2	60	-
OMF3	100	-
OSi	-	Only silica
MF1-OTES1	20	1:1
MF1-OTES2	20	1:2
MF1-OTES 3	20	1:3
MF1-OTES 4	20	1:4
MF2-OTES 1	60	1:1
MF2-OTES 2	60	1:2
MF2-OTES 3	60	1:3
MF2-OTES 4	60	1:4
MF3-OTES 1	100	1:1
MF3-OTES 2	100	1:2
MF3-OTES 3	100	1:3
MF3-OTES 4	100	1:4

## 4.3 Results

### 4.3.1 Surface characterization

Both in the cotton and in the polyester IR spectrum (Figure 30, Figure 31) it can be noticed at  $2923\text{ cm}^{-1}$  and at  $2853\text{ cm}^{-1}$  the  $\text{CH}_2$  groups and at  $2956\text{ cm}^{-1}$  the  $\text{CH}_3$  groups characteristic of alkyl chain of precursor, melamine derivative resin or the fabric. However, the signal of these band is more intense for the treated sample compare to untreated. In all treated samples the characteristic band of triazine group is situated around  $813\text{ cm}^{-1}$  and between  $1471\text{ cm}^{-1}$  and  $1546\text{ cm}^{-1}$ . Cotton samples show at  $3500\text{-}3000\text{ cm}^{-1}$  the characteristic bands of cellulose hydrogen bonded O-H stretching vibrations [91] while for the polyester samples a very intensive band was observed at  $1728\text{ cm}^{-1}$  due to stretching vibrations of C=O group [92]. After 5 cycles wash, the intensity of the bands ascribe to the silica precursor decrease in particular for treated PET samples showing a not perfectly adhesion of the film on the fabric surface. It could be due to less reactive functional groups on the surface of polyester compared to the cotton surface.

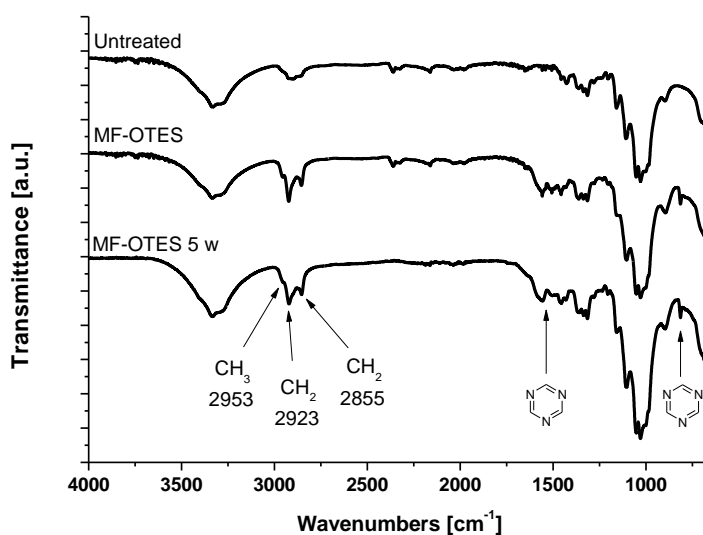
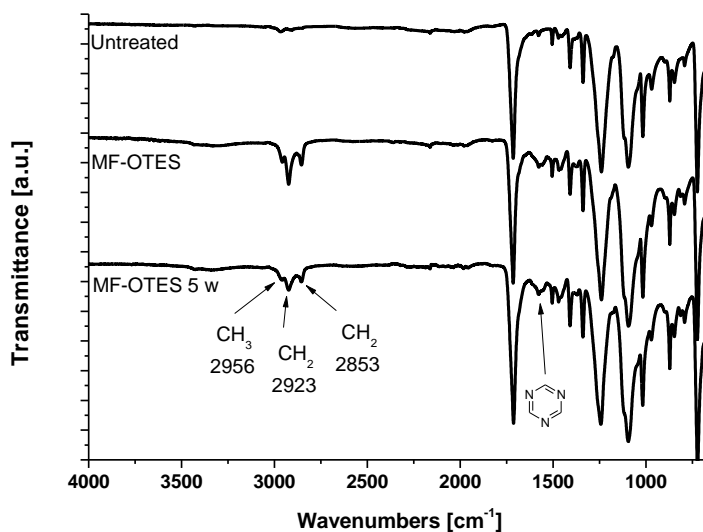


Figure 30. IR spectra of cotton fabric before and after washing cycles.



**Figure 31.** IR spectra of PET untreated, treated and treated after washing cycles.

### 4.3.2 Water-repellent properties

The nature of polymer, fiber type, twisting, fabric construction, finishing agents or dyeing, as well as the deposition of HOIMs films onto fabric surface can influence the repellent properties of textiles. For these reasons different tests were performed to have a better evaluation and comprehension of the water-repellent properties of textiles.

In Table 19, contact angle (CA) measurements of the untreated and treated samples are reported don't distinguish among the molar ratio. Untreated cotton sample is hydrophilic and the fabric is immediately wetted but, when it was treated with MF-OTES sols prepared with 60 g/L or 100 g/L of resin the water CA values were observed between 120°-130°. At the same time all PET samples treated with MF-OTES sols have shown an increase of water CA to values higher than 130° indicating that treatments with MF-silica sols increase the water repellency also for polyester. Comparing these results with those obtained on the samples treated with only resin (OMF) and precursor (OSi), a synergistic effect between the cross-linker

and the silica precursor is observed when MF and OTES are used together. In fact, the contact angle of the mixture (MF-OTES) are higher than respectively reference samples (OMF and OSi). In particular, the contact angle are not measurable for the cotton fabrics treated with only silica precursor or only 60 g/L melamine derivative because the fabrics are still hydrophilic. Whereas, CA of the mixture is about 120-130°.

**Table 19.** Contact angle (CA) measurement.

	MF [g/L]	Molar ratio MF:Si	Contact angle	
			Cotton	PET
MF1	20	1:1-4	---	131-150
OMF1	20	---	---	115
MF2	60	1:1-4	120-130	135-150
OMF2	60	---	---	120
MF3	100	1:1-4	120-130	138-140
OMF3	100	---	120	125
OSi	---	---	80	130
UnPET	---	---	---	50
UnCotton	---	---	---	---

In Figure 32 are reported the contact angle hysteresis values ( $h$ ) of treated cotton samples. On the x axis there are the molar ratios MF:Si (also called MF:OTES) = 1:1, 1:2, 1:3 and 1:4 while on the y axis are reported the hysteresis values. The repellency of the samples increases with the concentration of resin used and it seems to be influenced from the molar ratio MF:Si. Similar trends are observed for polyester samples in which the less hysteresis ( $h=10^\circ$ ) is observed for the sol prepared with 100 g/L of melamine derivative (Figure 33).

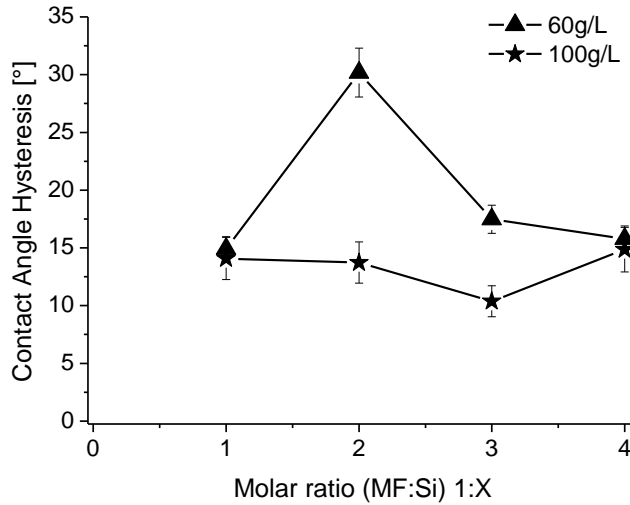


Figure 32. Hysteresis test results of cotton samples treated at different molar ratio (MF:Si).

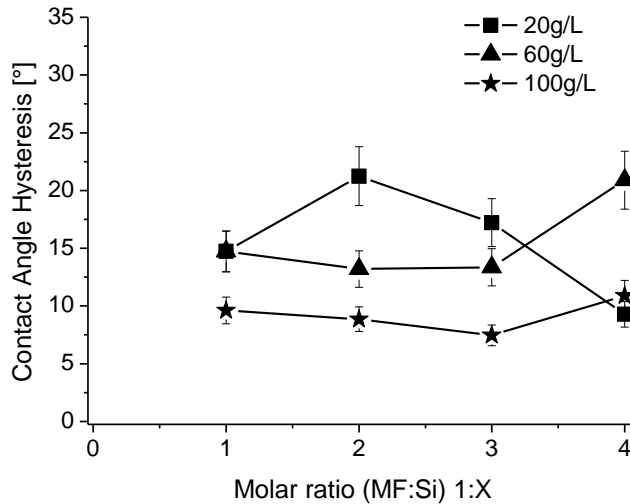
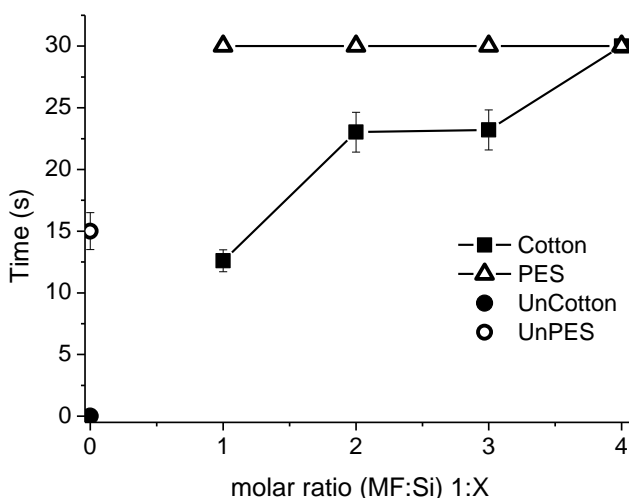


Figure 33. Hysteresis test results of cotton samples treated at different molar ratio (MF:Si).

In Figure 34, Figure 35 and Figure 36 the drop test results on polyester and cotton fabrics are reported. The test measures the time required to absorb a drop of water. On the x axis there are the molar ratio MF:Si = 1:1, 1:2, 1:3 and 1:4 while on the y axis the absorption times (seconds) are reported.

The untreated cotton is wetted immediately after the deposition of water drop, confirming a good hydrophilic behavior of the cellulosic fibers. At the same time, untreated polyester shows a certain repellency, the drop is absorbed within 15 s. The deposition of MF-Si film improves the repellency of textile, in fact higher repellency was observed for all treated samples compared to untreated fabrics. Water drop is not absorbed during the acquisition time (30 s) for the treated PET (MF-OTES) realized using 20 g/L, 60 g/L and 100 g/L of MF concentrations, while the same time is observed only for 60 g/L and 100 g/L of MF for the treated cotton fabrics. In the previous samples the results are not influenced by the kind of substrates or molar ratio MF:Si, while for the MF1-OTES sols (MF = 20g/L) applied on cotton fabrics, the repellency is strongly influenced from the molar ratio and it increases going from 1:1 to 1:4 molar ratio. The best repellency for the samples using 20 g/L of MF was measured for 1:4 molar ratio (MF:Si).

In Figure 37 the results of only MF and only precursor are reported. It's interesting to note that the all PET samples treated with the only silica sol or only MF show the same repellent behavior than mixture MF:Si. The test doesn't seem to be able to distinguish between the several samples. For this reasons other test, following reported, were performed. Nevertheless, the synergistic effect of mixture MF:Si is confirmed on treated cotton samples, except for MF3-OTES in which the same water repellency can be obtained using 100g/L of resin.



**Figure 34.** Drop test results of cotton and PET samples treated at different molar ratio (MF:Si) for 20g/L MF.

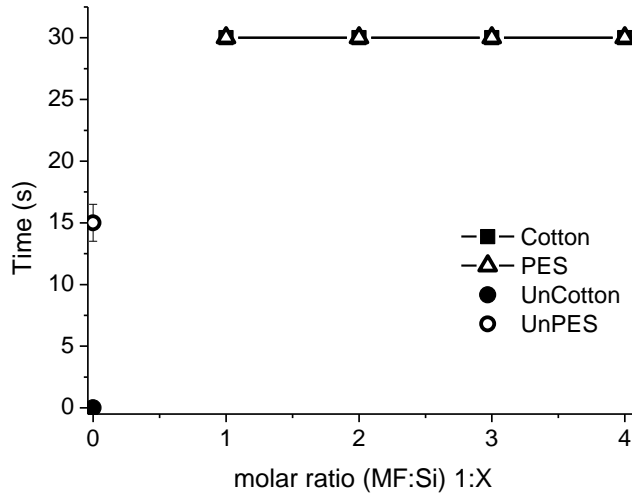


Figure 35. Drop test results of cotton and PET samples treated at different molar ratio (MF:Si) for 60g/L MF.

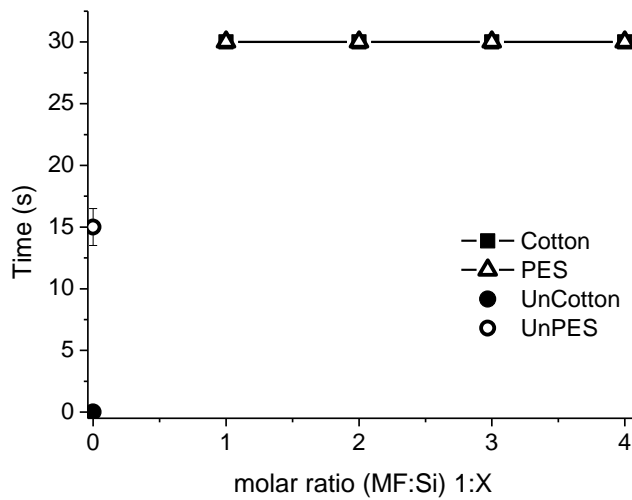
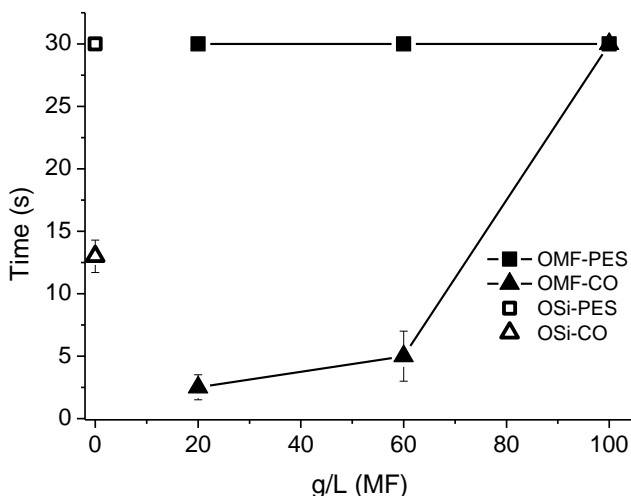


Figure 36. Drop test results of cotton and PET samples treated at different molar ratio (MF:Si) for 100g/L MF.



**Figure 37.** Drop test results of cotton and PET samples treated with only melamine derivative (OMF: 20 g/L – 60 g/L - 100 g/L) and only silica precursor (OSi).

In Figure 38, Figure 39 the DuPont test results for polyester and cotton fabrics treated by MF-OTES are reported. On the x axis there are the molar ratio MF:Si = 1:1, 1:2, 1:3 and 1:4 while on the y axis there is grade of repellency from 0 to 8. DuPont test method can be used to determine the effectiveness of a protective finish that is capable imparting a low energy surface on all types of fabrics, by evaluating the wettability of the sample to a selected series of water/alcohol solutions with different surface tensions. In Figure 38 the results for PET fabrics are reported. The untreated sample shows a lower repellency than all treated fabrics. The best results are both the 60 g/L and 100 g/L MF concentration samples independently from the molar ratio MF:Silica used.

The MF1-OTES treated cotton samples (20 g/L MF) sols have shown the same wettability as the untreated cotton fabric (Figure 39). Practically, the deposition of the different films with different molar ratio MF:Si does not change the repellency of the substrate. Nevertheless, increasing the MF concentration it is possible to reduce the wettability. The repellency of the film can be increased using low or higher share of silane. The best result has been obtained for 100 g/L of MF with molar ratio 1:4.



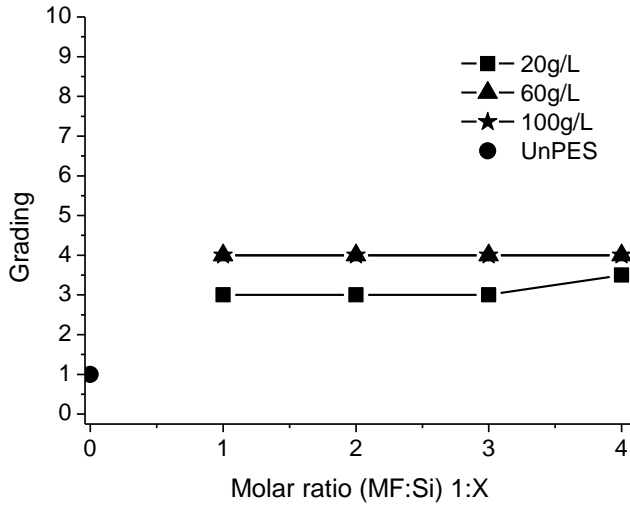


Figure 38. DuPont test results of PET samples treated at different molar ratio (MF:Si) compared to untreated PET.

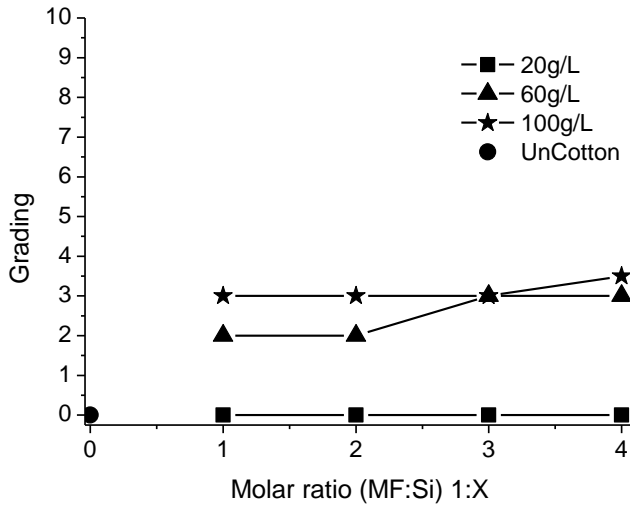
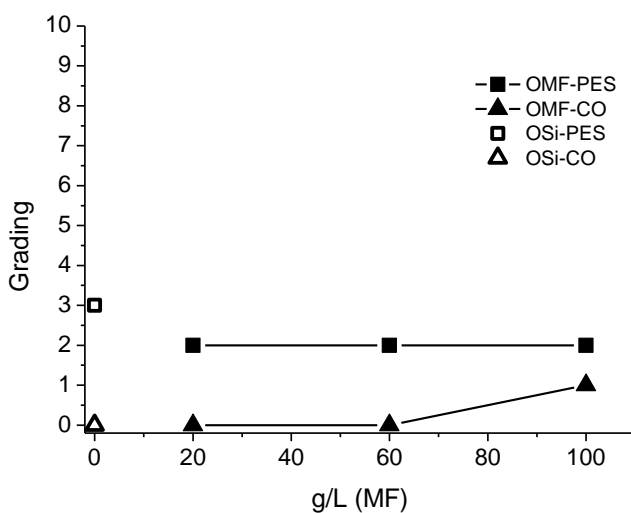


Figure 39. DuPont test results of Cotton samples treated at different molar ratio (MF:Si) compared to untreated cotton.

The repellency obtained for the fabrics treated by OMF and OSi solution is lower than mixture results (MF-Si), excepted for the MF1-OTES (1-3) films realized on PET in which similar repellency can be obtained with the application of only silica precursor (Figure 40). In all other samples (PET and cotton) the synergistic effect of the mixture on the repellency properties is observed.



**Figure 40.** DuPont test results of cotton and PET samples treated with only melamine derivative (OMF: 20 g/L – 60 g/L - 100 g/L) and only silica precursor (OSi).

In the Figure 41 and Figure 42 the water uptake results for polyester and cotton fabrics treated by MF-OTES are reported. On the x axis there are the molar ratios MF:Si = 1:1, 1:2, 1:3 and 1:4 while on the y axis there is percentage of weight variation.

The untreated samples both cotton and PET show a similar wetting behavior, their weight increased about 225% after the their immersion in the solution. Nevertheless, the water uptake of the fabric depends from the nature of the substrate. In fact, PES surface is only wetting due to surface energy and capillary structure, while for cotton, water there is also absorption by the fibre itself. The deposition of repellent HOIMs improves the repellency of all samples compared to reference samples. In particular the increase of weight is less than 10% for the treated PET samples. The results are similar for all molar ratios and the MF

concentrations except for 20 g/L of resin and molar ratio equal 1:1. In particular, the best results are observed for the sample treated by MF3-OTES (100 g/L of resin) solution yield have values around 1%.

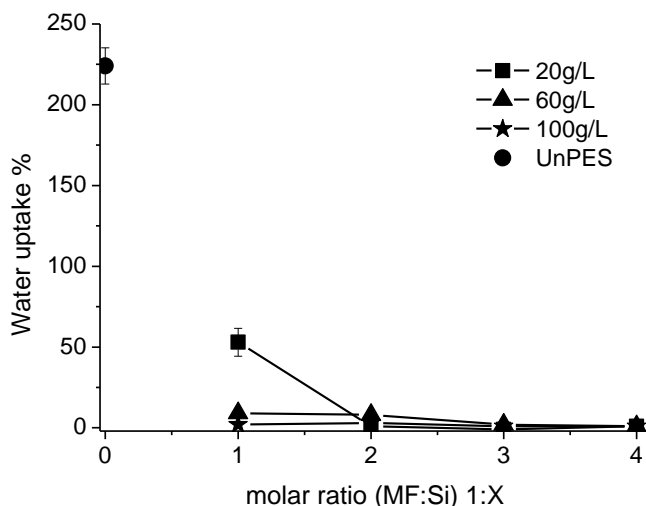


**Figure 41.** Water uptake test results of PET samples treated at different molar ratio (MF:Si) compared to untreated PET.

Cotton repellency is strongly influenced, as it has already been observed with the previous repellency methods, from the concentration of MF and MF:OTES molar ratio. Similar trends are observed for all samples but the repellency improves increasing the MF and the precursor concentrations. The best results is observed for molar ratio 1:4 for 100 g/L of MF used.

In Figure 43 the OMF and OSi results are reported. For PES treated samples good water repellent properties can be obtained using OSi but the same performance are not reached applying only MF. However, the best results is obtained using at the same time MF and silica precursor. The lowest water uptake measured for cotton fabrics treated with pure MF or silica precursor is about 100%. It is much higher than the best result obtained with the mixture.

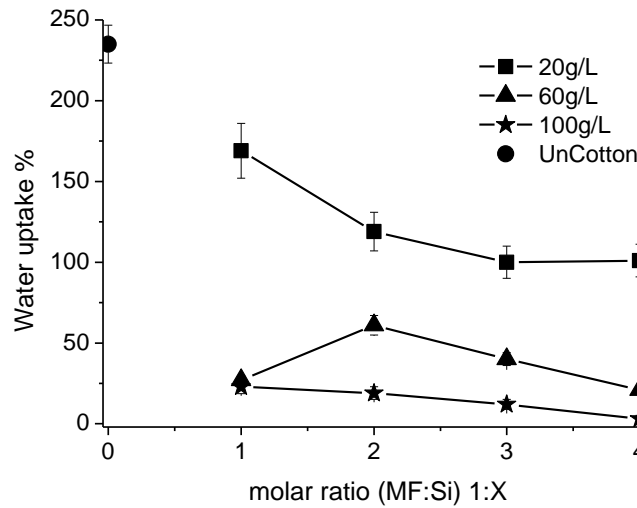


**Figure 42.** Water uptake test results of cotton samples treated at different molar ratio (MF:Si) compared to untreated cotton.

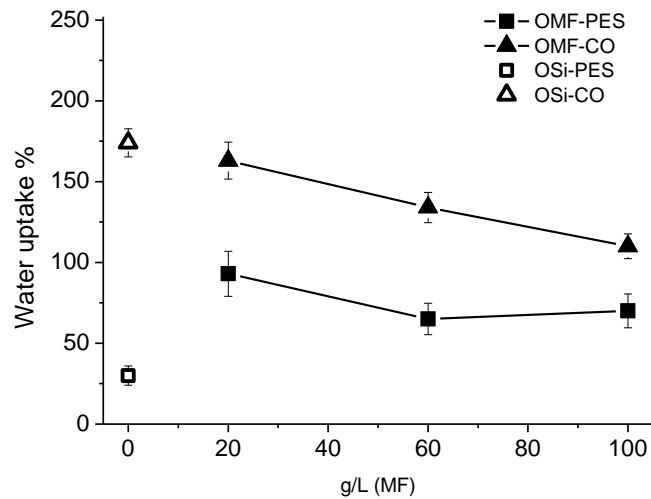


**Figure 43.** Water uptake test results of cotton and PET samples treated with only melamine derivative (OMF: 20 g/L – 60 g/L - 100 g/L) and only silica precursor (OSi).

Good repellency are obtained for the most of samples prepared. In particular, an interesting synergistic effect between silica precursor and melamine based crosslinking was observed in almost all tests. The importance of this effect on the repellency depends from several parameters (substrate, molar ratio, etc.). A possible mechanism hypothesis, regarding the increase of repellency when melamine derivative resin and silica precursor are used, it could be explained with a better orientation of alkylic chain of the precursor that is realized when MF crosslinker is used. The oriented alkyl groups generate the water repellency. In Figure 44 are shown a schematic representation of possible interactions between the hydrolized precursor, MF resin and substrate. In Figure 45, 3D structures of possible interaction between MF and OTES are reported. In particular are shown the orientation of the alkyl chain.

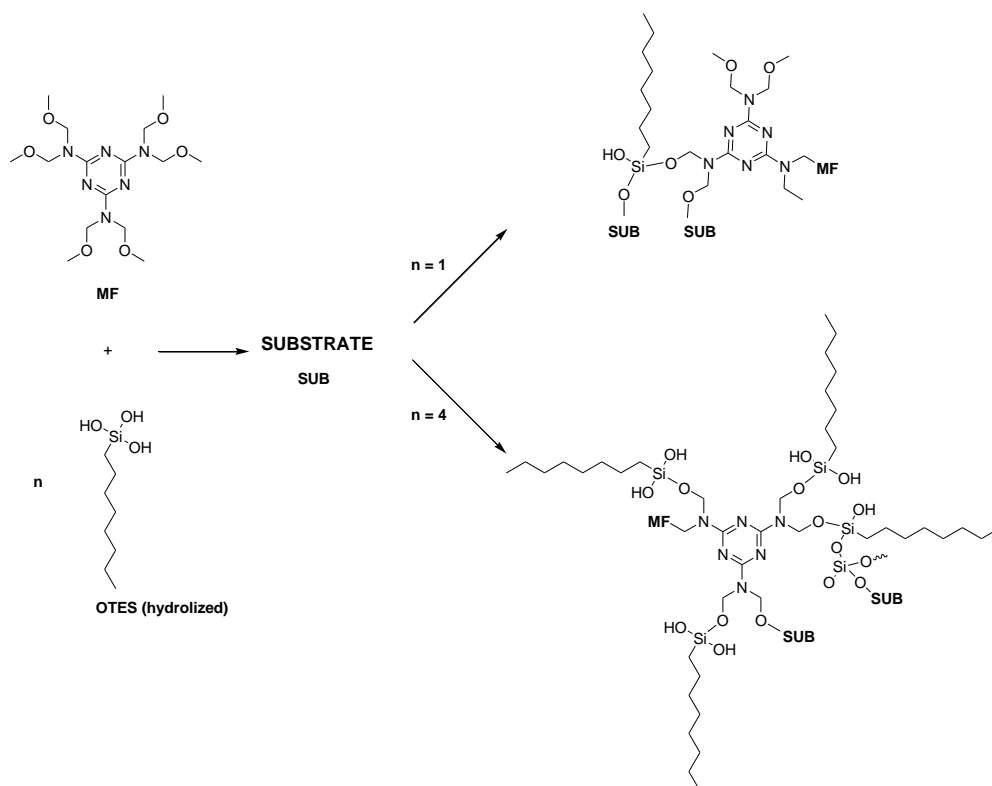


**Figure 44.** Schematic representation of possible interaction of MF and OTES on the fabric surface. Molar ratio (MF:OTES: 1:1 and 1:4).

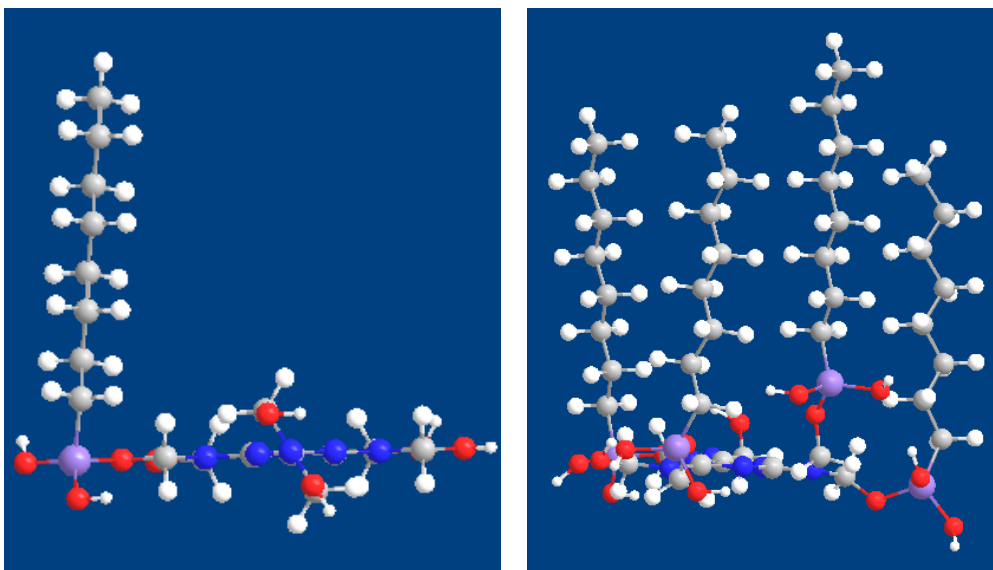


Figure 45. 3D structures of possible interaction between MF and OTES. Orientation alkyl chain.

#### 4. 4 Conclusion

Water repellent hybrid films were realized onto cotton and PET fabrics. The proposed hybrid compounds for textile finishing may be helpful for the development of new fluorocarbon free water repellents, that could constitute a possible alternative to the well established commercially available treatments for cotton and polyester.

The sol synthesis was performed at room temperature by sol-gel process using octyltriethoxysilane as precursor and melamine derivative resin as cross-linker. The investigations were performed as function of three melamine concentrations and four molar ratio MF:precursor (1:1-4). FT-IR analysis of treated samples have showed an increase of the intensity bands due to  $\text{CH}_3$  bonds compared to untreated samples.  $\text{CH}_3$  bonds are observable both in the precursor (alkyl chain) and in the crosslinker. This band is also confirmed after 5 washing cycles. Nevertheless, an important decrease of band intensity of the network is observed for the PET samples after laundering.

It was presented that the hydrophobic properties of coated textiles are significantly determined by melamine derivative concentration and molar ratio between melamine derivative and silane. An interesting synergic effect is obtained

when melamine derivative resin and silica precursor are used in mixture. In fact higher repellency is obtained for the samples treated by the mixture compared to the application of only resin or silica precursor on the fabric. Increasing both the melamine concentration and molar ratio a good hydrophobic properties can be performed and the best results are obtained for 100 g/L of resin and 1:4 molar ratio (MF:precursor) for cotton samples. Nevertheless, good water repellency has already been obtained using 60 g/L of resin both for cotton and polyester. In particular, the best hydrophobic behavior is observed for PET samples in which advanced contact angle was measured between 130°- 150° and hysteresis in the range of 10°- 20°.

# Chapter 5

## Self Cleaning Finishing

### 5.1 State of the art

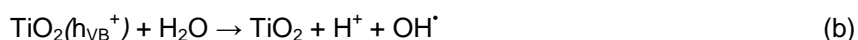
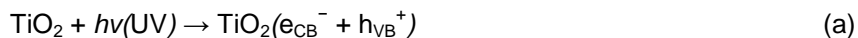
Textile materials are commonly present in our life. Everyone wears clothes of natural, artificial or man-made fibers as well as apartments are usually equipped with carpets or curtains. All these materials can easily become dirty during the use and, consequently, have to be cleaned.

The maintenance process is usually energy-consuming [93] and requires a lot of water and surfactant. Moreover, they cannot be considered environmental friendly because they cause water pollution and eutrophication phenomena [94]. Considering the number of worldwide user and the millions of meters of textile product every years, It can easily understand the cost saving (environmental, energy, money) due to the use of textiles easy to clean and/or self-cleaning. Basically two types of self-cleaning surfaces are distinguished in literature – photoactive or photocatalytic surfaces [95], based for example on photocatalytically



active TiO<sub>2</sub> and surfaces, often named Lotus surfaces [96]. The combination of both types in a single coating is also described [97]. In particular, the research topic of this PhD thesis on the self cleaning surfaces has regarded the development of photoactive TiO<sub>2</sub> sols and films.

Crystalline TiO<sub>2</sub> has received much attention in the recent years due to its interesting properties as photocatalyst [98]. Moreover, inexpensiveness, excellent chemical stability and nontoxicity of TiO<sub>2</sub> make it attractive for practical applications. In fact, TiO<sub>2</sub> is widely employed for several applications in many industrial and research areas as water and air purification [99,100,101], sterilization/disinfection [102], antifogging [103] and superhydrophilic effect [104]. Recently, it is also studied for innovative applications regarding the conversion of solar energy into electricity by DSSC (Dye-Sensitized Solar Cell) [105] and hydrogen production by water photosplitting [106]. TiO<sub>2</sub> can be used as textile finishes to impart some specific effects (UV-absorber, self cleaning, antistatic, antimicrobial and flame retardant) to the fabric [29]. In the photocatalytic process the TiO<sub>2</sub> is activated when it is irradiated with light of an energy greater than its band gap energy. The photocatalytic breakdown reaction proceeds via intermediate steps ending in the mineralization of the organic to water, CO<sub>2</sub> and mineral acids. The initial step is the electron–hole pair formation, followed by their separation. Photogenerated hole (h<sub>VB</sub><sup>+</sup>) can oxidize directly the organic molecule or react with water to produce OH• radicals. Whereas, the electron in the conduction band (e<sub>CB</sub><sup>-</sup>) can reduce organic molecules or forms superoxide radical anion O<sub>2</sub><sup>•-</sup>. The lifetimes of the electron and the hole influence the redox reaction. The most important reactions causing the degradation of organic molecules (e.i. dyes) on the fabric surface are the following [107]:



Thus, it evidences that reducing the band gap of  $\text{TiO}_2$  can enhance its photocatalytic performance through more efficient utilization of lower energy photons. The band gap of titania depends on its crystal phase, particle size and crystallinity.  $\text{TiO}_2$  has three distinct crystalline structures: rutile, anatase, and brookite. Among the common crystalline forms of titania, rutile ( $E_g = 3.0$  eV or  $\lambda_{bg}$  413 nm) anatase (3.2 eV or  $\lambda_{bg}$  387 nm), are generally recognized to be the most active phases as opposed to the brookite form [108]. So,  $\text{TiO}_2$  due to its wide band gap (3.0-3.2 eV) is able to absorb only in the UV range. For this reasons, most of studies involved ultraviolet (UV) photons as the major exciting light sources. Considering that the UV light range is about 5% in the solar irradiation [109], intuitively, it is desirable to enhance the photocatalytic performance of  $\text{TiO}_2$  to utilize photons from the near-visible to visible region. Recently, a considerable number of studies were devoted to the development of efficient visible light sensitive photocatalysts and to photocatalytic properties improvement [110-116]. Nitrogen [110,111], sulfur [112,113], carbon [114,115], fluorine [116] and transition metal selective doping as well as the particle size of photocatalyst have been investigated in order to achive a red shift of the absorbance. Narrowing of the band gap of  $\text{TiO}_2$  upon doping was often considered responsible for the enhanced visible light activity of these materials.

The most commonly used techniques for deposition of  $\text{TiO}_2$  film on various substrates are: sol-gel, reactive sputtering, pulsed laser deposition, evaporation, chemical vapor deposition and spray pyrolysis [117,118]. Amongst the above mentioned methods, the sol-gel technique is widely used for its low processing cost, simplicity and ability to produce thin and uniform films on wide surface substrates. Sol-gel application is compatible with textile processes because it doesn't require new equipments for its application. In fact, pad or exhaust processes can still be considered the most suitable [29].

The use of stable colloidal solutions are preferred because they can permit an uniform and homogeneous deposition of the  $\text{TiO}_2$  and can reduce problems during the application. Unfortunately, the hydrolysis and the condensation reaction of titania take place quickly. These reactions cause agglomerate/aggregate phenomena that can lead either to a gelling or precipitation of solution. For these reasons, stable  $\text{TiO}_2$  sols are usually obtained preparing  $\text{TiO}_2$  in alcohol or mixture of alcohol/water [119]. Alcohol is a suitable solvent to improve stability of metal oxide

sols. Under these conditions, stable titania sols can be achieved with highly diluted sols, while higher TiO<sub>2</sub> concentrations will lead to agglomeration and precipitation. Stable TiO<sub>2</sub> sols can also be obtained in pure water but only at very low pH values or using acetyl acetone [120]. However, the use of alcohol as solvent and low pH-value can give rise to a lot of problems for storage and application, e.g., inflammable and corrosive substances could be dangerous, while the acetyl acetone is suspected to be teratogenic.

The first aim of this study (Part A) is to investigate possibilities for the preparation of stable aqueous titania sols without the addition of alcohols, glycol or acetyl acetone at suitable pH for the industrial application. Synthesized sols have been tested to study the influence of different TiO<sub>2</sub> precursor concentrations, of synthesis temperature, of acetate buffer and using chitosan as stabilizer. Chitosan ( $\beta$ -(1,4)-*N*-acetyl-Dglucosamine) is a biodegradable polymer obtained by deacetylation of chitin [121]. It is the second most abundant biopolymer on earth and found mainly in invertebrates, insects, crustaceans, algae, fungi and yeast [122,123]. Recent investigations confirm the suitability of chitin and its derivatives in chemistry, biotechnology, medicine, veterinary, dentistry, agriculture, food processing, environmental protection, and textile production. On the biomedical field, chitosan and its derivatives have a great number of applications ranging from wound dressings, contact lenses and drug delivery systems [122]. It is used to control release from different delivery systems: microparticules, liposomes, vesicles, gels, suspensions [122,124,125]. Chitosan is also used in cosmetics, food and nutrition and textile industry [122]. Moreover, it is a biodegradable cationic biopolymer and could assist in the reduction of pollutants in residual waters by adsorption and chelation of heavy metal ions, and, by an efficient electrostatic action, can also act in the coagulation of colloidal particles [126,127]. This characteristic was evaluated to increase the stability of TiO<sub>2</sub> sol as possible retardant of hydrolysis/condensation reactions. The stability of the sols were evaluated using different analysis: FT-IR, turbidity, dynamic light scattering and viscosity.

In the second research topic (Part B), self-cleaning TiO<sub>2</sub> films were realized on cotton fabric starting from several TiO<sub>2</sub> sols prepared in a mixture of alcohol/water in which chitosan was not used. The aims of this study are: (a) to develop a simple synthesis of TiO<sub>2</sub> at low temperature by sol-gel technique to finish cotton fabrics, (b) to investigate the photocatalytic properties by the dyestuff

degradation directly on solid phase, (c) to realize the optical characterization of the film realized on finished textile fabrics, (d) to establish the correlation between the photo bleaching of the treated textiles and the catalyst, the precursor concentration and the presence of polyethylene glycol (PEG) as a dopant, (e) to investigate the change in the mechanical properties under daylight exposure. Activity research is to increase efficiency of the photocatalytic process changing the acid used as catalyst with or without dopant (PEG). For these reasons sols were realized at two different precursor concentrations. As well described previously, the enhancement in the efficiency of the photocatalytic process can be imparted modifying particle size, crystal microstructure and morphology of TiO<sub>2</sub> nanoparticle. It can be realized by annealing or with solvothermal treatment [128,129]. Regarding calcinations, it cannot be performed to improve the amorphous-anatase transformation, otherwise it would destroy the textile polymer while solvothermal treatment has not been used because it required a lot of energy. In fact, the textile treated or TiO<sub>2</sub> powder has to be treated in boiling water for long, mostly using autoclave. For these reasons the application was performed at low temperature at 120°C for 5 min.

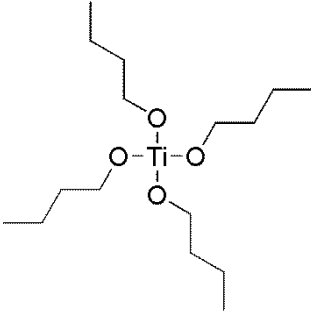
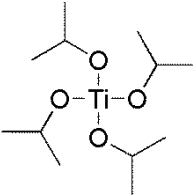
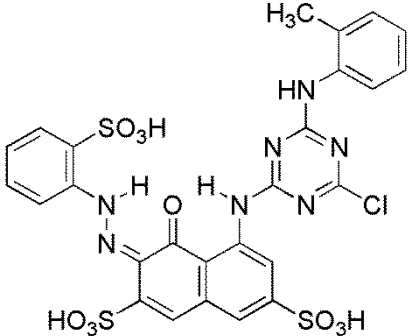
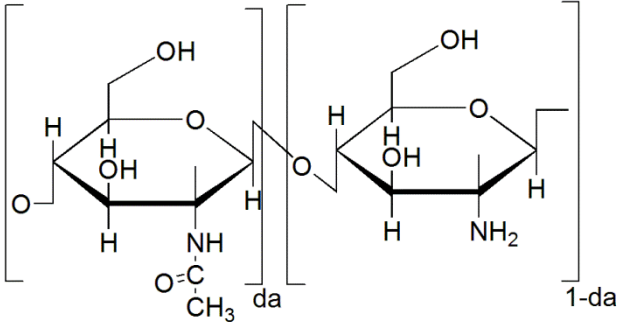
## 5.2 Experimental setup

### 5.2.1 Materials

#### *- Part A: Study of sol stability*

Titanium (IV) butoxide (Ti(OCH<sub>2</sub>CH<sub>2</sub>CH<sub>2</sub>CH<sub>3</sub>)<sub>4</sub> or TBT; 97%), hydrochloric acid (HCl; 37%), acetic acid (CH<sub>3</sub>COOH; glacial, ≥ 99.85%), ethanol (C<sub>2</sub>H<sub>5</sub>OH, absolute, ≥ 99.8%), sodium acetate (CH<sub>3</sub>COONa; anhydrous, ≥ 99.00%), ammonia solution (NH<sub>4</sub>OH; 30%) and sodium chloride (NaCl;XXX) were purchased from (Sigma-Aldrich/Merck), while chitosan 100 (deacetylation > 95% (1-da), Mw 95 kDa) was provided from ChiPro GmbH, Germany. All chemicals were used as received. The chemical structures of the compounds used are shown in Table 20.

**Table 20.** Name, code and chemical structures of the precursors, dyestuff and chitosan.

Name	Code	Chemical formula
Titanium (IV) butoxide	TBT	
Titanium tetraisopropoxide	TTIP	
Procion red PX4B	PR	
Chitosan	CH	

Where **da** is average degree of acetylation

**- Part B: Optical and photo activity characterization**

Titanium tetraisopropoxide ( $\text{Ti}(\text{OCH}(\text{CH}_3)_2)_4$  or TTIP; 97%), hydrochloric acid (HCl; 37%), nitric acid ( $\text{HNO}_3$ ; 69%), acetic acid ( $\text{CH}_3\text{COOH}$ ; glacial,  $\geq 99.85\%$ ), ethanol ( $\text{C}_2\text{H}_5\text{OH}$ , absolute,  $\geq 99.8\%$ ) and PEG 1000 were purchased from (Sigma-Aldrich/Merck). The procion red PX4B (PR) dyestuff used for the evaluation of the photocatalytic activity was provided by Dystar (Italy). All chemicals and the dyestuff were used as received. The fabric was a 100% cotton of basis weight  $237 \text{ gr/m}^2$ , previously scoured and bleached. The chemical structures of the used compounds are shown in Table 20.

**5.2.2 Nanosol preparation and coating process**

A series of sols were synthesized to evaluate the effect of different (i) solvent, precursor (ii) sol-gel route, (iii) catalysts, (iv) pH values and (v) stabilizer/dopant (chitosan/PEG) both on the sol stability and the photo-activity properties of the resulting material.

**- Part A: Study of sol stability**

$\text{TiO}_2$  sols was realized in aqueous solution without adding any alcohol. The sols were prepared in two different main approaches, in the preliminary test called “single-step” the precursor was added at least in the water solution at the appropriate condition. In the “two-step”, the titania precursor was mixed with 100% acetic acid either in presence of chitosan or not and, after in a second step, the sols were neutralized to reach the suitable pH adding alkaline solution.

- Method 1: single-step; pure  $\text{TiO}_2$  sol. Preliminary test.

100 mL of pure  $\text{TiO}_2$  sol was prepared adding 1 mL of titanium butoxide in an acid solution. The acid solution was prepared with an amount of an acid suitable to adjust the desired pH values. Either hydrochloric or acetic acid were used as catalyst in the pH values between  $\text{pH} = 1$  and  $\text{pH} = 4$ . The resulting solution was stirred at room temperature for 1 hour and 45 min. The procedures used to prepare the sol by single-step method are reported in the Figure 46.

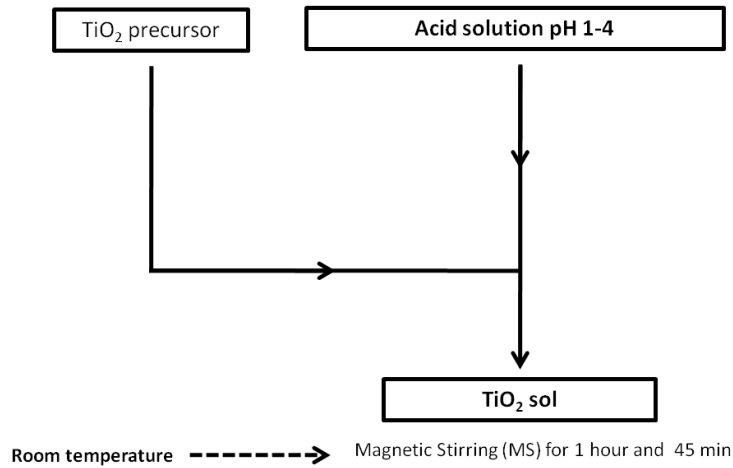


**Figure 46.** Single-step process; pure  $\text{TiO}_2$  sol. Titania precursor was dissolved in an acidic solution of a given pH-value. MS and US are magnetic stirring and ultrasonic treatment.

- Method 2: single-step; Chitosan- $\text{TiO}_2$ . Preliminary test.

The Chitosan- $\text{TiO}_2$  sol was synthesized as variation of method 1. Chitosan (0.25%<sub>wt</sub>) was dissolved in the acid solution at the same pH conditions used for method 1 before the addition of  $\text{TiO}_2$  precursor. The procedures used to prepare the sol are illustrated in the Figure 47.

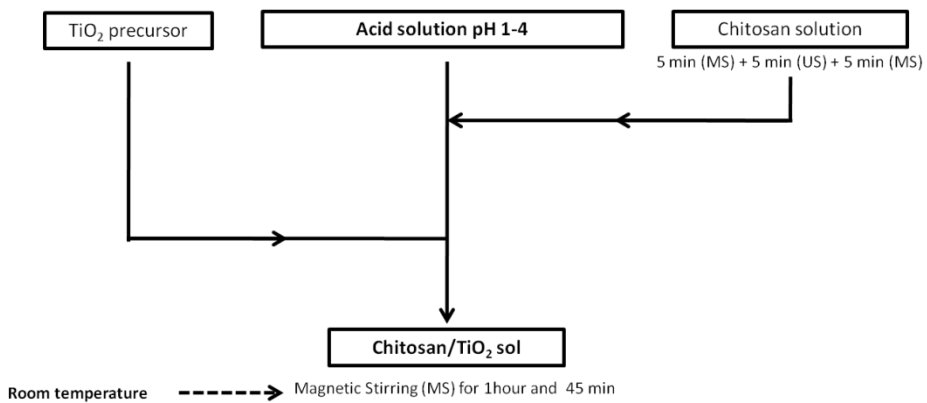


**Figure 47.** Single-step process; Chitosan-  $\text{TiO}_2$  . Titania precursor was dissolved in an acidic solution of a given pH-value contain a certain amount of chitosan. MS and US are magnetic stirring and ultrasonic treatment.

- Method 3: Two-step; pure  $\text{TiO}_2$  sol.

100 mL of pure  $\text{TiO}_2$  sol in acetate buffer was prepared mixing two different solutions called  $\text{TiO}_2$  acid sol (A) and neutralizing solution (B), respectively.  $\text{TiO}_2$  acid sol (A): 1 mL of titanium butoxide precursor was dissolved in a flask containing glacial acetic acid (3 mL) under vigorous magnetic stirring. The solution was stirred for 15 minutes and, then, was sonicated for 5 minutes. The solution prepared showed a light yellow color. Solution B was obtained adding 3 mL of sodium acetate (2 M) to 94 mL of distilled water. The final sol was obtained adding drop by drop the solution B into solution A within 10 minutes. The sol resulting was stirred vigorously for 1 h and 30 minutes before characterization. This way, the titania precursor is allowed to react with acetic acid first before hydrolysis is initiated. Moreover, the pH values of the sol is slowly shifted from the starting acid pH value to  $\text{pH} = 4$ .

Several sols were prepared as variation of method 3 to investigate the influence of buffer and  $\text{TiO}_2$  concentration:

- Acetate buffer concentration: 2% (1 mL  $\text{CH}_3\text{COOH}$ , 1 mL  $\text{CH}_3\text{COONa}$ ), 6% (3 mL, 3 mL), 18% (9 mL, 9 mL).
- $\text{TiO}_2$  concentration: 0.25%<sub>v/v</sub> - 0.5%<sub>v/v</sub> - 1.5%<sub>v/v</sub> (for 6% acetate buffer).  
0.5%<sub>v/v</sub> - 1.5%<sub>v/v</sub> - 3%<sub>v/v</sub> (for 18% acetate buffer).

The procedures used to prepare the sol are reported in the Figure 48:

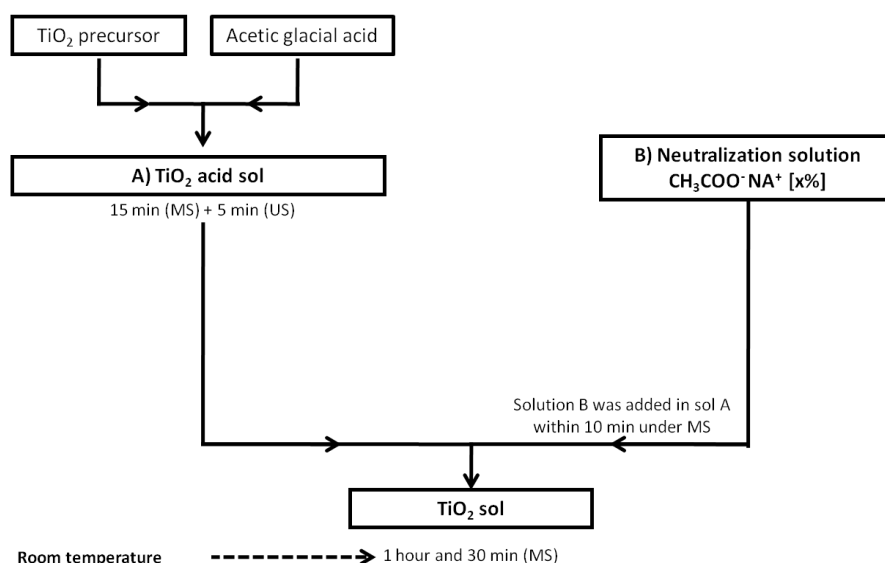


**Figure 48.** Two-step process; pure  $\text{TiO}_2$  sol were prepared adding titania precursor in acetate buffer solution. MS and US are magnetic stirring and ultrasonic treatment.



- Method 4: Two-step; Chitosan-TiO<sub>2</sub> sol.

Method 4 is a variation of method 3, in which the Chitosan-TiO<sub>2</sub> sol was prepared starting from three different solutions (A, B, above mentioned, and solution C). The chitosan solution (C) was prepared dissolving the chitosan powder (0.25 g) in 5 mL of distilled water, previously acidified with 0.4%v/v of acetic glacial acid and stirred/sonicated to obtain an homogeneous solution. The solution C appears a clear yellow solution of high viscosity. Chitosan solution was added into A and, after stirring, the resulting mixture was mixed with solution B.

Variation of method 4:

- Acetate buffer concentration: 2% (1 mL CH<sub>3</sub>COOH, 1 mL CH<sub>3</sub>COONa), 6% (3 mL, 3 mL), 18% (9 mL, 9 mL).
- TiO<sub>2</sub> concentration: 0.25%<sub>v/v</sub> - 0.5%<sub>v/v</sub> - 1.5%<sub>v/v</sub> (for 6% acetate buffer). 0.5%<sub>v/v</sub> - 1.5%<sub>v/v</sub> - 3%<sub>v/v</sub> (for 18% acetate buffer).
- Chitosan concentration: 0.125%<sub>w/v</sub> - 0.5%<sub>w/v</sub>.
- Temperature synthesis: 95°C. The sol prepared mixing solution A,B,C was stirred at 95° for 1 hour and 30 minutes before the sol characterization.
- pH values: 3 – 5.
- Alkali (instead of CH<sub>3</sub>COONa): NaOH and NH<sub>4</sub>OH (NH<sub>3</sub>).
- Route sol preparation: The sol (prepared mixing solution A,B,C) was stirred before the characterization for different time or by different equipments.
  - Magnetic stirring: *STD* (1hour and 30 min); *6 h* (6 hours).
  - *Ultrasonic treatment* (US): the stirring of *STD* preparation was replaced by ultrasonic treatment (1 hour and 30 min).  
Ultrasonic equipment: model: Sonorex RK 102 Transistor; BANDELIN electronic.

The procedures used to prepare the sol (method 4) are reported in the Figure 49.

- Method 5: single-step buffer; Chitosan-TiO<sub>2</sub> sol in buffer solution.

Method 5 is a particular variation of method 4. 100 mL of sol was prepared adding 1 mL of titanium butoxide directly in 99 mL of buffer solution (3 mL CH<sub>3</sub>COOH, 3 mL CH<sub>3</sub>COONa (2M), 93 mL water ) in which previously was dissolved 0.25g of chitosan. This sol was prepared specifically for turbidity measurement.

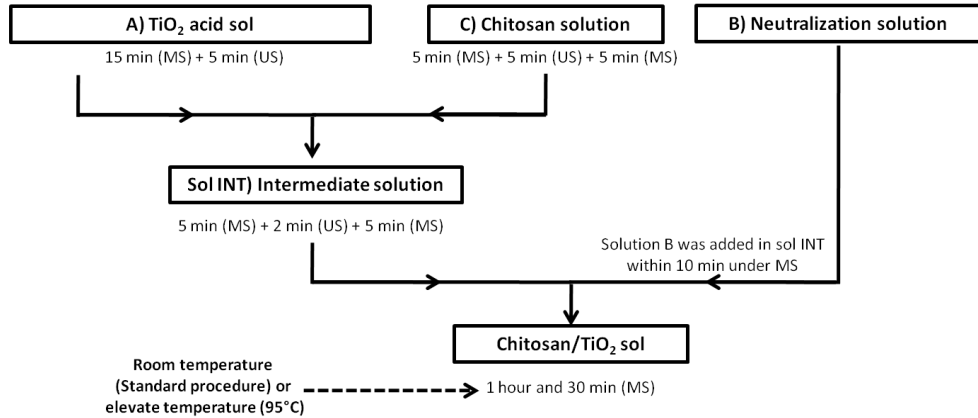


**Figure 49.** Two-step process; Chitosan-TiO<sub>2</sub> sol were prepared adding titania precursor to an acetate buffer solution containing chitosan. MS and US are magnetic stirring and ultrasonic treatment.

FT-IR measurements were performed on the liquid solution (e.i. pure acetic acid, pure acetic acid-TiO<sub>2</sub>), on solid (e.i. chitosan) and “Xerogel” prepared from the sol (80°C for 10 minutes, e.i. pure acetic acid-TiO<sub>2</sub>, TiO<sub>2</sub> sols, Chitosan-TiO<sub>2</sub> sols, chitosan acetate). For FT-IR measurements were also synthesizes the following samples:

- TiO<sub>2</sub> in pure CH<sub>3</sub>COOH: 1 mL of titanium butoxide was mixed with 3 mL of pure acetic acid. The samples was stirred and sonicated for 15 minutes and 5 minutes, respectively, before any measurements.
- Chitosan acetate for FT-IR measurement was synthesized as following: 0.25g of chitosan was dissolved in 3 mL of pure CH<sub>3</sub>COOH and 3 ml of CH<sub>3</sub>COONa (2M). Distilled water was added for achieving a final volume of 100 mL. The solution was stirred for 2 hours, after, the solution was applied on glass slide and it was dried at 80°C for 10 minutes to remove the solvent.

#### - Part B: Optical and photo characterization

A second group of TiO<sub>2</sub> sols was prepared by mixing titanium isopropoxide with aqueous, alcoholic solution using absolute ethanol as a solvent. Each sols were prepared with different acids (acetic, hydrochloric, nitric acid) either in presence of dopant (PEG) or not. Precursor concentrations in the solutions were fixed at 0.025 M and 0.25 M, where the TTIP/H<sub>2</sub>O/acid molar ratio were 1:4:0.15 and 1:40:0.15, respectively. The obtained transparent sol was left under magnetic stirring for 1h and was stored for 2 days before application. This procedure was used to obtain the

three sols by hydrolysis catalyzed with acetic, nitric or hydrochloric acid. An amount of 100 mL of each sol was doped, with PEG in a molar ratio TTIP:PEG=1:0.05. The samples have been coded as a in function of the kind of acids, the presence of PEG and the sol concentration used as summarized in Table 21.

Before applying the sol-gel solutions, the textile fabrics were washed in 2% non-ionic detergent at pH 7 and 40°C for 20 min to remove the residual impurities from the cotton surface; after, they were rinsed several times with de-ionized water, dried. The cleaned samples were conditioned under standard atmospheric pressure at 65 ± 4% relative humidity and 20 ± 2°C for at least 24 hours prior to all the experiments [130].

The cotton fabrics were impregnated for 30 seconds in the sols and, after, passed through a two-roll laboratory padder (Mathis AG, Switzerland) at nip pressure of 3 bar yielding 70% wet pick-up. After padding, the solvent evaporated and a solid film formed through the well-known sol-gel polymerization route after drying (10 min, 60°C) the fabric were cured at 120°C for 5 min.

The amount (wt%) on weight fabric (owf) of material deposited on the samples was determined and for this reason each sample was weighed before ( $W_0$ ) and after the padding and thermal treatment ( $W_1$ ), using Mettler balance ( $\pm 10^{-4}$  g) to determine the amount of charged material (add-on%) as following (Equation 10):

$$Add - on \% = \frac{(W_1 - W_0)}{W_0} \quad (\text{Equation 10})$$

Table 21. Experimental setup codes.

Conc. TiO <sub>2</sub> (M)	Dopant	Molar ratio TTIP/H <sub>2</sub> O/acid/PEG	Reference	Code		
				Acetic Acid	Hydrochloric acid	Nitric acid
0			UN			
0.025	NO	1:40:0.15:0		A1	H1	N1
0.25		1:4:0.15:0		A2	H2	N2
0			UNP			
0.025	PEG	1:40:0.15:0.05		A1P	H1P	N1P
0.25		1:4:0.15:0.05		A2P	H2P	N2P

## 5.3 Results

### 5.3.1 Part A: Study of sol stability

#### 5.3.1.1 FT-IR Characterization

Infrared spectroscopy was used to try to follow the polycondensation process in order to obtain useful information on possible interaction between the substances into the sols:  $\text{TiO}_2$ , chitosan and buffer. In particular, infrared spectroscopy study was performed on the samples (in acetate buffer) realized on two-step process either in presence of chitosan or not. Here are reported the characterization of the samples realized with: 1%v/v  $\text{TiO}_2$ , 6% acetate buffer, with (0.25%wt) or without chitosan, synthesized at room temperature or  $95^\circ\text{C}$ . However, similar results are obtained for the other samples synthesized at different concentration of % buffer, precursor and chitosan. The most interesting results are reported in the following paragraphs.

In Figure 50 the spectrum of pure acetic acid is reported. The absorption band at  $1755\text{ cm}^{-1}$  is attributed to C=O stretching (monomer), at  $1709\text{ cm}^{-1}$  C=O stretching (dimer), at  $1409\text{ cm}^{-1}$  to  $\text{CH}_3$  asymmetric deformation and at  $1289\text{ cm}^{-1}$  the  $\text{CH}_3$  symmetric deformation and COH bending.

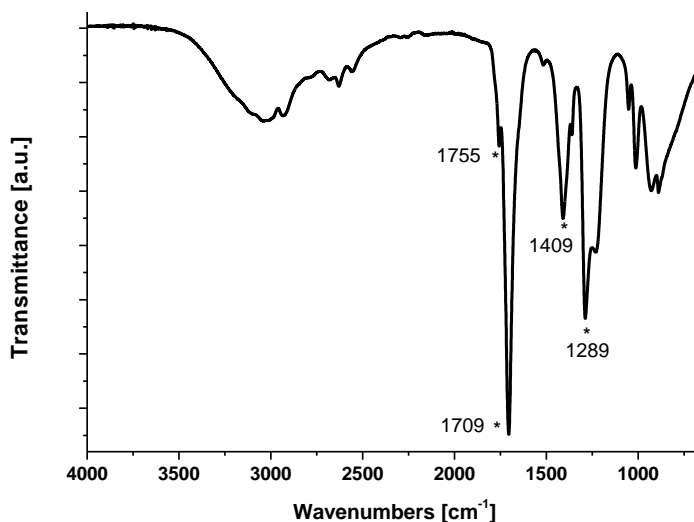


Figure 50. FT-IR spectrum of pure acetic acid.

Two interesting bands are observed around 1500 – 1400  $\text{cm}^{-1}$  for the sol prepared dissolving  $\text{TiO}_2$  (Titanium butoxide) in pure acetic acid (Figure 51). Referring to literature these could be assigned to acetate ligands. The frequency separation ( $\Delta < 130 \text{ cm}^{-1}$ ) between the  $\nu_{\text{asym}}$  (COO) at 1533  $\text{cm}^{-1}$  and  $\nu_{\text{sym}}$  (COO) at 1413  $\text{cm}^{-1}$  suggests that  $\text{CH}_3\text{COO}^-$  acts as bidentate ligand. The titanium is directly bonded to the acetate but it would be difficult to say whether the acetate is chelating (bonded to one Ti) or bridging (binding to two Ti) ligand. However, some shoulder suggest that both the coordinations are likely to occur [131, 132, 133, 134].

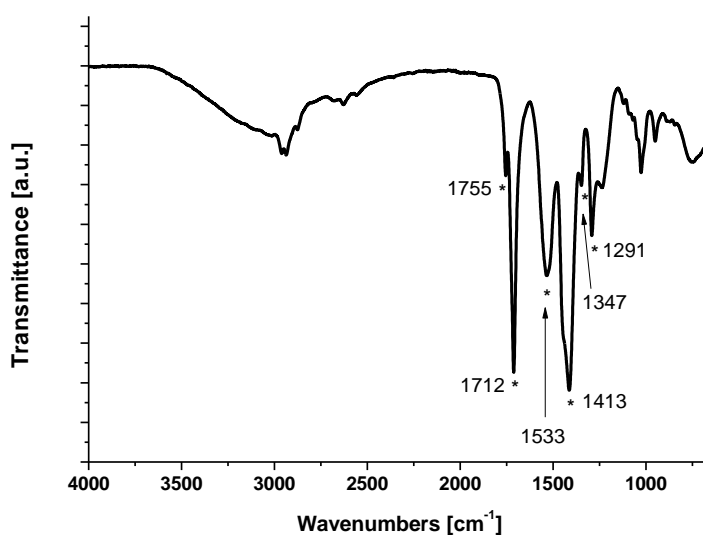
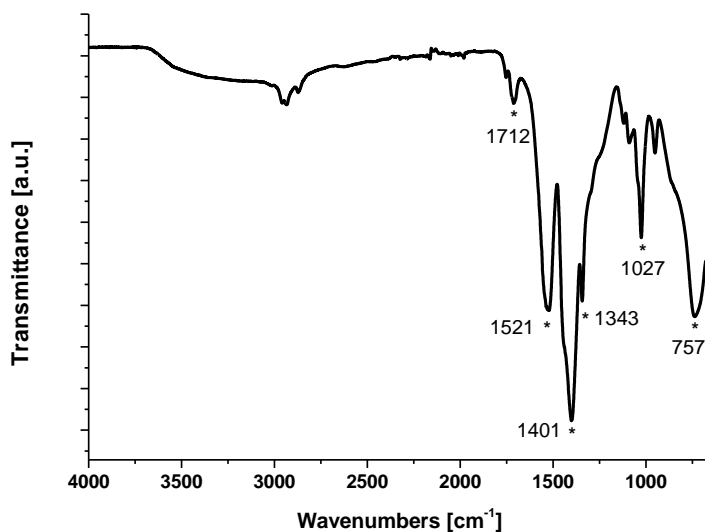


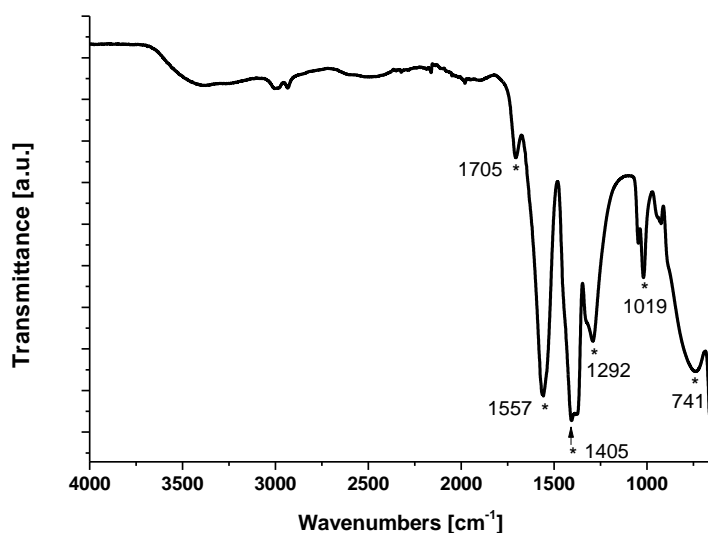
Figure 51. Infrared spectrum after the addition of  $\text{TiO}_2$  precursor to acetic acid.

Figure 52 shows the infrared spectrum of the xerogel obtained after drying of the previous sol (see Figure 51) for 10 min at 80°C. The two bands at 1521  $\text{cm}^{-1}$  and 1401  $\text{cm}^{-1}$  are still visible indicating the presence of acetate groups. Moreover, The spectrum of xerogel exhibits a signal 757  $\text{cm}^{-1}$  that should be ascribed to absorption bands of the Ti-O and O-Ti-O flexion vibration [135].



**Figure 52.** Infrared spectrum of xerogel (80°C for 10 min) derived from addition of TiO<sub>2</sub> precursor to acetic acid.

In Figure 53, the xerogel FT-IR spectrum derived from stable TiO<sub>2</sub> sol prepared in buffer solution (stable sol: clear and homogeneous sol which does not show precipitation) is reported. It shows similar bidentate ligand bands as the previous xerogel, reported in Figure 52. In particular, the band at about 1557 cm<sup>-1</sup> is shifted about 30 cm<sup>-1</sup> (in previous spectra was at 1520 cm<sup>-1</sup>) while a new band at 1292 cm<sup>-1</sup> appears. The bands at 1292 cm<sup>-1</sup> and 1705 cm<sup>-1</sup> could be attributed to the  $\nu(\text{COO})$  vibration of an acetate ligand and the large frequency separation ( $\Delta\nu = 413$  cm<sup>-1</sup>) between  $\nu_{\text{sym}}$  (1292 cm<sup>-1</sup>) and  $\nu_{\text{asym}}$  (1705 cm<sup>-1</sup>) suggest an unidentate acetate ligand. However, these two bands (around 1705 cm<sup>-1</sup> and 1292 cm<sup>-1</sup>) cannot be assigned only to free acid acetic because the intensity seems to be too low to justify it. This suggests that some monodentate acetate ligands should be linked to the titanium.



**Figure 53.** Characteristic Infrared spectrum of xerogel (80°C for 10 min) derived from stable TiO<sub>2</sub> sol prepared in buffer solution.

Generally, acetate could react with the titanium alkoxide precursor according to the scheme reported in Figure 54 [133]:

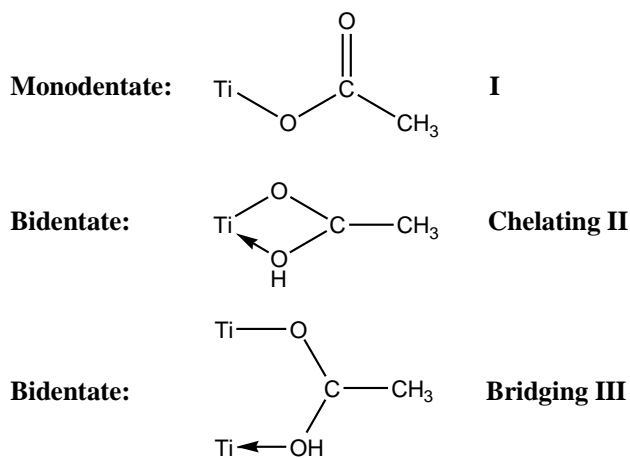


**Figure 54.** Possible reactions of the acetate anion with Titanium.

The position and splitting of the acetate ligands bands have been reported in literatures [134] and they are shown in Table 22.

**Table 22.** Stretching vibration of acetate ligands in different Ti(IV)-acetate complex according to [134].

Coordination mode	$\nu_{\text{asym}}(\text{COO})$ $\text{cm}^{-1}$	$\nu_{\text{sym}}(\text{COO})$ $\text{cm}^{-1}$	$\Delta\nu$ $\text{cm}^{-1}$
Monodentate I	1720	1295	425
Bidentate chelating II	1550	1470	80
Bidentate bridging III	1590	1430	160

Nevertheless, the stretching vibration infrared bands obtained from stable  $\text{TiO}_2$  sols synthesized in this research are different. They are shown following in Table 23.

**Table 23.** Stretching vibration of acetate ligands in different Ti(IV)-acetate complex ( $\text{TiO}_2$ -buffer; Chitosan- $\text{TiO}_2$ ) in this research. 6% buffer; 1%v/v  $\text{TiO}_2$ .

Coordination mode	$\nu_{\text{asym}}(\text{COO})$ $\text{cm}^{-1}$	$\nu_{\text{sym}}(\text{COO})$ $\text{cm}^{-1}$	$\Delta\nu$ $\text{cm}^{-1}$
Monodentate I	1705	1292	414
Bidentate chelating II	1557	---	
Bidentate bridging III	---	1405	

In the characteristic FT-IR of xerogel derived from the unstable  $\text{TiO}_2$  sol prepared in buffer solution the band at about  $1292 \text{ cm}^{-1}$  due to the monodentate ligand disappear completely or is strongly reduced and, at the same time, the intensity of bidentate bands increased strongly (Figure 55). The behaviour is observed both for the unstable sols synthesized at room temperature (about  $20^\circ\text{C}$ ) and  $95^\circ\text{C}$ . These interactions involved in the sol could explain the variation of the sol stability over time.



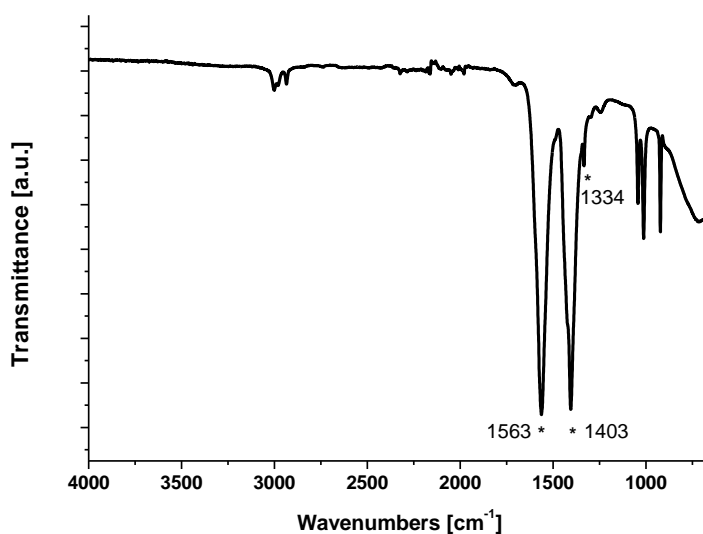


**Figure 55.** Infrared spectrum of xerogel (80°C for 10 min) derived from unstable TiO<sub>2</sub> sol (in buffer solution) synthesized at room temperature and 95°C.

The IR spectrum of pure chitosan shown in Figure 56 exhibits an adsorption band from 3600 to 3100 cm<sup>-1</sup> and 1030 cm<sup>-1</sup> due to hydroxyl (-OH) functional groups; at 2936 and 2886 cm<sup>-1</sup> assigned to -CH stretching vibrations in -CH and -CH<sub>2</sub>. Adsorption bands at 1615 cm<sup>-1</sup> (amide I), 1514 cm<sup>-1</sup> (amide II), and 1377 cm<sup>-1</sup> (amide III) [136,137]. The band at 1157 cm<sup>-1</sup> is due to C-O-C in the pyranose ring while the band at 1065 cm<sup>-1</sup> is due to CO stretching vibrations. In the chitosan acetate spectrum (Figure 57), there were shifts of amide bands and the appearance of a band at 1555 cm<sup>-1</sup> due to the formation of -NH<sub>3</sub><sup>+</sup> CH<sub>3</sub>COO<sup>-</sup> [138].

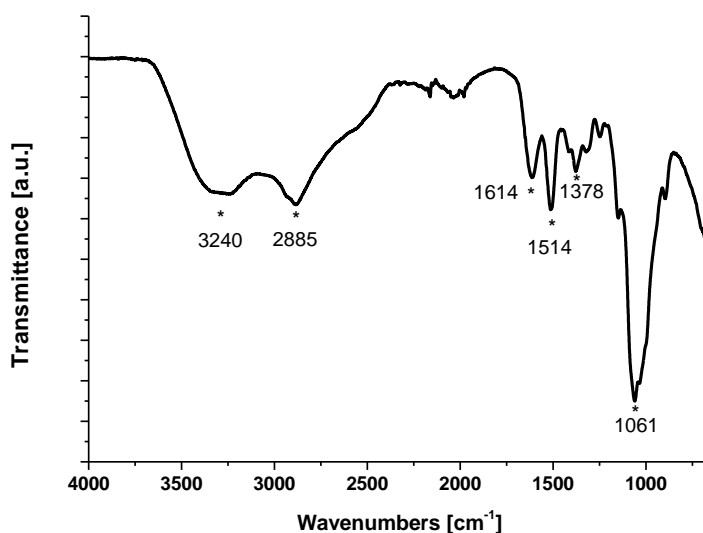


Figure 56. FT-IR of pure chitosan.

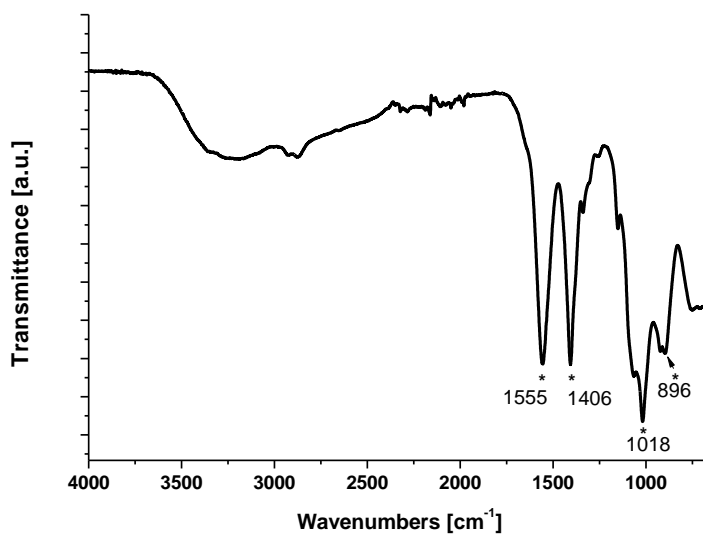


Figure 57. FT-IR of chitosan acetate.

The protonation of  $\text{-NH}_2$  groups of chitosan and, consequently, the electrovalent bond between chitosan and acetate improves the solubility of chitosan molecules. In Figure 58 the chitosan acetate formula is reported:

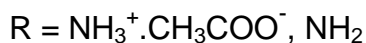
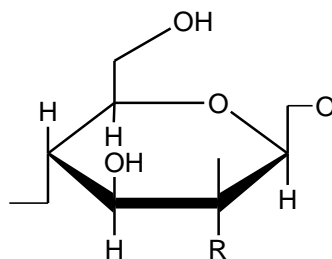


Figure 58. Structural formula of chitosan acetate.

The characteristic spectrum of stable Chitosan-TiO<sub>2</sub> sols (xerogel) is reported in Figure 59. In the range of 1000-1100 cm<sup>-1</sup> the characteristic bands of chitosan due to hydroxyl (-OH) functional groups are observed. Two new bands appear at 1291 cm<sup>-1</sup> and 1702 cm<sup>-1</sup> that suggest the formation of unidentate acetate ligand between the titania precursor and acetate anion. The characteristic bands of titania bidentate acetates are overlapped to the chitosan acetate bands in which the main peaks are around 1561 cm<sup>-1</sup> and 1405 cm<sup>-1</sup>. It is interesting to notice some shoulder that suggest possible interaction between chitosan, acetate and titania.

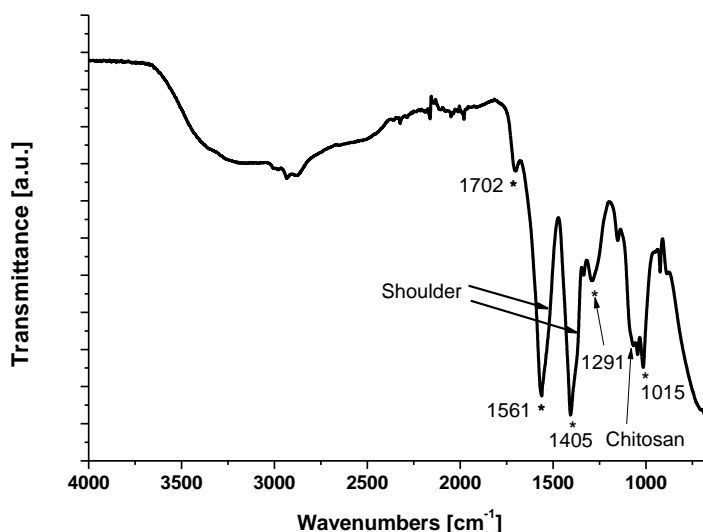
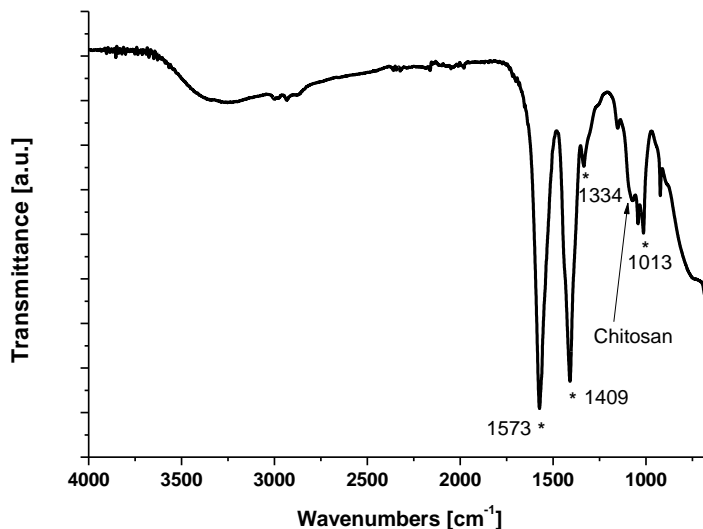


Figure 59. FT-IR of xerogel (80°C for 10 min) derived from the Chitosan-TiO<sub>2</sub> stable sols.

As shown for the xerogel of unstable  $\text{TiO}_2$  sols (Figure 55), also for the xerogel of unstable Chitosan- $\text{TiO}_2$  sols (Figure. 60), the bands corresponding to the monodentate ligand disappear completely or are strongly reduced while the intensity of the bands at  $1573 \text{ cm}^{-1}$  and  $1409 \text{ cm}^{-1}$  increases strongly. Moreover, the shoulders observed in the stable sol are not present in unstable sols xerogels.



**Figure. 60.** FT-IR of chitosan acetate and xerogel (80°C for 10 min) derived from Chitosan- $\text{TiO}_2$  unstable sols.

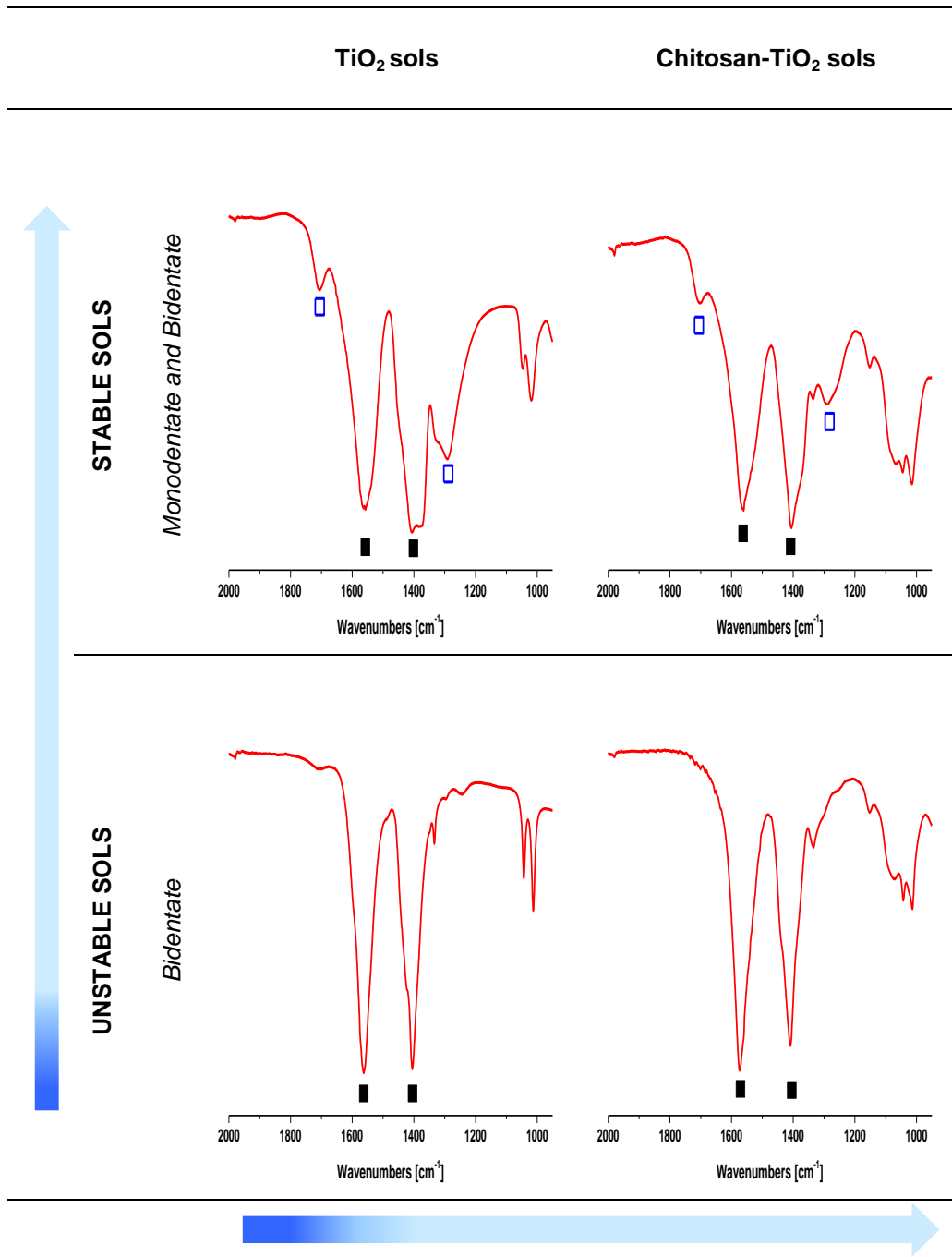
It's interesting notice that the sols prepared with chitosan show a greater stability over time than the pure  $\text{TiO}_2$  sols (see also the turbidity measurement). This different behavior could probably be explained by two different mechanisms that may act simultaneously. In the first, chitosan reduces the amount of acetate ion available through the formation of chitosan acetate. So, the rate of condensation to form the bidentate acetate- $\text{TiO}_2$  species may be slowed. At the same time, in the second way the chitosan may interfere in the aggregation phenomena (or particles growth) for steric hindrance reducing the growth of titania particles.

A schematic comparison of stable and unstable sols with and without chitosan is shown in Table 24.

**Table 24.** Schematic comparison of stable and unstable sols with and without chitosan.

Characteristic bands for xerogels derived from stable and unstable sols.

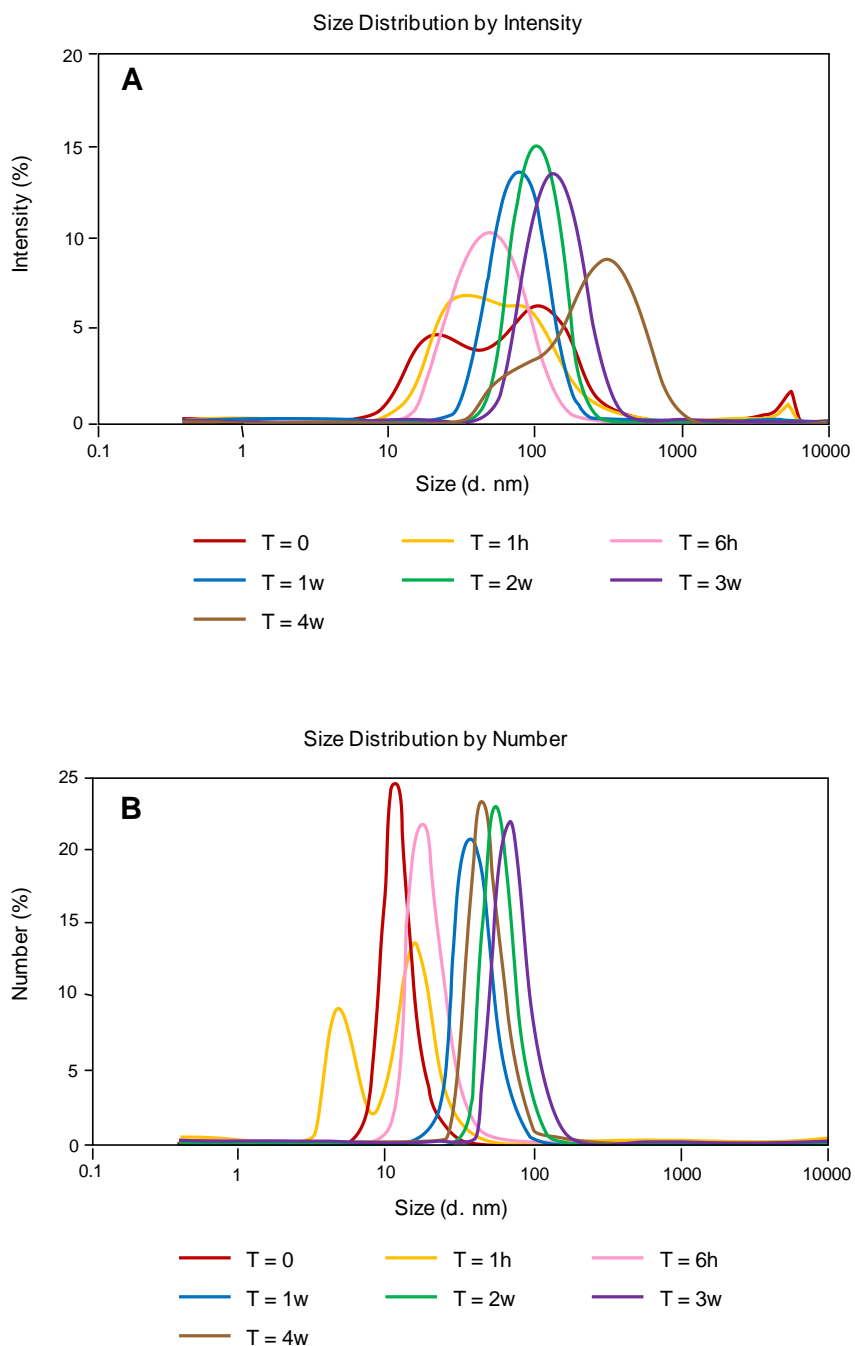
Monodentate bands (□); Bidentate bands (■).



### 5.3.1.2 DLS measurement

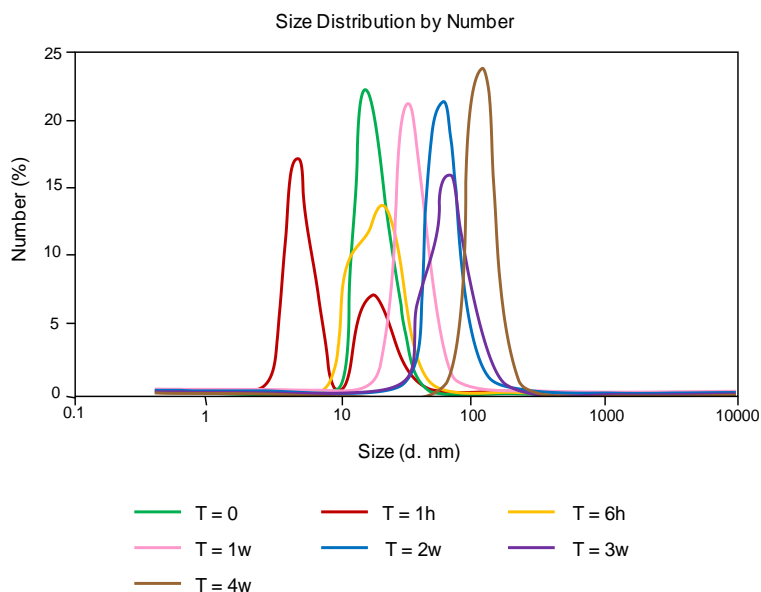
Dynamic light scattering (DLS), detects the fluctuations of the scattering intensity due to the Brownian motion of particles in solution. The statistics of the scattering signal are analyzed with a correlator, the resulting correlation function may be inverted to find a size distribution for the particles in solution. So, dynamic light scattering was used as a complementary tool for the characterization of sol stability to distinguish between a homogenous monodisperse and an aggregated sample. The intensity and number distributions produced by a typical algorithm are reported and the contributions in terms of % intensity and % number are shown as a function of particle diameter. The most interesting results of the stable Chitosan-TiO<sub>2</sub> samples (two-step) are following reported.

Figure 61A, B show the results of DLS measurement performed at different aging times of Chitosan-TiO<sub>2</sub> sample (0.25%<sub>v/v</sub> TiO<sub>2</sub>, 6% buffer). It is clearly visible that particle size is timing dependent. During aging of the sol the particles size increases due to the aggregation phenomena or growth of particles which are detected as variation of intensity signal of the DLS analysis. The stability of sol is usually reduced with the increasing of particle size. In particular in Figure 61A, a double peak in the sample just prepared is observed, that became only one after 6 hours of aging. The maximum intensity is observed after 2 weeks of aging, whereupon, the intensity decreases and a broad peak is observed after 4 weeks. Except for the measurement at 1 hour, only a peak has been observed for the other samples concerning the number distribution. At 1 hour a double peak was observed indicating the formation of smaller particles after the preparation of the sol. Perhaps, it could be due to the interaction between the chitosan and acetate anion with the titania. In particular in excess of acetate, some titania aggregate could be destroy in smaller particles by acetate anion effect to form acetate TiO<sub>2</sub>. After this initial step, the condensation of acetate titania starts and it brings to the aggregation of the particles.



**Figure 61.** DLS analysis of Chitosan-TiO<sub>2</sub> samples (0.25%v/v TiO<sub>2</sub>: 6% buffer). A) Intensity (%); B) Number distribution (%). h: hours; w: week.

Similar results are observed for the Chitosan-TiO<sub>2</sub> sample (0.25%<sub>v/v</sub> TiO<sub>2</sub>) in which the maximum intensity was measured after four week (Figure 62). Also, the increase of the number of smaller particles immediately after the preparation of sol were detected.



**Figure 62.** DLS analysis of Chitosan-TiO<sub>2</sub> samples (0.5%<sub>v/v</sub> TiO<sub>2</sub>; 6% buffer). A) Intensity (%); B) Number distribution (%). h: hours; w: week.

Figure 63A, B shows the DLS results of the samples prepared at different Chitosan-TiO<sub>2</sub> concentrations (18% buffer) at T=0 of aging. High polydispersity data are observed for all samples due to the considerable aggregation phenomena (or particles growth). Similar intensity distribution are observed for the samples prepared with TiO<sub>2</sub> concentration lower than 1.5 percentage, while a broad peak (about 50 nm Z-average) and a significant peak (particles bigger than 1 μm) for 3%<sub>v/v</sub> TiO<sub>2</sub> are observed.



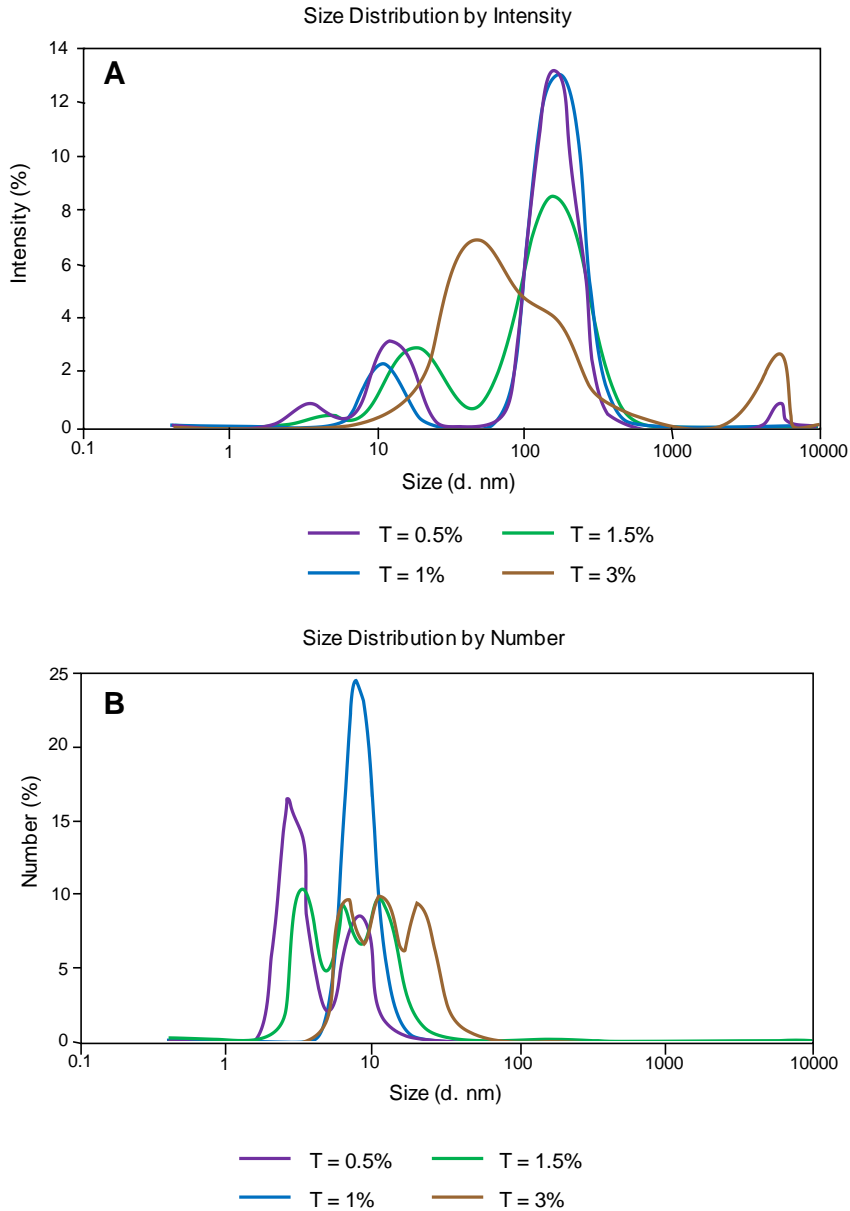


**Figure 63.** DLS analysis of Chitosan-TiO<sub>2</sub> samples (0.5%, 1% 1.5%, 3%v/v TiO<sub>2</sub>; 18% buffer). A) Intensity (%); B) Number distribution (%).

Figure 64A, B shows the results of the DLS analysis for the Chitosan-TiO<sub>2</sub> sols (0.25%<sub>v/v</sub>, 0.5%<sub>v/v</sub>, 1.5%<sub>v/v</sub> TiO<sub>2</sub>) prepared with 6% of buffer at T=0 of aging. The intensity (%) signal of Chitosan-TiO<sub>2</sub> sols increases with the titanium dioxide concentration and, only, for 0.25%<sub>v/v</sub> TiO<sub>2</sub> are detected two different particles

species. Similar behaviour is observed for number distribution which for all sample is very close to the Z-average size. It is obvious the particles size depends from the concentration of the precursor in the sol. In fact, the probability of the particles to react and form bigger particles (aggregation or growth) increases with the increasing of the TiO<sub>2</sub> concentration.

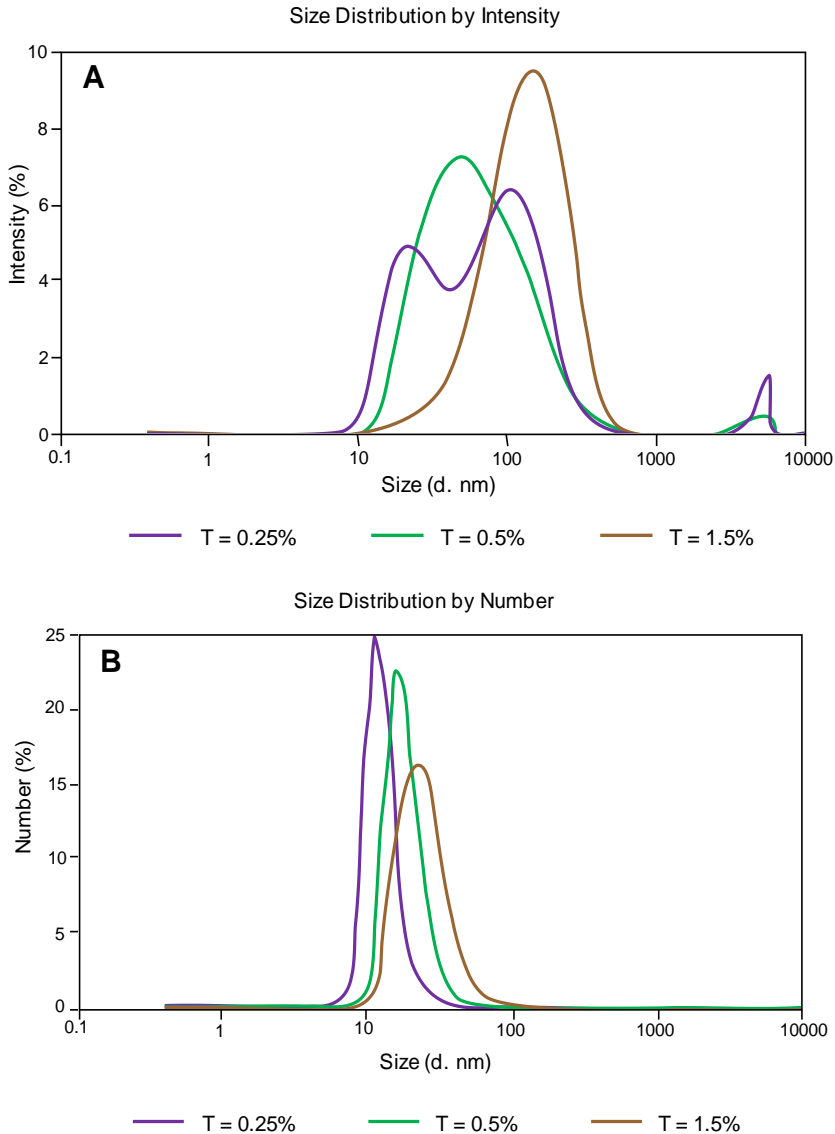


**Figure 64.** DLS analysis of Chitosan-TiO<sub>2</sub> samples (0.25%, 0.5% 1.5%v/v TiO<sub>2</sub>; 6% buffer). A) Intensity (%); B) Number distribution (%).

### 5.3.1.3 Turbidity measurement

Turbidity measurements were performed to investigate the stability of the sols over time. The appendix shows the photos of all samples prepared, as shown in the graphs of this paragraphs.

#### **Discussion: single-step procedure; preliminary test; method 1 and 2.**

Preliminary tests (single-step procedure) were performed to understand the stability of  $\text{TiO}_2$  synthesized in aqueous solution. The sols were catalyzed with HCl or acetic acid at different pH in the range from pH 1 to pH 4 with a resolution of 1. Stable sols have been observed only for  $\text{pH} \leq 1$  for hydrochloric acid and  $\text{pH} \leq 2$  for acetic acid (Figure 65). The turbidity measurements have shown low and quite constant NTU (nephelometric turbidity unit values) for more than 700 hours indicating a good stability over time.

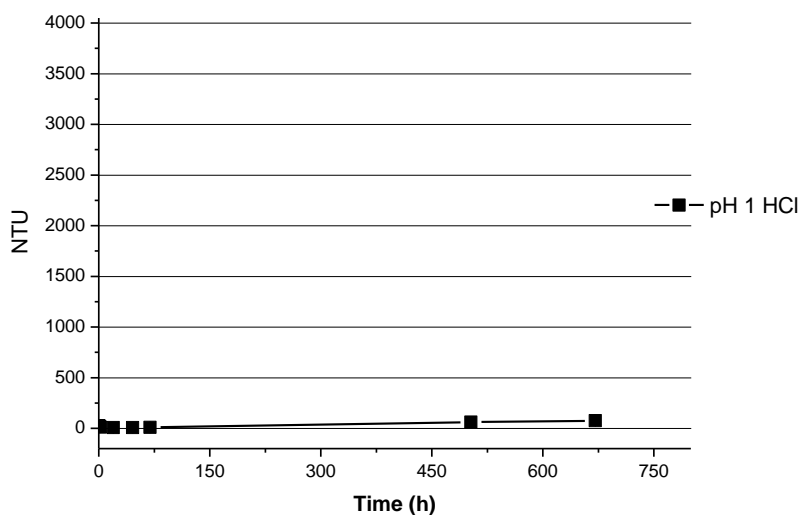


**Figure 65.** Turbidity measurement. Single-step process.  $\text{TiO}_2$  Sol at pH 1 in HCl.

Unfortunately, the solutions, so realized, are too corrosive to be used easily for industrial applications and they could damage the textile substrate reducing its mechanical properties. When pH values have been shifted toward  $\text{pH} > 1$  for hydrochloric acid and  $\text{pH} > 2$  for acetic acid a white precipitate has been observed (see appendix for photos). In these experimental conditions, all samples synthesized haven't allowed to prepare a stable sol and over range NTU values have been

measured. No differences in the sol stability have been observed adding chitosan during the preparation of the previous solutions (pH values >1 for hydrochloric acid and pH values >2). In fact, all samples appeared still unstable with a white precipitate into solution and over range turbidity values were observed. For these reasons no turbidity results have been follow reported.

Finally, for the sols prepared with stoichiometric amount of catalyst, the sol stability depends from the pH values of the solution and the kind of acid used as catalyst. Moreover, no significant effects was observed adding chitosan as stabilizer.

***Discussion: two-step procedure; method 3 and 4.***

Starting from the results of preliminary tests (single-step process), a two-step process has been investigated. The idea has been to solubilize initially the precursor in strongly acid solution, to delay the addition of water and to shift slowly the pH of solution. In this way it is wanted to reduce/decrease the TiO<sub>2</sub> aggregation phenomena due to the hydrolysis/condensation reaction of titania.

Each sol was prepared mixing an acid TiO<sub>2</sub> sol catalyzed by acetic acid in presence or absence of chitosan and a neutralization solution (acetate solution) to reach pH 4 which is particularly suitable for industrial applications. In particular, the titania precursor was initially dissolved in pure acetic acid solution in which acetate can act as a chelating ligand and react, with the titanium alkoxide precursor to form Ti(OR)<sub>x</sub>(AC)<sub>y</sub>.

Initially, the influence of different acetate buffer concentrations (2%, 6%, 12% and 18% of CH<sub>3</sub>COOH/CH<sub>3</sub>COONa) on stability of TiO<sub>2</sub> sol (1%v/v TiO<sub>2</sub>, pH4) have been intensity study. In Figure 66 are showed the stability sol results in terms of turbidity measurement for the samples prepared without chitosan. A completely different turbidity trend is observed in comparison with the samples prepared at the same pH condition by single-step process (Figure 65) in which over range values were observed. In Figure 66, even if there are some small differences between the samples, all sols achieve similar asymptotic NTU values after 700 hours of aging. However, the better stability results have been observed when the concentration of buffer increases such that higher was the buffer concentration lower NTU values was observed.

Acetate buffer (acetic acid/sodium acetate) used exhibits chelating agent characteristics and modify the precursor to form  $Ti(OR)_x(AC)_y$ . This modified precursor can decrease the rate of the hydrolysis reaction and thus prevent sedimentation, because the acetate functional group is more difficult to hydrolyze than the OH functional group [139]. However, this is true only for short time, in fact, the condensation reactions proceed bringing over time to the formation of a white gel of titanium dioxide.

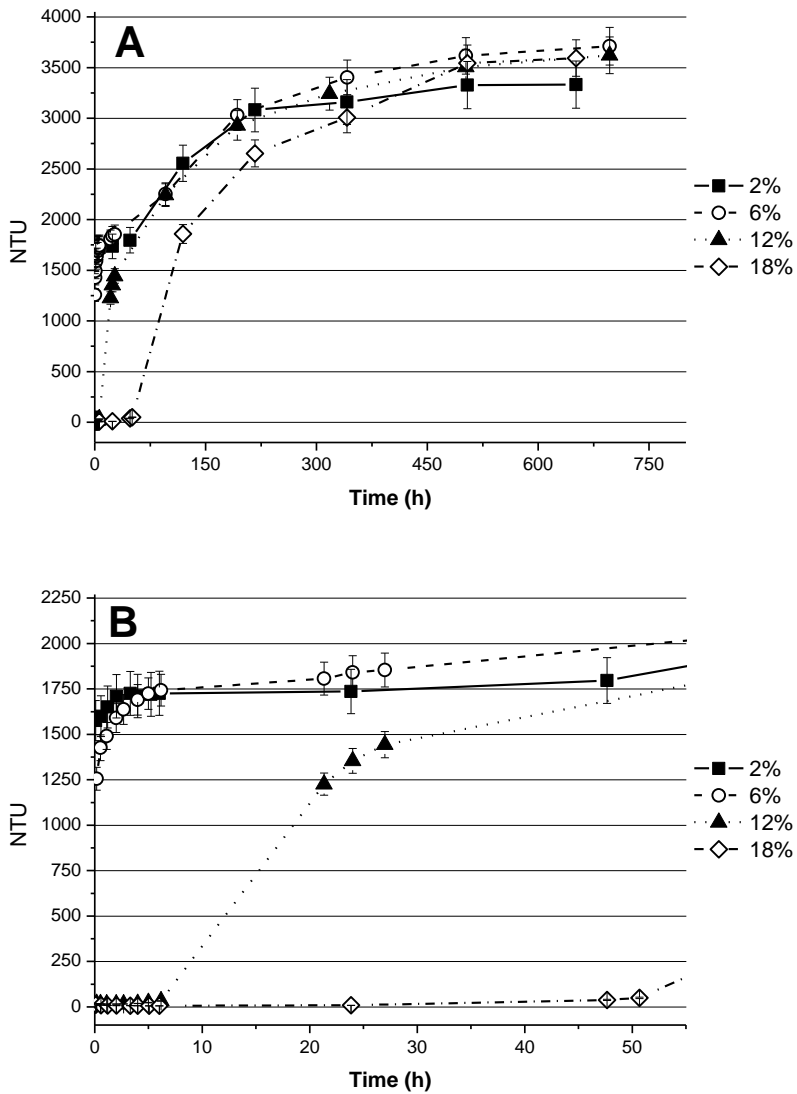


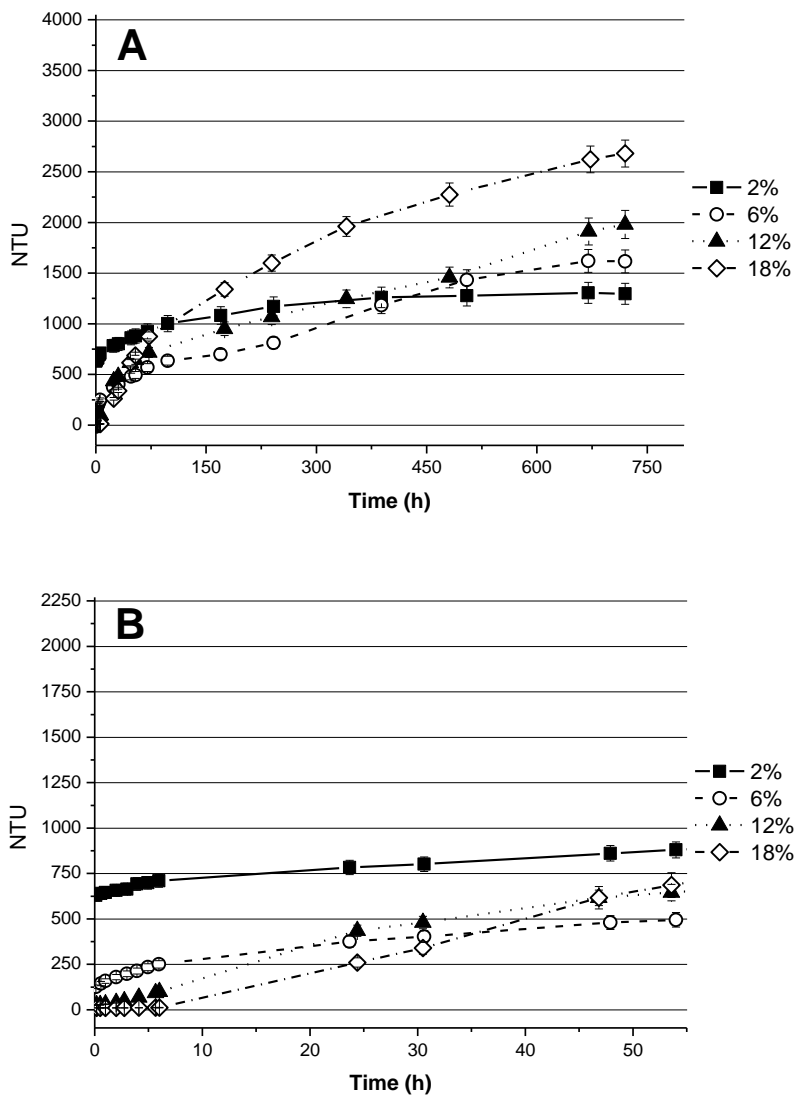
**Figure 66.** Turbidity measurement. Influence % Buffer  $CH_3COOH/CH_3COONa$  (2%, 6%, 12%, 18%). Kost = 1 %v/v  $TiO_2$  precursor at pH 4. B) Detail.

Comparing the results, above mentioned, with those obtained in presence of chitosan at the same condition (Figure 67A, B), it's clearly visible as chitosan samples show lower NTU values at 700 hours than reference samples. This is also confirmed by photos (see appendix). Moreover, for most of them are not still observed asymptotic trend that, instead, was measured for all samples without chitosan. The stability is strongly influenced by the amount of buffer used. It increases with the increasing of the buffer concentration from 2% to 18%. Nevertheless, this behavior could be true only up to certain short aging time, after that, in fact, a opposite trend was observed: the sol prepared with 18% of buffer shows higher NTU values than the sol prepared with 2% of buffer at about 700 hours of aging.

It's interesting notice the stability results in first about "15 hours" of aging for the samples prepared either in presence of chitosan (Figure 67) or not (Figure 66). For buffer concentration lower or equal to 6% the stability of sols prepared with chitosan is higher than pure  $\text{TiO}_2$  sols, while for buffer concentration higher than 9% the stability of Chitosan- $\text{TiO}_2$  samples is lower than  $\text{TiO}_2$  sols. Perhaps, for the samples prepared with low amount of buffer, acetate anion concentration don't seem to be enough to reduce the aggregation (or growth) of the particles. Consequently, the chitosan could acts as stabilizer reducing the aggregation phenomena (or growth particles) by steric hindrance effect (main effect on the stability). In the other hand, for high concentration of buffer the main effect on the sol stabilization could be due to the acetate anion. In presence of chitosan the available acetate anion required to stabilize the sol is reduced due to the formation of chitosan acetate and, consequently, the stability is lower than pure  $\text{TiO}_2$  samples.

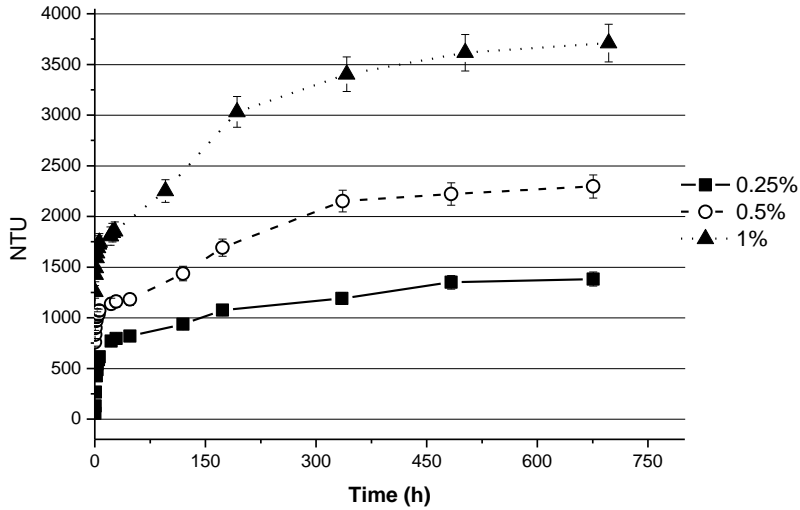
Over time the condensation reactions of acetate titania proceed bringing to the formation of unstable sol (white gel) for all sols. Chitosan acts reducing the condensation rate and the aggregation phenomena or growth particles by chemical bond interaction and steric impediment (see FT-IR measurement).

Finally, the use of chitosan in the two step process improves the sol stability, playing an important role on the stabilization of  $\text{TiO}_2$ . However, the aging and buffer concentration are important for the preparation of stable sol.



**Figure 77.** Turbidity measurement. Influence % Buffer  $\text{CH}_3\text{COOH}/\text{CH}_3\text{COONa}$  (2%, 6%, 12%, 18%). Kost = %  $\text{TiO}_2$  (1%v/v), chitosan (0.25%wt) at pH 4. B) detail.

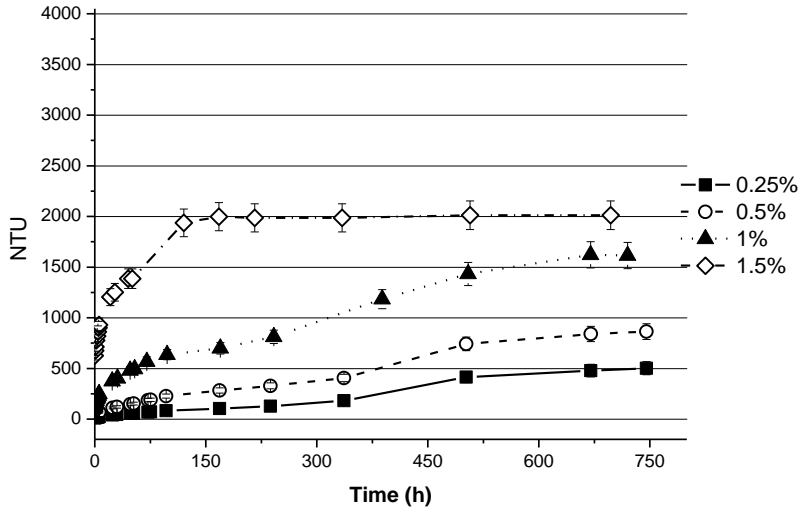
As shown in Figure 68, Figure 69 and Figure 70 the stability of sols depends on the concentration of  $\text{TiO}_2$  precursor used. The stability is inverse proportion to the  $\text{TiO}_2$  concentration both for the samples without (Figure 68) and chitosan (Figure 69, Figure 70). In particular, the  $\text{TiO}_2$  sols prepared with 6% of buffer show similar trends but only shifted (Figure 68).



**Figure 68.** Turbidity measurement. Influence %TiO<sub>2</sub>. Kost = % buffer CH<sub>3</sub>COOH/CH<sub>3</sub>COONa (6%) at pH4.

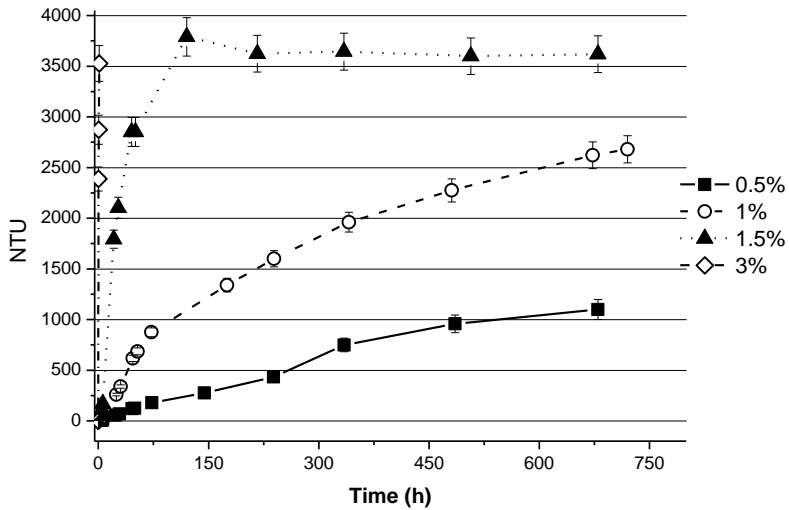
The use of chitosan stabilizes the sols (in Figure 69) in which only a sample (1,5% Chitosan-TiO<sub>2</sub>) shows asymptotic trend after about 700 hours. Generally, the samples realized with chitosan show lower turbidity compare to the pure TiO<sub>2</sub> sols. It's interesting to note, as the turbidity of 1,5% Chitosan-TiO<sub>2</sub> sample is comparable to 0,5%TiO<sub>2</sub>: the chitosan sample is three time more concentrated but with similar turbidity value of the sample prepared without chitosan. This results can be useful to understand the positive effect of chitosan on the stabilization of the sol.





**Figure 69.** Turbidity measurement. Influence % TiO<sub>2</sub>. Kost = % buffer CH<sub>3</sub>COOH/CH<sub>3</sub>COONa (6%), 0.25%wt chitosan at pH 4.

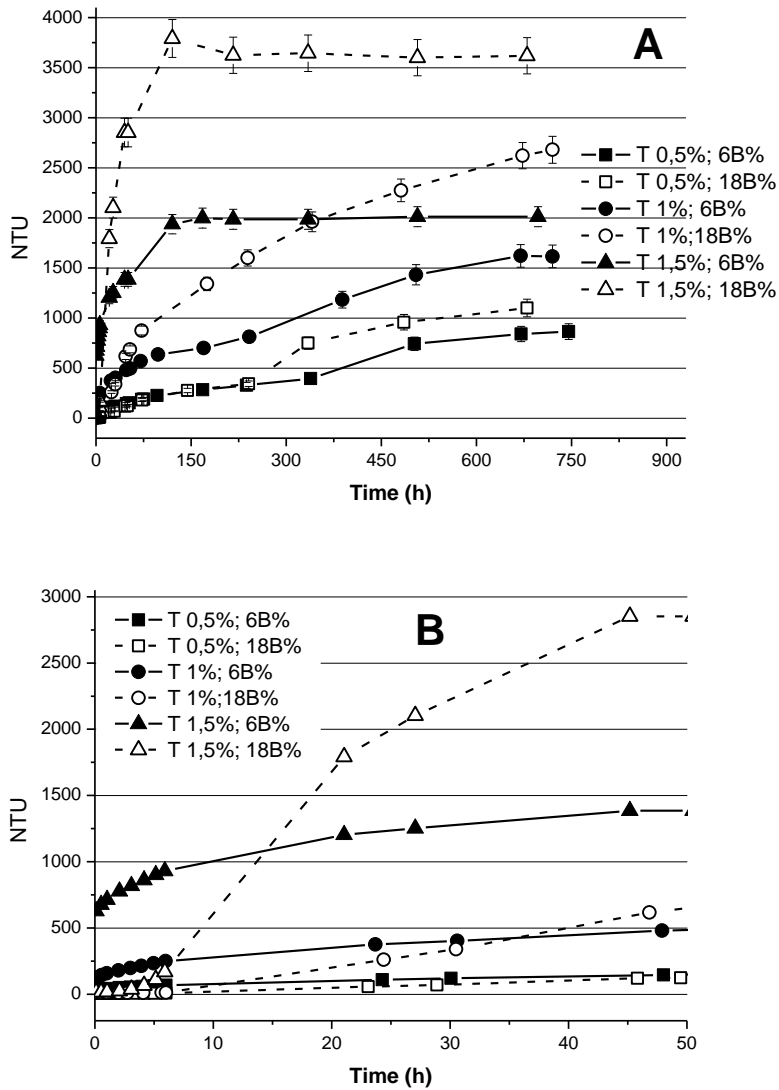
As shown in Figure 70, the stability of these samples changes strongly using different percentage of buffer (Figure 69).



**Figure 70.** Turbidity measurement. Influence % TiO<sub>2</sub>. Kost = % buffer CH<sub>3</sub>COOH/CH<sub>3</sub>COONa (18%), 0.25%wt chitosan at pH 4.

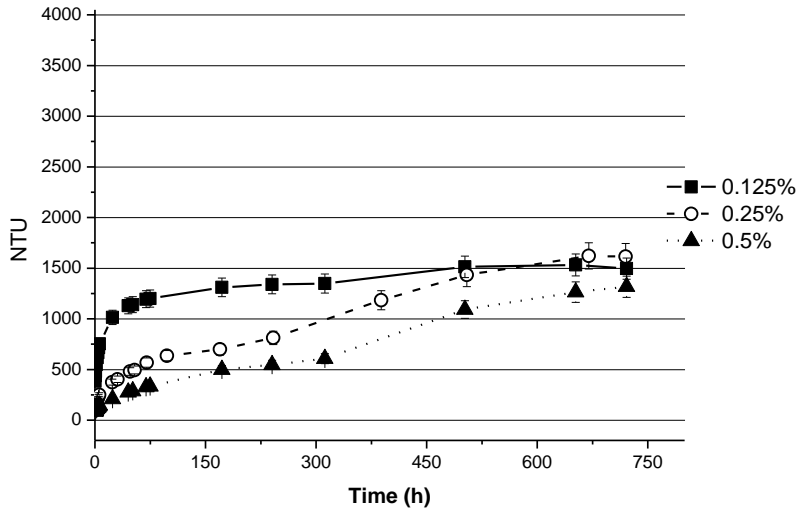
A better visualization of the results regarding the influence of the TiO<sub>2</sub> concentration is obtained overlapping the data in the Figure 69 and Figure 70, it is reported in

Figure 71. For the samples prepared with the same  $\text{TiO}_2$  concentration a partially overlap of the turbidity is observed. In particular, the overlap is longer reducing concentration of precursor. This behavior could be explain with the increase of condensation reaction rate increasing the amount of titania precursor in solution. Moreover, NTU values for the samples prepared with 18% of buffer are higher than the results of 6% buffer and increase quickly with  $\text{TiO}_2$  concentration. It's is due to bigger acetate- $\text{TiO}_2$  network obtained increasing the amount of acetate and titania.



**Figure 71.** Turbidity measurement. Relationship %  $\text{TiO}_2$  (0.5%, 1%, 1.5%v/v) and % Buffer  $\text{CH}_3\text{COOH}/\text{CH}_3\text{COONa}$  (6% and 18%). Kost = 0.25%wt chitosan at pH 4. B) Detail.

In Figure 72 the stabilizing effect of chitosan seems to be confirmed, a decreasing of turbidity is observed increasing the chitosan concentration.



**Figure 72.** Turbidity measurement. Influence % Chitosan (0.125%, 0.25%, 0.5%). Kost = % buffer CH<sub>3</sub>COOH/CH<sub>3</sub>COONa (6%), %TiO<sub>2</sub> (1%v/v) at pH 4.

In the Figure 73, Figure 74 and Figure 75 the results of Mass ratio of: %TiO<sub>2</sub>:%Buffer = 1:12; %Chitosan:%TiO<sub>2</sub> = 1:2; %Chitosan:%Buffer = 1:48 are reported respectively.

In particular, for the mass ratio: %TiO<sub>2</sub>:%Buffer = 1:12, a quasi linear and stable behavior is observed for the 0.5%TiO<sub>2</sub>:6%Buffer sample. Nevertheless, the sol becomes quickly unstable increasing the amount of TiO<sub>2</sub> and Buffer and it's already appeared unstable for the 1.5%TiO<sub>2</sub>:18%Buffer (1.5:18) after short time (Figure 73).

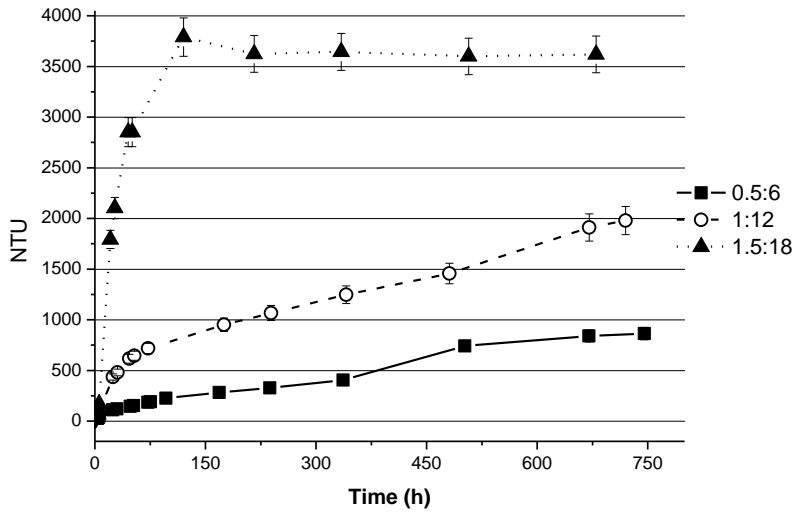


**Figure 73.** Turbidity measurement. Mass Ratio; % TiO<sub>2</sub> : % Buffer = 1:12. Kost = chitosan (0.25%wt) at pH 4.

Moreover, the increasing of chitosan is not enough to stabilize the enhanced of TiO<sub>2</sub> for the same mass ratio (Figure 74). Nevertheless, all samples show low turbidity.

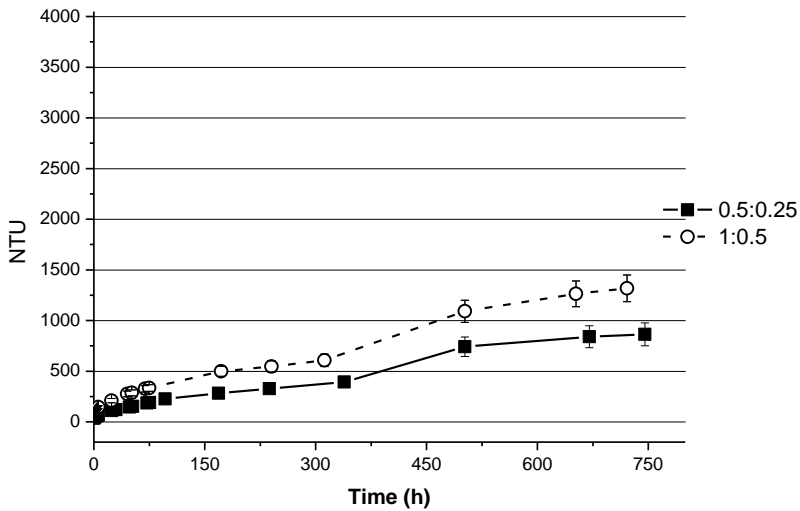


**Figure 74.** Turbidity measurement. Mass Ratio; % Chitosan : % TiO<sub>2</sub> = 1:2. Kost = % buffer CH<sub>3</sub>COOH/CH<sub>3</sub>COONa (3%) at pH 4.

Finally, in Figure 75 the results for the samples with the same Mass ratio (%Chitosan:%Buffer=1:48) are reported. High amount of chitosan and buffer seem to improve the stability of sol for short aging time. Nevertheless, after about 400 hours the sols prepared with the same molar ratio but with less amount of a buffer and chitosan are preferred.

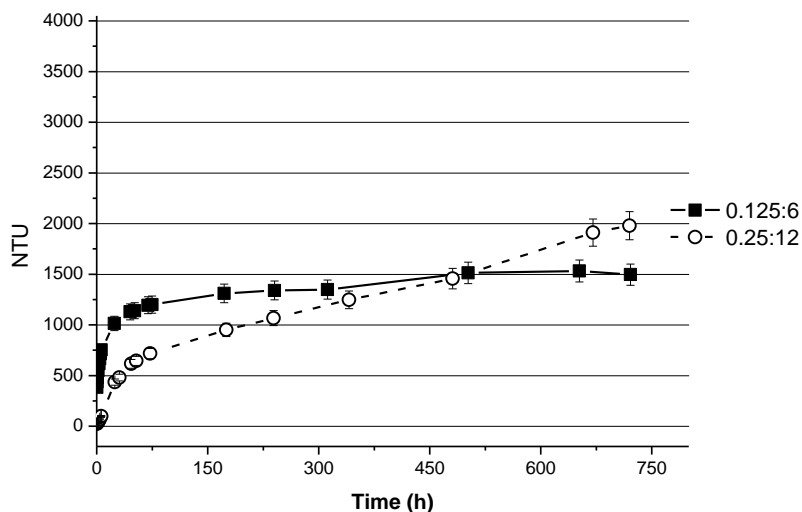


**Figure 75.** Turbidity measurement. Mass Ratio; % Chitosan : % Buffer = 1:48. Kost = % TiO<sub>2</sub> (1%v/v) at pH 4.

A complete different behaviour is observed comparing the same sample (1%<sub>v/v</sub> TiO<sub>2</sub>, 6% buffer and 0.25%<sub>w/t</sub> chitosan) synthesized at room temperature and 95°C. The sol synthesized at room temperature is initially clear and seems more stable than at 95°C. The room temperature trend evolves as shown in the previous figures in which the turbidity increases gradually to reach an asymptotic behaviour. Nevertheless, the samples realized at 95°C shows lower NTU values with the aging and it is still stable after two months. The mechanism of this interesting result is still under investigation, nevertheless it could be due the physical interaction among the substances in the sols. The result is still more interesting considering the behaviour of the same sol synthesized without chitosan. It appears immediately unstable and doesn't change its stability over time.

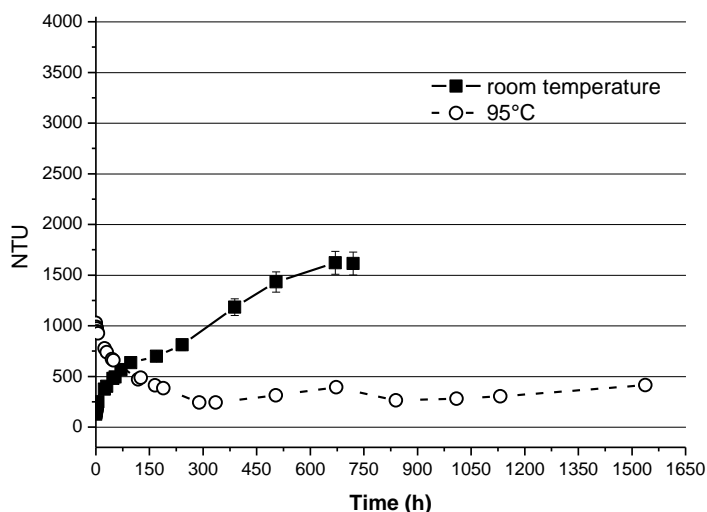


**Figure 76.** Turbidity measurement. Effect of temperature (room temperature and 95°C). Kost = % TiO<sub>2</sub> (1%v/v), chitosan (0.25%wt) at pH4.

Finally, the influence of the route of sol preparation were investigate. Slight difference are shown compare the follows samples: Standard (see method 3), 6 hours (the sample were stirred 6 hours and not 90 minutes before starting the data collection) and by ultrasonic treatment (the 1 hour and 30 minutes of magnetic stirring was replaced by ultrasonic treatment).

Nevertheless, the procedure to prepare the sol strong influence the stability of the solution. Stable sols were obtained only when the precursor was initially dissolved in pure acetic acid by two-step procedure. Whereas, when the precursor was added in acetate solution (CH<sub>3</sub>COOH/CH<sub>3</sub>COONa water solution- Method 5) the sols were immediately unstable (see appendix; one way/step 6%B). In this case, when the precursor is added in the solution, hydrolysis and condensation reactions take place immediately before acetate-TiO<sub>2</sub> is formed.

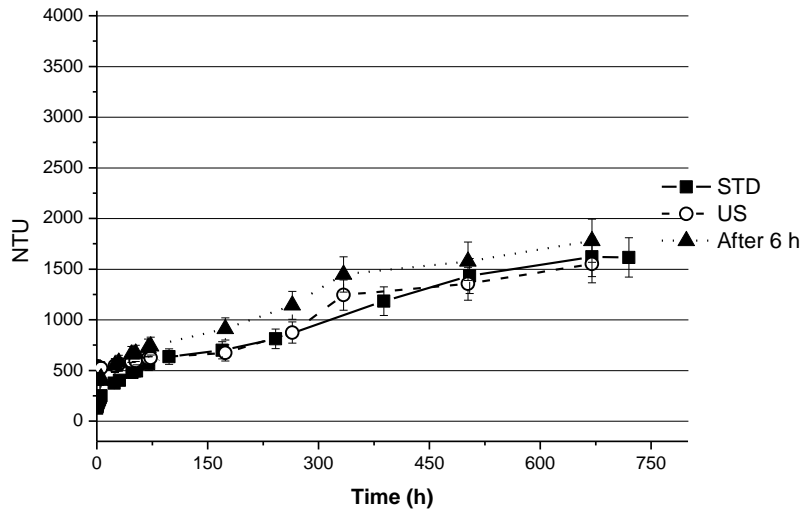


**Figure 77.** Turbidity measurement. Effect of sol-gel route: Kost = % TiO<sub>2</sub> (1%v/v), chitosan (0.25%wt) at pH 4.

The stability of sol in presence of chitosan was investigated at several pH condition in the range from pH 3 to pH 5 (resolution 1 unit). As shown in the Figure 78, the turbidity results have completely different stability behavior over time than single-step process prepared at the same pH condition, in fact no over range data were collected. For all samples were not observed a linear trend but a quickly enhanced of turbidity and, then, progressive stabilization of NTU values were measured. The samples at pH 4 shows the stability.

The stability of sols seem to be only slight influenced from the kind of alkali used (Figure 79). Perhaps, the difference between ANA and NaOH or NH<sub>3</sub> samples could be ascribe to salt concentration present in the sols.

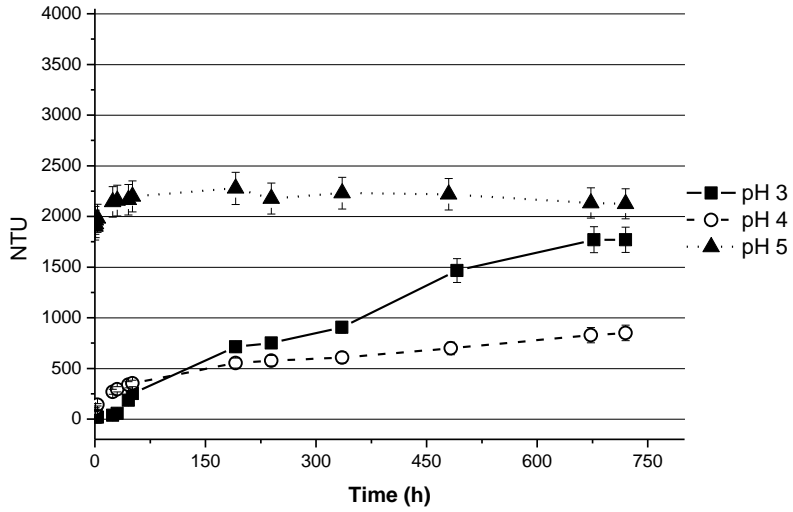


Figure 78. Turbidity measurement. Two-step process: influence of pH: 3, 4, 5; Kost = % TiO<sub>2</sub> (1%v/v), % Chitosan (0.25%wt).

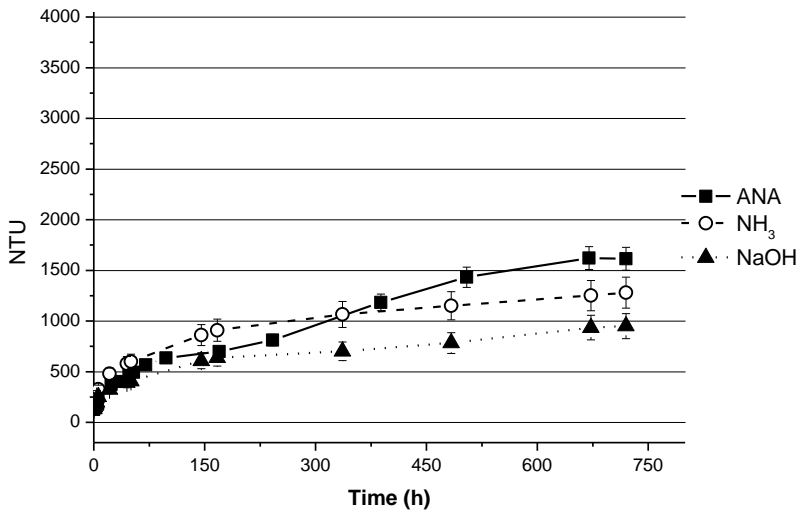


Figure 79. Turbidity measurement. Influence of different alkali: CH<sub>3</sub>COONA (AcA), ammonia NH<sub>4</sub>OH (NH<sub>3</sub>) and NaOH. Kost = % TiO<sub>2</sub> (1%v/v), Chitosan (0.25%wt).



#### 5.3.1.4 Viscosity measurement

All the samples realized shown higher viscosity than water, that is about 0.001 Pa x s at 20°C. The most of samples have a viscosity between 0.002-0.004 Pa x s that is very similar. Nevertheless, some interesting comment can be do. The most interesting results of two-step preparation are following reported.

Weak differences are observed comparing the samples realized with or without chitosan for different % of buffer (Figure 80, Figure 81), as well as the percentage of buffer used doesn't seem influenced the viscosity of the solutions (Figure 82). Slight differences are obtained comparing the viscosity results of the sample prepared with at 6% and 18% of buffer. In particular, difference in the viscosity are observed only for the higher concentration of precursor used.

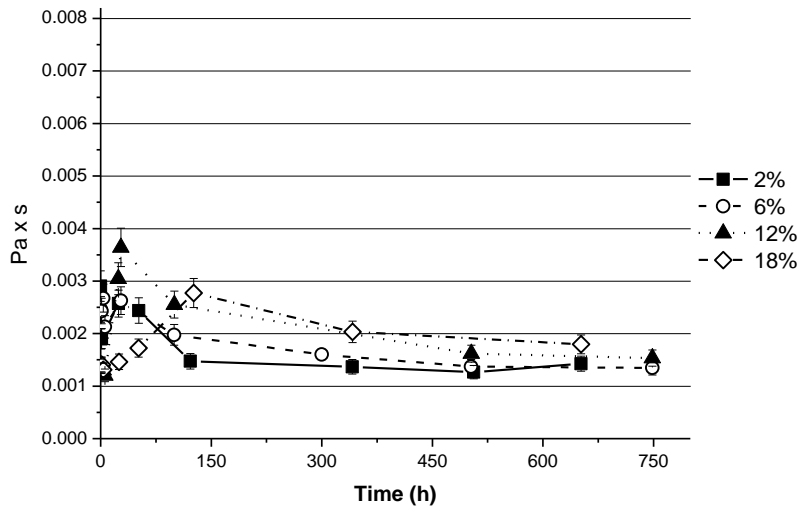


**Figure 80.** Viscosity measurements. Influence % Buffer (2%, 6%, 12%, 18%). Kost = %TiO<sub>2</sub> (1%v/v) at pH 4.

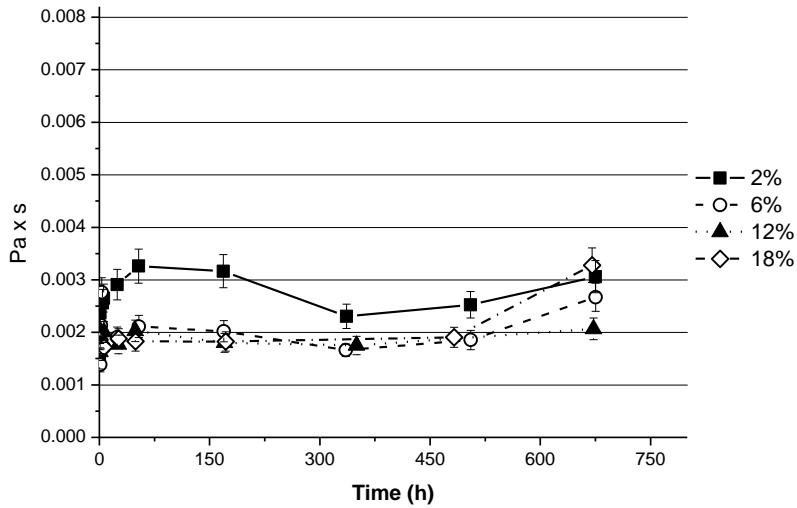


**Figure 81.** Viscosity measurements. Influence % Buffer (2%, 6%, 12%, 18%). Kost = % TiO<sub>2</sub> (1%v/v), chitosan (0.25%wt) and pH 4.

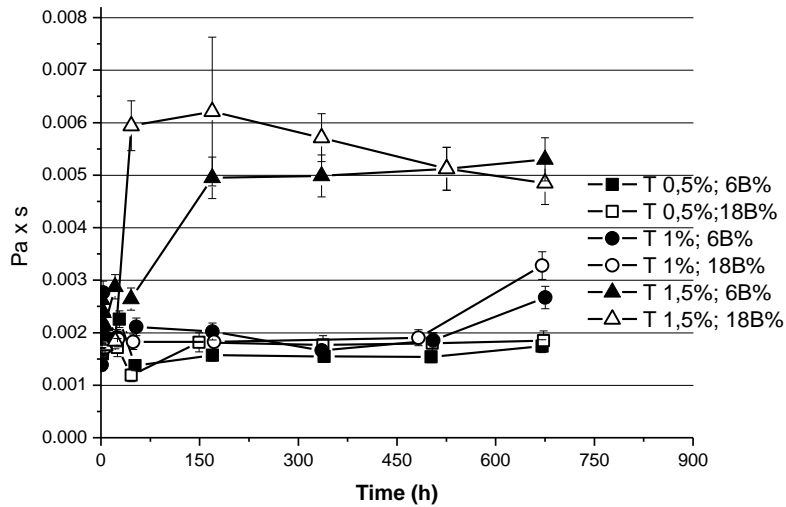


**Figure 82.** Viscosity measurements. Relationship % TiO<sub>2</sub> (0.5%, 1%, 1.5%v/v) Vs %Buffer CH<sub>3</sub>COOH/CH<sub>3</sub>COONa (6% and 18%). Kost = 0.25%wt chitosan at pH 4.

0.25%<sub>wt</sub> and 0.5%<sub>wt</sub> of chitosan in solution don't influence the sol viscosity that is about 0.02 Pa x s (Figure 83). Nevertheless, the viscosity of the sol prepared with chitosan (0.125%) is about 0.4 Pa x s. it is due to the strong aggregation reaction in involving chitosan.

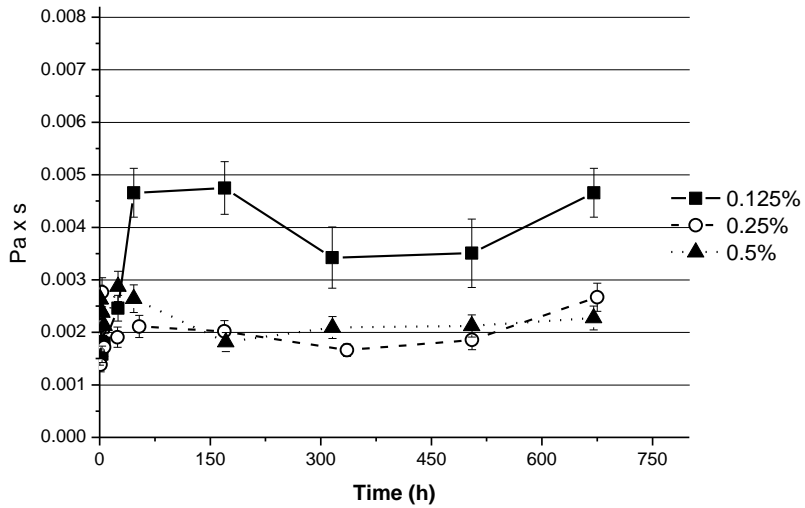


**Figure 83.** Viscosity measurements. Influence % Chitosan (0.125%, 0.25%, 0.5%wt). Kost = % buffer  $\text{CH}_3\text{COOH}/\text{CH}_3\text{COONa}$  (3%),  $\text{TiO}_2$  (1%v/v), at pH 4.

Slight differences of viscosity are also observed for the samples prepared at pH 3, 4 and 5. In particular, lower values are reported for the pH 4 while the higher values are obtained for the sample at pH 5 (Figure 84).

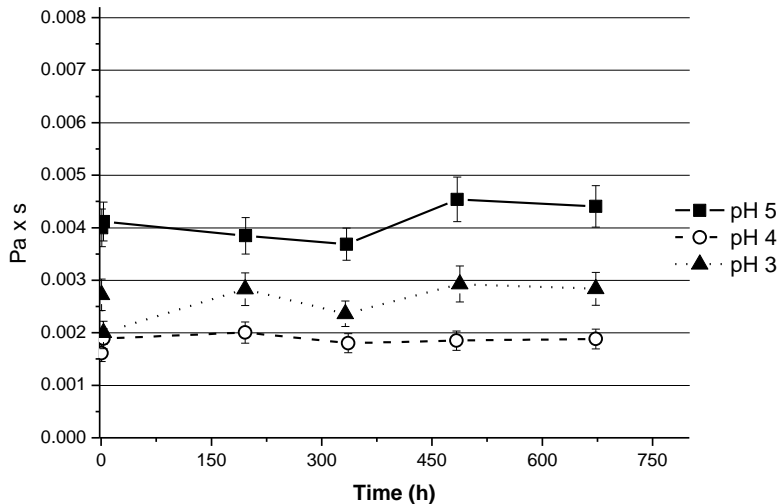


**Figure 84.** Viscosity measurements. Two-step: influence of pH: 3, 4, 5. Kost:  $\text{TiO}_2$  (1%v/v), %Chitosan (0.25%wt).

The Figure 85 and Figure 86 show the changing in the viscosity at different mass ratio of %TiO<sub>2</sub>:%buffer (1:2) and %chitosan:%Buffer (1:48), respectively. The viscosity of the sample 1.5:18 (%TiO<sub>2</sub>:%buffer) and 0.25:12 (%chitosan:%Buffer) is 0.06 Pa x s and 0.04 Pa x s, respectively. All other samples the viscosity is similar and it is equal 0.02 Pa x s.

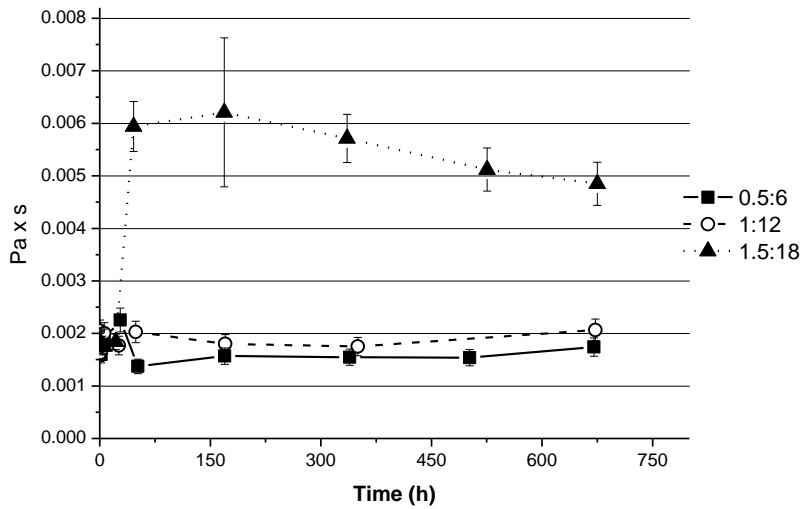


Figure 85. Viscosity measurements. Mass Ratio; % TiO<sub>2</sub> : %Buffer = 1:12. Kost = chitosan (0.25%wt) at pH 4.

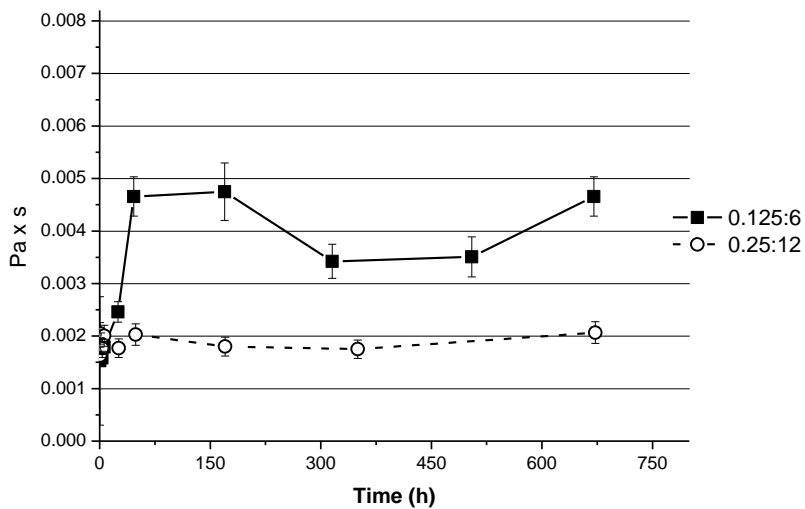


Figure 86. Viscosity measurements. Mass Ratio; % Chitosan : %Buffer = 1:48. Kost = %TiO<sub>2</sub> (1%v/v) at pH 4.

No difference in the sol viscosity are obtained compare the sample prepared with several alkali at pH 4, synthesized at 95°C and with mass ratio % Chitosan : % TiO<sub>2</sub> = 1:2. The viscosity is about 0.02 Pa x s.

### **5.3.2 Part B: Optical and photo activity characterization**

#### **5.3.2.1 Surface characterization**

In order to find evidence of any relevant change in the fabric surface due to treatments with the hybrid sols, analysis by scanning electron microscopy (SEM) was performed. Images for treated and untreated cotton fabrics are shown in Figure 87 SEM measurements were carried out to investigate the difference between the surfaces of the untreated cotton fabric and the modified nano-TiO<sub>2</sub> samples, both undoped and doped by PEG. The textile surfaces (Figure 87B, D) treated by undoped sols for both the concentrations used (0.025 M and 0.25 M) show agglomerated particles and several fractures in the titania coating, that disappear when PEG is added in the sols indicating excellent inter-particle connectivity and high inter-layer attachment. The presence of PEG in both sols makes the hybrid thin film more homogeneously distributed on the fiber surface (Figure 87C, E).

The composition of the films was determined by energy dispersive X-ray analysis (Figure 88). For treated cotton fabric surfaces, titanium and anion of the catalyst acid were the only detected elements in addition to fabric reference.

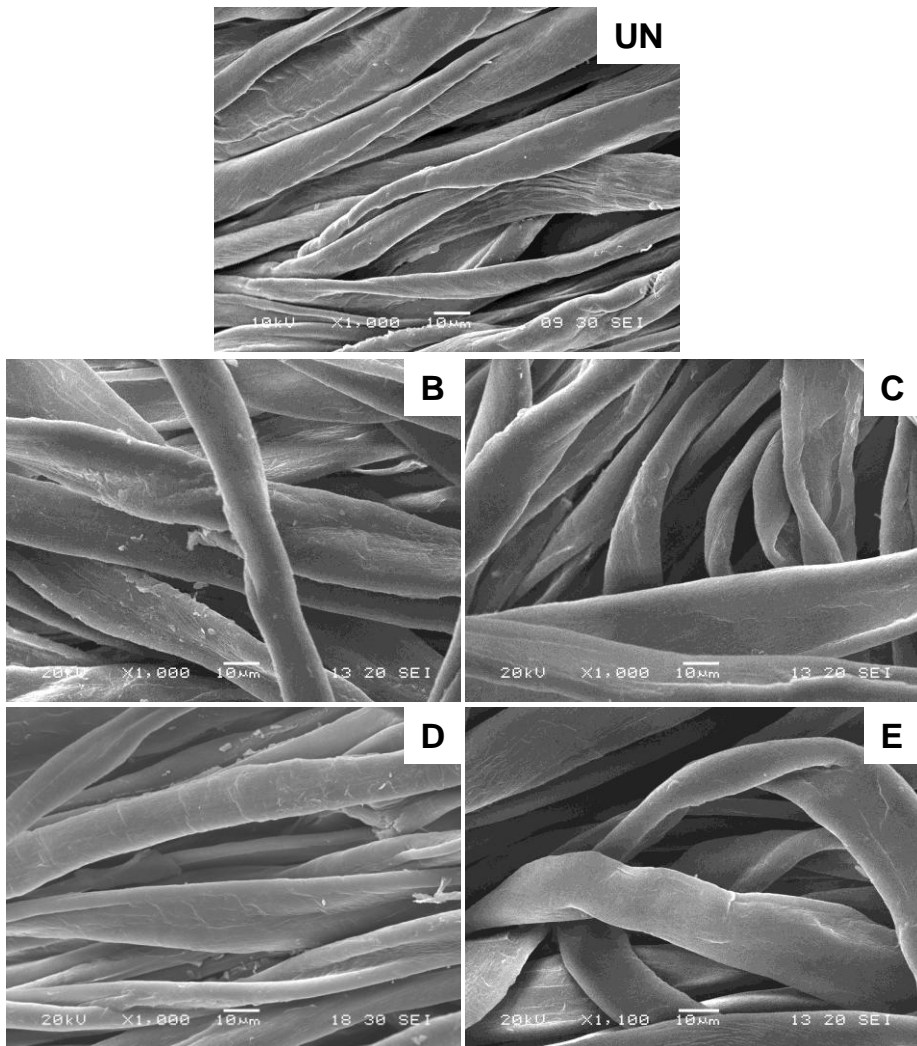


**Figure 87.** SEM images of cotton samples: UN) cotton fabric untreated; cotton fabric samples treated by: B) 0.025M HCl TiO<sub>2</sub> sol, C) 0.025M HCl TiO<sub>2</sub> sol doped, D) 0.25M HCl TiO<sub>2</sub> sol, E) 0.25M HCl TiO<sub>2</sub> sol doped.

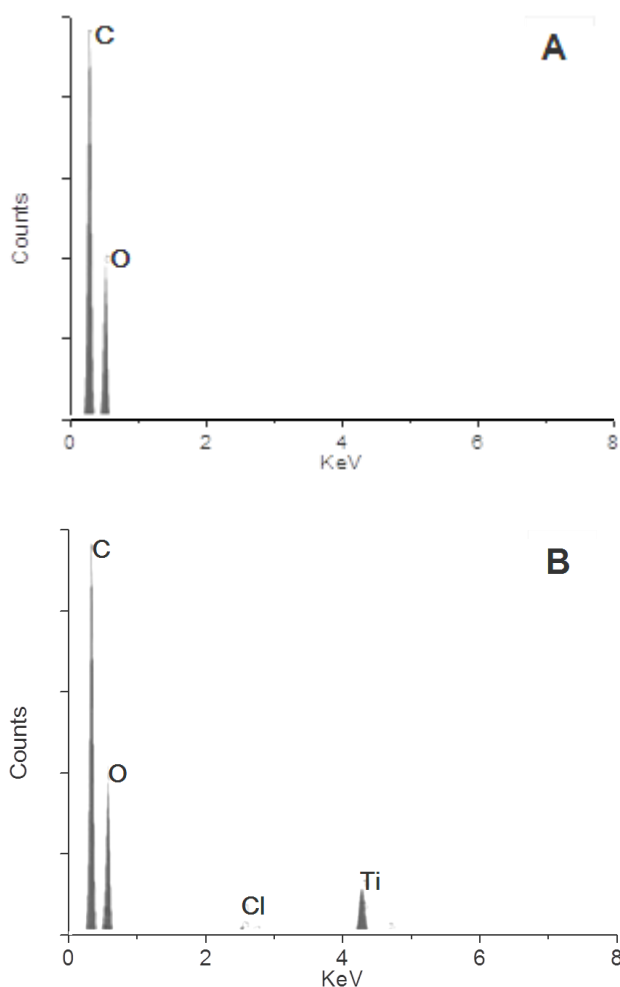


**Figure 88.** EDX spectrum for untreated (A) and treated by HCl TiO<sub>2</sub> sol (B) cotton fabric surface.

### 5.3.2.2 Optical characterization

Optical properties were investigated in the UV and visible region by the diffuse reflectance spectra measurement from 250 nm to 800 nm and results are shown in Figure 89 and Figure 90. The presence of TiO<sub>2</sub> on all treated samples is confirmed by the strong light absorption in the UV region when compared to the untreated samples. For all reflectance curves of the treated samples, three distinct zones can be identified: a first zone ( $\lambda < 300$  nm) with a strong absorption characteristic of TiO<sub>2</sub>, a second zone ( $300 \text{ nm} < \lambda < 400$  nm) of transition where the

reflectance value decreases quickly, and a third zone ( $\lambda > 400$  nm) with low absorption values. Particularly, comparing the samples realized with the same concentration (0.25 M and 0.025 M  $\text{TiO}_2$  sol) with and without PEG (Figure 89A, B), the absorption spectra have shown a general overlapping.

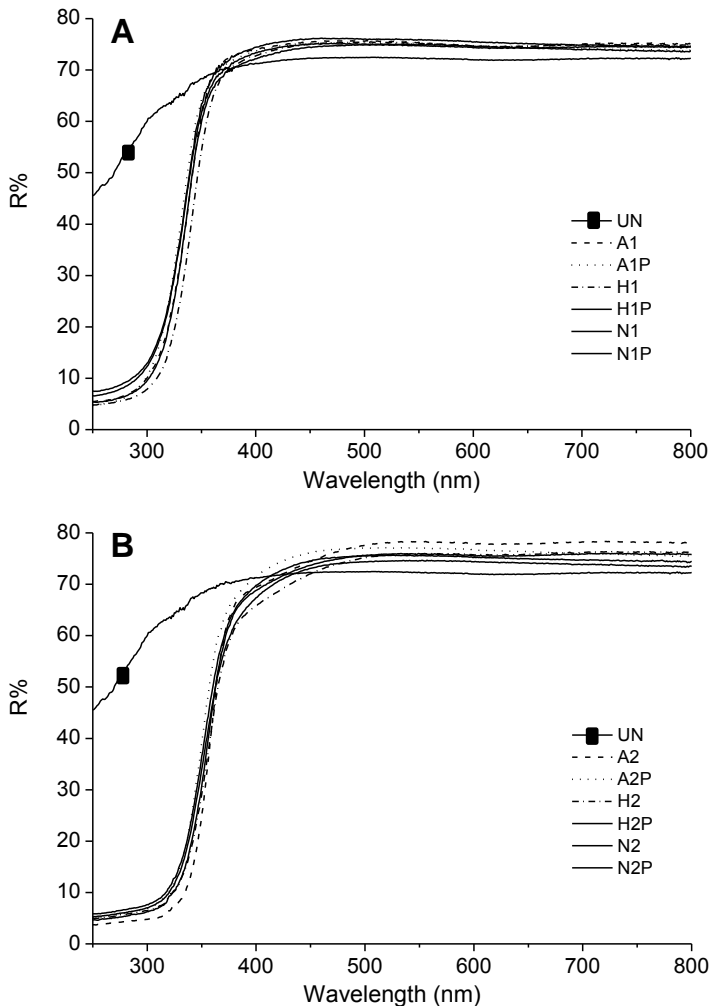


**Figure 89.** Diffuse reflectance spectra of treated sample. A) doped/undoped  $\text{TiO}_2$  (0.25M) samples; B) doped/undoped  $\text{TiO}_2$  (0.025M) samples.

On the other hand, comparing the influence of the concentration of each sol using different acid on reflectance spectra (Figure 90A, B), a strong blue shift of about 25 nm was found for the fabrics treated with 0.025 M  $\text{TiO}_2$  sol. In the  $\text{TiO}_2$  semiconductor the shift of the absorption onset, corresponding to electron transition



from the top of valence band to the bottom of conduction band, has been thoroughly explained by quantum confinement in thin layers [140].

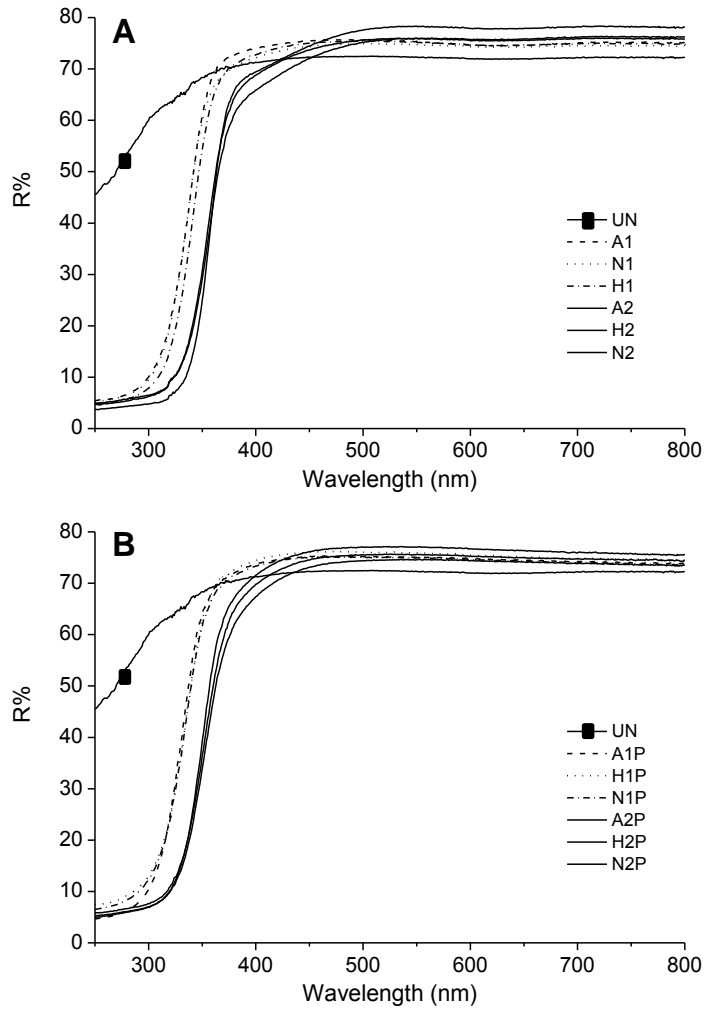


**Figure 90.** Diffuse reflectance spectra of treated sample. A) 0.025/0.25M TiO<sub>2</sub> samples; B) doped 0.025/0.25M TiO<sub>2</sub> samples.

To investigate the crystal phase composition of TiO<sub>2</sub> thin film realized on cotton fabric in the different conditions, XRD analysis was performed. The known bulk structure of titanium oxide, such as anatase, rutile, and brookite were not detected by XRD. No detectable diffraction peaks and the XRD pattern of the treated samples didn't reveal any difference with cellulose. Although it is not possible to exclude the presence of some undetected short range order, these films

can be called amorphous [141,142]. All samples (acid, PEG, concentration) have shown the same XRD pattern with amorphous characteristics. This indicates that the recipe preparation and the conditions used in the application process seem not to change the crystalline structure of the titania coating from amorphous to anatase and rutile forms, what is normally carried out by increasing the temperature of calcinations or by other methods, like low temperature hydrothermal treatment [143,144,145]. Since XRD analysis of treated and untreated samples has shown the same pattern, Tauc plot analysis was realized in order to further study the local structure of the TiO<sub>2</sub> based amorphous film and to investigate differences in the energy gap of each sample. The band gap energy of the thin films have been obtained by plotting the modified Kubelka–Munk function against the energy of excitation source, where the band gap is obtained from the intercept of energy axis at Y = 0 as shown in Figure 91 for H1, H2, H1P and H2P samples. The energy gap values of all samples are reported in Table 25.

**Table 25.** Energy gap of TiO<sub>2</sub> thin film  $E_g \pm 0.01$  eV.

TiO <sub>2</sub> conc. (M)	Acids	No PEG		PEG	
		Code	Energy Gap (eV)	Code	Energy Gap (eV)
0.025	Hydrochloric	H1	3.51	H1P	3.53
	Nitric	N1	3.52	N1P	3.53
	Acetic	A1	3.53	A1P	3.62
0.25	Hydrochloric	H2	3.34	H2P	3.37
	Nitric	N2	3.36	N2P	3.38
	Acetic	A2	3.37	A2P	3.42

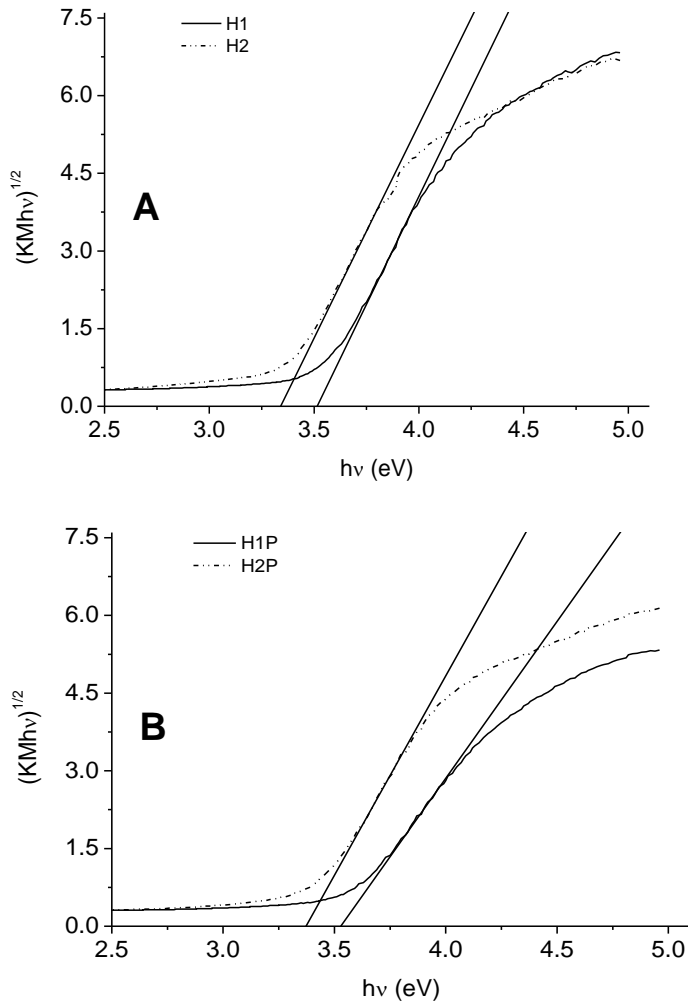


**Figure 91.** Energy gap of H1, H2, H1P and H2P measured by Tauc plot analysis.

The calculated band gap energy values are found to be in the range of 3.3 – 3.6 eV which are higher than the values usually accepted for the crystalline  $\text{TiO}_2$  phases like anatase and rutile crystals, respectively 3.2 eV and 3.02 eV [146]. This is in agreement with the results observed from XRD analysis and reflectance spectra mentioned before that have shown a non crystalline thin film. In particular, comparing data at constant concentration, the difference in the band gap among mineral acids and organic acid is negligible for undoped sols, whereas samples containing PEG show slightly higher values. In fact, e.g. for 0.25 M  $\text{TiO}_2$  samples

the energy gap values have been found about 3.38 eV (H2P and N2P) and 3.42 eV (A2P) for the mineral and organic acid respectively, while for 0.025M sols they were 3.53 eV (H1P and N1P) and 3.62 eV (A1P). In particular, even if in some cases exist very small differences between the  $E_g$  values, some interesting similar trends can be observed. In fact, an increase in the semiconductor band gap can be measured when PEG or acetic acid are used individually or together: the highest values are observed when both of them are used together for each  $\text{TiO}_2$  concentration. This increase in the band gap energy with increasing the content of PEG and acetic acid can be attributed to structural interruption in the titania framework by these molecules resulting in larger energy gap between the valence band and conduction band which reduces the recombination rate of electrons and holes at the time of UV exposure [147]. The addition of PEG to hydrolyzed precursor could bring to the formation of titanium glycolate complex that is not present in the inorganic network of titania as shown in Figure 92.

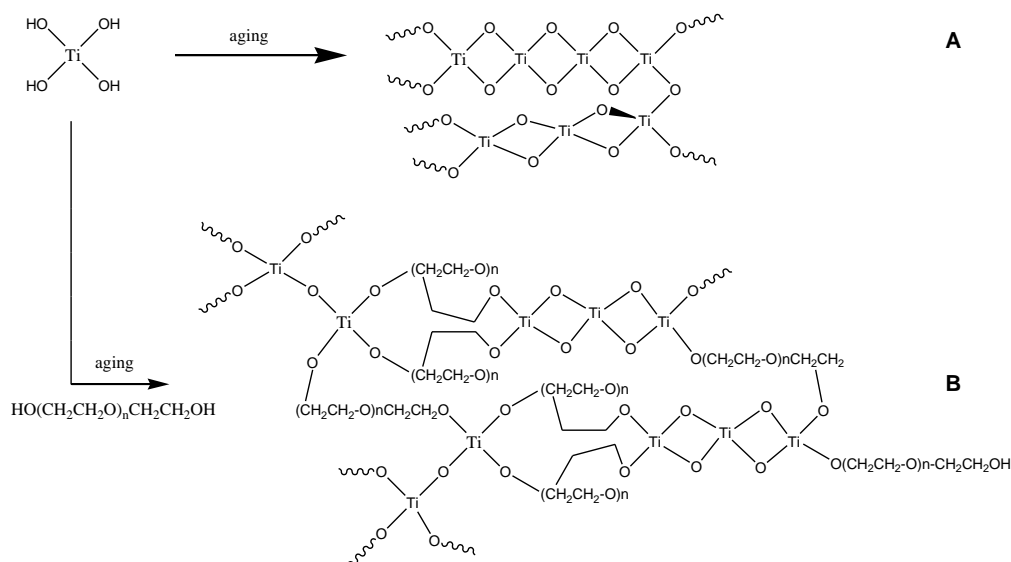


**Figure 92.** Schematic illustration of  $\text{TiO}_2$  inorganic network (A) and a possible mechanism of cross linked titania glycolate (B).

The literature reports [148] that amorphous titanium glycolates with well defined rod-like or plate-like microstructures having hexagonal and cuboidal facets could be thus obtained at room temperature. Of course the characteristics of the sol

depend on the time of stirring, the kind of polyethylene glycol used and the aging of mixture of titanium alkoxide. This assumption could be in agreement with the XRD pattern observed for the doped  $\text{TiO}_2$  samples, where no distinct diffraction peak were detected. Moreover, as well known, the transformation from amorphous titanium glycolate to anatase occurs in the range of 450–550°C; while the phase transformation from anatase to rutile takes place between 750°C and 880°C. The sols synthesized and tested in this research were instead prepared at room temperature and cured onto textile fabric at 120°C. So, using the  $\text{TiO}_2$ -PEG sols a complete inorganic matrix was not realized but only a  $\text{TiO}_2$  cluster break from organic PEG structures, as confirmed by several papers [149], where PEGs are commonly used like templates to realize a high porosity crystalline  $\text{TiO}_2$  after calcination at high temperature. This could be the reason why the titania amorphous structure shows a weakly shift of the energy gap values. At the same time, the acetic acid does not act only as an acid catalyst like  $\text{HCl}$  and  $\text{HNO}_3$ , but also as a ligand and changes the alkoxide precursor at the molecular level, therefore modifying the whole hydrolysis condensation process. Acetate can act as a chelating ligand and react, with the titanium alkoxide precursor to form  $\text{Ti}(\text{OR})_x(\text{AC})_y$  according to the scheme reported in Figure 54 [150]. It is following reported:

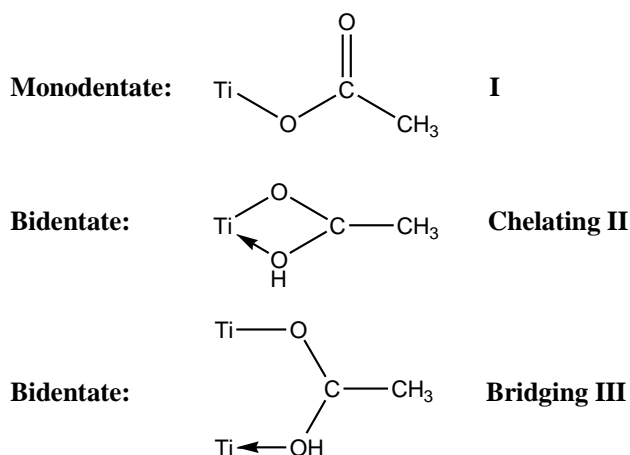


Figure 93. Possible reactions of the acetate anion with Titanium [Figure 54].

Since chelating acetates can only be removed upon heating above 200°C, temperature that has never been used in this research, the presence of these bonds in our acetate TiO<sub>2</sub> matrices could be confirmed. Finally, also the concentration of the sol plays an important role. In fact, the energy gap values between 3.51-3.62 eV regarding the samples treated by 0.025 M sols are higher than the energy gap of the samples treated by 0.25 M sols (3.34 - 3.42 eV). The larger band gap is normally explained by the quantum size effect, which results in a shift of the band gap to higher values for grain sizes smaller than 20 nm [151].

Sol concentration influences also the amount of TiO<sub>2</sub> deposited (add-on%) onto textile fabric after the application of the solution. For samples treated with 0.025M TiO<sub>2</sub> sols (with and without PEG) an add-on% of about 0,20% for all types of acid used was observed (Figure 94), while for the 0.25 M sols add-on% values were influenced by the presence of PEG and by the nature of the acid used. In fact, in the presence of HCl and HNO<sub>3</sub> add-on% were 2.5% and 1.4% respectively for the sols with and without PEG, whereas in the presence of acetic acid under the same condition the values were equal to 3.5% and 2.3%. The highest add-on% measurement is probably due to the presence of CH<sub>3</sub>COO<sup>-</sup> anion into the matrix network.

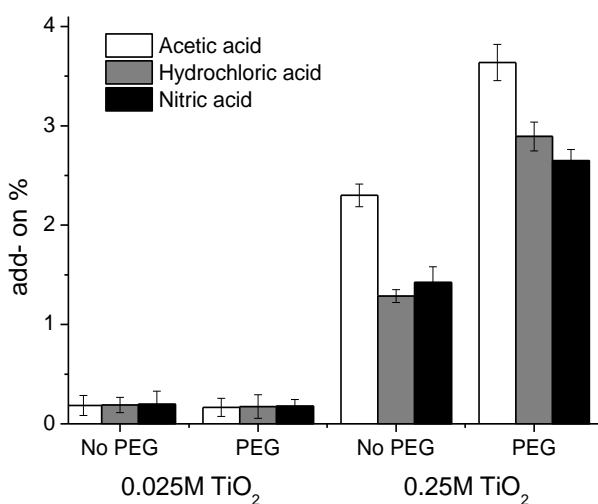


Figure 94. Add-on % on textile fabrics.

### 5.3.2.3 Photodegradation of dyestuff

The photocatalytic activity of the TiO<sub>2</sub> films on cotton fabric have been investigated under UV and visible sources. The detailed mechanism of the photocatalytic oxidation process has been widely discussed by many authors. As well known, TiO<sub>2</sub> excites electrons from the valance band to the conduction band when irradiated by UV light, whenever the light energy is greater than the band gap energy (e.g. Eg: 3.2 eV). The resulting electrons and holes can be separated to participate in a red-ox reaction with chemicals coming from the outside. For example, when water is added, oxygen is reduced to a super-oxide radical and a hydroxyl ion is oxidized to a hydroxyl radical. Photocatalytic degradation of organic substrates as dyes is due to the combination of these radicals with highly oxidant species (peroxide radicals). Being the resulting •OH radical a very strong oxidizing agent (standard redox potential +2.8 V), it can quickly oxidize most of azo dyes to the mineral end-products. In heterogeneous photocatalysis a similar role of reductive pathways has been also observed in the degradation of several dyes even if with a minor relevance than oxidation.

Figure 95 shows the percentage of dyestuff degradation under UV exposure as a function of exposure time for samples prepared from different sols with organic and mineral acids, undoped (Figure 95A) and doped (Figure 95B). In all cases, there is an evident influence on the dyestuff degradation rate by the acid used especially for the undoped samples. In fact, after only 30 minutes of UV exposure it is possible to observe a degradation rate correlated to the acid used according to the order: H > N > A. This influence becomes more pronounced increasing the exposure time and it is proportional to the concentration of sol used for the samples preparation. After 2 hours of exposure, samples realized by 0.25 M sols showed an enhancement of degradation kinetic from organic acid to mineral acid film: it was equal to about 50%, 35% and 20% for H, N and A, respectively. However, the complete degradation of the dye applied onto the sol treated fabrics has never been observed. This is in agreement with the TiO<sub>2</sub> loading on the substrate and, consequently, with the thickness of the film applied on the textile fabrics. As well known from the open literature, the loading of TiO<sub>2</sub> and the thickness of film could strongly influence the photocatalytic activity. Nevertheless, in some cases a reduction of the activity at

higher catalyst loading is reported maybe due to deactivation of activated molecules by collision with ground state molecules.

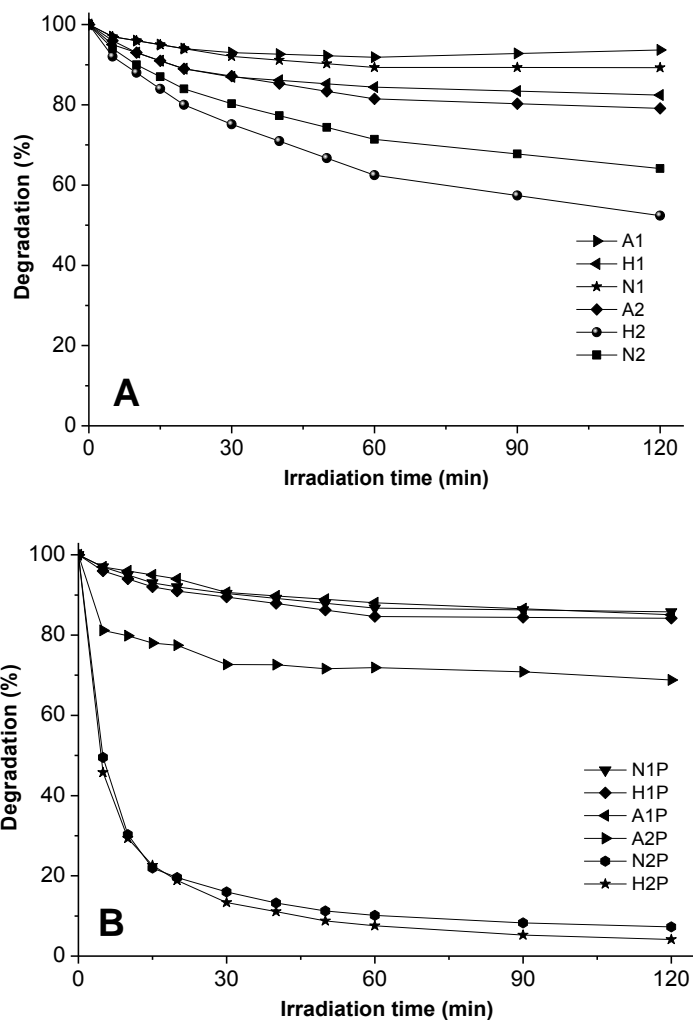


**Figure 95.** Photocatalytic activity undoped  $\text{TiO}_2$  treated samples by: 0.25M  $\text{TiO}_2$  and 0.025 M  $\text{TiO}_2$  sols. UV source.

Moreover, a good correlation seems to be observed plotting the rate of bleaching ( $k$ ) against  $\text{pK}_a$  of acids, Figure 96. In particular, better  $R^2$  is obtained for 0.25 M  $\text{TiO}_2$  samples ( $R^2=0.99$ ) than 0.025 M  $\text{TiO}_2$  samples ( $R^2=0.96$ ).



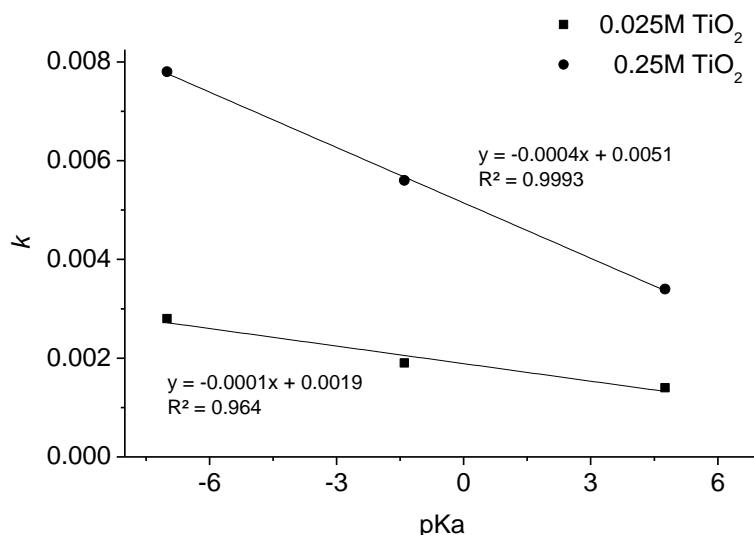


**Figure 96.** Relationship between pKa and  $k$  (for Hydrochloric, Nitric and Acetic acids, from left to right) of undoped TiO<sub>2</sub> treated samples.

The addition of PEG (Figure 95B), proportionally to the concentration of the sols used, dramatically increases the dyestuff degradation rate under UV light, particularly with mineral acids, while organic acids seem to have a lower influence. Nevertheless, it was not possible to verify a correlation between the rate of bleaching and pKa of the acids used. The effect of PEG is already evident after 5 minutes: the dyestuff degradation on treated fabrics with mineral acid doped sols is about 50%. After 60 minutes the bleaching rate decreases and after two hours of UV light exposure dyestuff complete degradation was observed only for the samples treated in the mineral acid sols.

Figure 97 shows the rate of decomposition under visible source for the samples treated by different sols with organic and mineral acids, undoped (Figure 97A) and doped (Figure 97B). In all cases, except for 0.25 M doped treated samples in the presence of mineral acids (H<sub>2</sub>P and N<sub>2</sub>P), the bleaching rates are particularly slow and only after two hours of exposure a difference can be appreciated. Even under visible exposure the faster dyestuff degradations are observed for the samples treated by hydrochloric or nitric acid TiO<sub>2</sub> sols synthesized with PEG confirming the effect of the polyethylene glycol. However, differently from UV-light

exposure, even after two hours of exposure under visible light a complete dyestuff degradation didn't take place.

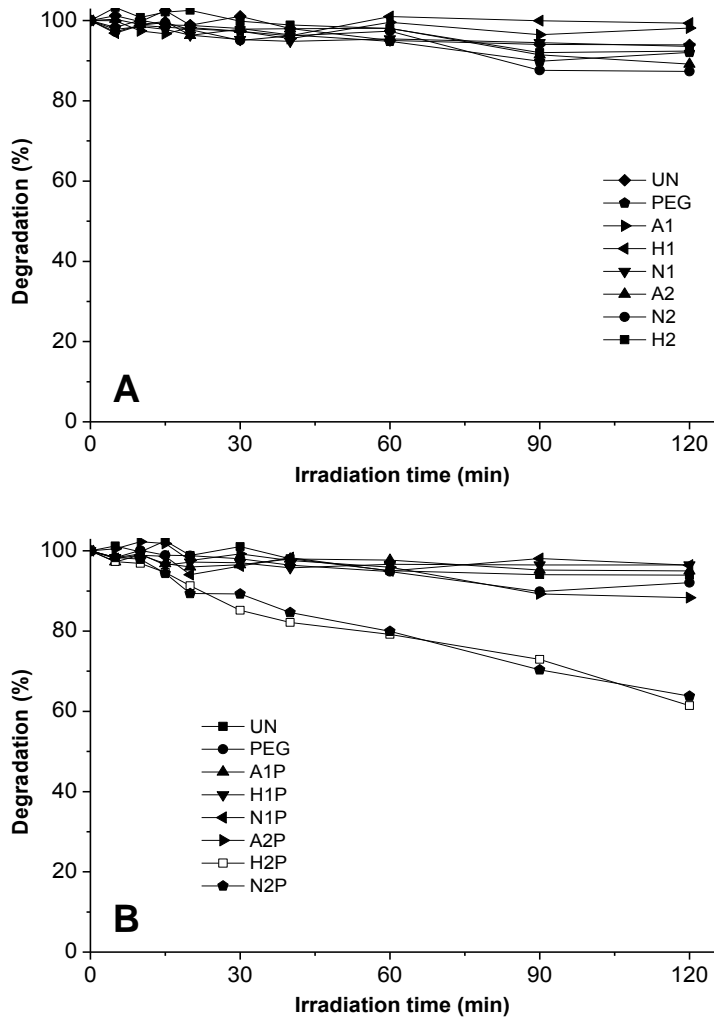
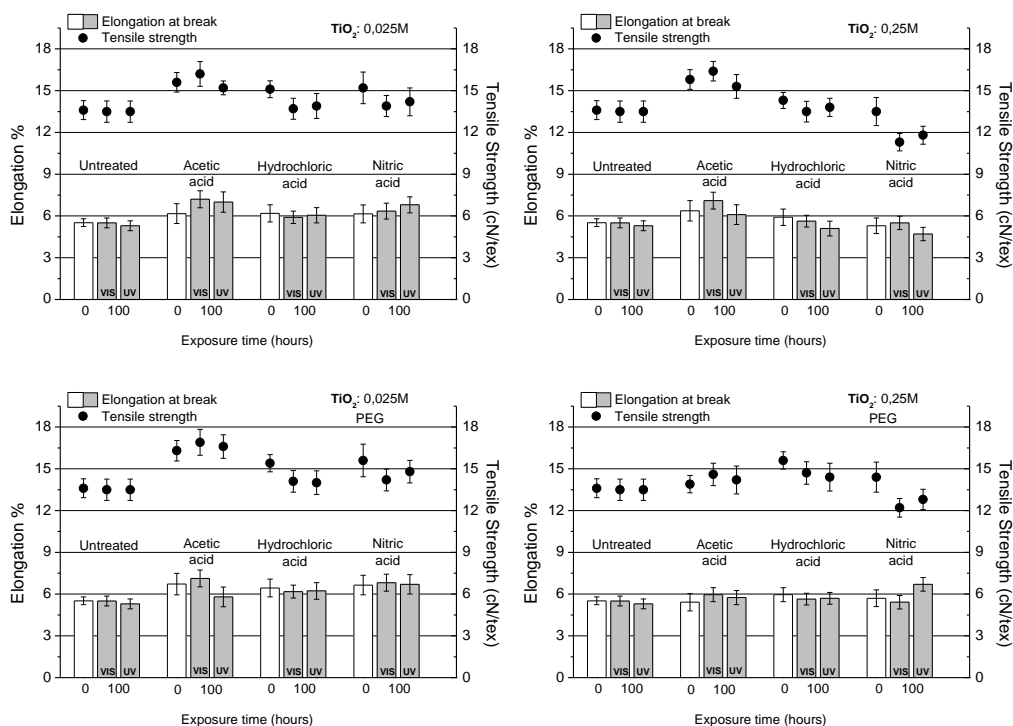


Figure 97. Photocatalytic activity undoped TiO<sub>2</sub> treated samples by: 0.25M TiO<sub>2</sub> and 0.025 M TiO<sub>2</sub> sols. Visible source.

#### **5.3.2.4. Mechanical properties**

Usually, most chemical finishes applied to fabrics cause undesirable changes in fabric performance such as decrease in tensile properties. Since the photocatalytic activity of the applied films could influence mechanical properties of the treated fabrics, all samples were checked before and after exposure under UV and visible light. The textile properties, such as elongation and tensile strength are discussed and the results are reported in Figure. 98. As evidenced in Figure. 98, mechanical properties variations as bis as 15% as a maximum are reported after the application of the film on the fabric, compared to the untreated cotton sample. Similar differences are observed between the samples before and after 100 hours of exposure under visible light. However, the rate of modification depends on the sol-gel used like catalyst, sol concentration, presence of PEG and irradiating source. Generally, cotton fabrics treated by acetic acid sols show an interesting increase in the tensile strength values after the exposure under visible exposure. A possible reason could be the formation of esteric bond due to a possible radicals reaction between the acetic anion and the hydroxyl groups on the fabric surface. This reaction could partially modify the cellulose ring and consequently the mechanical properties. At the same time, the samples treated by the mineral acid sols show a reduction of mechanical properties in particular under visible exposure compare to sample treated by sol catalyzed with acetic acid. In particular under both visible and UV exposure, all fabrics treated using sol catalyzed with nitric acid show the worst tensile strength performances, while it doesn't seem to influence strongly the elongation properties. As expected, a certain decrease in the tensile strength has been observed. Such a decrease could be tolerable for home-textile and most technical textile, even if it could be critical for architectural textiles.



**Figure 98.** Mechanical properties of treated and untreated samples before and after visible/UV exposure for 100 hours.

## 5.4 Conclusion

In part A, stable aqueous titania sols were sensitized without the addition of alcohols, glycol or acetyl acetone at suitable pH for the industrial application. The stability of sols were investigate using dynamic light scattering analysis, turbidity and rheological measurements. Different synthesis sol condition such as, acetate buffer and  $\text{TiO}_2$  precursor concentrations, synthesis temperature and route of preparation, were study to evaluate possible effect on the sol stabilization with or without chitosan used as stabilizer. The stability of the aqueous  $\text{TiO}_2$  sols depends strongly on the sol-gel route, single-step o two-step as well as the pH values of the solution. The use of acetate buffer seems to increase the stability of the sol as it improves when chitosan is added. This increase of stability could be attributed to the interaction occurs between chitosan,  $\text{TiO}_2$  and acetate in the sol. Acetate buffer reacts with  $\text{TiO}_2$  precursor to form  $\text{Ti}(\text{OR})_x(\text{AC})_y$  that is more difficult to hydrolyze than the OH functional group. Chitosan could reduce the formation of bidentate

acetate-TiO<sub>2</sub> species and interfere in the aggregation phenomena (or particles growth) for steric hindrance. Increasing the TiO<sub>2</sub> concentration the sol stability is reduced while high synthesis temperature can be useful to have stable sol.

In part B, twelve different TiO<sub>2</sub> sols were synthesized for modification of textile cotton from titanium tetraisopropoxide using: three different starting acidic solutions (nitric, hydrochloric and acetic acids) as well as the addition of PEG-1000 onto two different (0.25 M and 0.025 M) concentration. All synthesis were carried out at room temperature and then applied onto textile fabrics at 120°C for 5 minutes. SEM observation analysis of coated TiO<sub>2</sub> textile samples showed that cotton fibers are uniformly covered. From the performed surface and the structural characterization it can be inferred that no crystalline phases are present in the coatings. The optical analysis performed by Tauc plot model show energy gap in the range of 3.3 eV and 3.5 eV which is higher than the values for anatase (3.2 eV). The photocatalytic activity increases: 1) increasing the concentration of the precursor used; 2) moving from acetic to nitric and finally to chloride acid; 3) using PEG as dopant in presence of mineral acids; 4) using UV source than visible light. In fact the slowing down of the decomposition at longer wavelength is evident, while the trend in the decomposition is maintained. The concentration and, consequently, the amount of TiO<sub>2</sub> on the substrate seems to play a fundamental role on the photocatalytic activity. The results for the 0.25 M TiO<sub>2</sub> sols, doped or undoped, don't show remarkable effect in the dyestuff bleaching. This does not mean the 0.025 M TiO<sub>2</sub> films cannot have a photocatalytic activity, but only that it is not possible to observe significant effects for the dyestuff concentration used after 2 hours long light exposure.

The PEG addition into mineral sol-gel solution increases dramatically the rate of dye degradation under UV exposure while it is less evident under light exposure. Moreover, the rate of degradation of undoped TiO<sub>2</sub> films seems to show an interesting linear correlation with pKa of the acid used. Finally, an expected decrease in the mechanical properties (lower than 15%) was observed after 100 hours of visible or UV light exposure. This acid polyethylene glycol-based sol-gel method could be useful in the preparation of TiO<sub>2</sub> fabric finishing with high photocatalytic activity for self-cleaning or environmental applications. Anyways further investigation are necessary to study the observed crystalline phase and the influence of polyethylene in the photocatalytic properties.

# Conclusion

Organic-inorganic hybrid thin films based on silica sols were developed by sol-gel process for flame retardant, hydro-repellent and self cleaning fabrics. The proposed hybrid compounds for textile finishing may be helpful for the development of new finishes, constituting a valid alternative to the well established commercially available treatments of textile. In fact, traditional treatments have several disadvantages: halogen flame retardants are hazardous materials for the workers during production and application as well as for the end-user who wears the treated cloths. Moreover, they can be responsible of water pollution. On the other hand, fluorocarbon compounds, that are the most used chemicals to confer hydro-repellent properties, are high expensive and a potential risk for human health in case of skin contact and for the environment in case of any emission of fluorine compounds during and after the textile impregnation. For these reasons a part of the research activity was focused on the development of halogen free flame retardant and fluorocarbon free hydro-repellent finishes.

The sol finishes can be easily applied with equipments already present in the textiles industry, allowing the company to save money. Moreover, they require a lower temperature for curing (120°C - 150°C) than traditional finishes (150°C - 170°C). In particular, the application of sols with hydro-repellent or self cleaning features can reduce the maintenance cost of fabrics and, consequently, they can be considered energy saving. Sol finishes can be used to impart multifunctional properties onto treated textile, mixing different organic molecules functionalizing or choosing appropriately the inorganic precursor. In this way, multifunctional properties has been realized with TiO<sub>2</sub> film onto cotton fabrics. Self cleaning and UV absorber properties have been obtained onto treated textiles.

Halogen free flame retardants hybrid films were realized on cotton fabrics as specific combination of silica precursors (APTES and DPTES), phosphorus donors (DEP and DPTES) and nitrogen donors (APTES and MF). The flame retardant study was developed using two main research approaches:

In the first one (part A) three new halogen-free hybrids finishes from the silica precursor with nitrogen functionality (APTES) were synthesized and used in order to develop flame retardant cotton fabrics. Starting from a sol containing

APTES, a second sol was obtained by addition of the diethylphosphite (DEP) to the first one; it was produced with the aim of exploiting the effectiveness of the P-N synergism in this system. Finally, in the third sol, the melamine derivate resin (MF) was added in order to enhance the adhesion of film on the fabric. The chemical structures of synthesized HOIMs were evaluated by FT-IR spectroscopy. Hydrogen bonding interaction were detected between the protonated functionality of silica precursor and the partially hydrolyzed diethylphosphite, while in the Si-P-C xerogel also covalent bonds linked the silica matrix to the M cross-linker. Thermal analysis of the treated cotton samples revealed that these sol-gel treatments are an efficient flame retardant finishing for cellulose fabrics producing a greater amount of char as compared to the untreated fabric both in nitrogen and in air atmosphere. In particular, a decrease of degradation temperature was observed for the fabrics treated with Si-P and S-P-C sols. The burning tests demonstrated that although the cotton sample treated with the pure silica sol burned, it left a residue replica of the original fabric structure. High levels of flame retardancy were observed for the hybrid Si-P and Si-P-C thin films: this positive effect was promoted by the remarkable char production due to the synergism phosphorus-nitrogen and also to the high cross-linking degree demonstrated by FT-IR spectra of samples pyrolyzed at 600°C. Unfortunately the proposed finishes showed a poor washing fastness due to weak interaction of DEP in the xerogel film.

In the second approach, hybrid phosphorus doped silica films on the cotton surface were obtained mixing a phosphorus silica precursor (DPTES) and N donors (APTES or MF). The phosphorus functionality is directly bonded with silica atom by covalent bond and, consequently, it cannot be removed so easily by washing cycles. Si-O-Si bonds of inorganic network, hydrogen bonding between phosphonyl groups and un-reactive OH groups of cellulose, and covalent bonds between silica matrix and melamine were observed by FT-IR. Thermal analysis showed significant enhancements of the thermal and thermo-oxidative stability of treated cotton, thanks to the formation of char, at the same time limiting the production of volatile species. All samples showed a reduced burning rate with a formation of a residue replica of original structure of the fabric.

Free fluorocarbon water repellent hybrid films were then realized onto cotton and PET fabrics using octyltriethoxysilane as precursor and melamine derivative resin as cross-linker. FT-IR spectroscopy confirmed the presence of xerogel films on

the fabric surface after deposition and polymerization of sols as well as after 5 washing cycles of the treated fabrics. In particular, the wash fastness of xerogel film depended on the chemical nature of fibers: a better adhesion was observed on the cotton fabrics. To have a better comprehension of the wettability of treated and untreated textiles, different tests were performed: contact angle, drop test, DuPont test and water uptake. The water repellency of the fabric was shown to be significantly influenced by cross-linker concentration and molar ratio MF:precursor. Generally, higher repellency properties were observed with the increase of both the MF concentration and molar ratio (synergistic effect resin-precursor). The best results were obtained using the sols prepared with 100 g/L of resin and 1:4 molar ratio (MF:precursor), whereas the films realized with 20 g/L of resins, especially for cotton, showed very low repellency. The treated polyester samples showed a contact angles and hysteresis between 130° - 150° and 10° - 20° respectively, while for cotton samples were in the range 120° - 130° and 15° - 25° except the sample at 20 g/L of resins that was hydrophilic.

The self cleaning study was finally developed in two main research directions. In the first one, stable aqueous titania sols were synthesized at suitable pH for the industrial application without the addition of alcohols, glycol or acetyl acetone. Preliminary tests were carried out to evaluate the stability at different pH conditions. Afterwards, acetate buffer solution was used to prepare at pH 4 the TiO<sub>2</sub> sols. The stability of sols was investigated using dynamic light scattering analysis, turbidity and rheological measurements. Different synthesis parameters such as acetate buffer and TiO<sub>2</sub> precursor concentrations, synthesis temperature and route of preparation, were studied to evaluate possible effects on the sol stabilization with or without chitosan. The stability of the aqueous TiO<sub>2</sub> sols was shown to strongly depend on the sol-gel route, single-step or two-step as well as the pH values of the solution. Stable TiO<sub>2</sub> sol was obtained only when titania precursor was directly dissolved in acetic acid and only after water has been added to reach the suitable pH (two-step process). The use of acetate buffer seems to increase the stability of the sol, because it was improved when chitosan was added. This increase of stability could be attributed to the interaction occurring between TiO<sub>2</sub>, acetate buffer and chitosan in the sol. Nevertheless, sol stability decreased when TiO<sub>2</sub> concentration was increased, whereas high synthesis temperature can be useful to have stable sol.



In the part B of the research, thin films based on  $\text{TiO}_2$  sols were developed by sol-gel process with high photocatalytic activity for self-cleaning or environmental applications. Different sols were synthesized for modification of textile cotton from titanium tetraisopropoxide using: three different starting acidic solutions (nitric, hydrochloric and acetic acids) as well as the addition of PEG-1000 (dopant) onto two different (0.25 M and 0.025 M) concentrations. All synthesis were carried out at room temperature and then applied onto textile fabrics at  $120^\circ\text{C}$  for 5 minutes. Morphological characterization revealed an homogeneous distribution of the doped films while several fractures were observed for the complete inorganic films. From X-ray diffraction performed on surface it can be inferred that no crystalline phases were present in the coatings. The optical analysis confirmed the absence of crystalline phase film. In fact, Tauc plot model showed energy gap in the range of 3.3 eV and 3.5 eV which is higher than the values for anatase (3.2 eV). The photocatalytic activity increased: 1) increasing the concentration of the precursor used; 2) moving from acetic to nitric and finally to chloride acid; 3) using PEG as dopant in presence of mineral acids; 4) using UV source than visible light. In fact the slowing down of the decomposition at longer wavelength was evident, while the trend in the decomposition was maintained. The concentration and, consequently, the amount of  $\text{TiO}_2$  on the substrate played a fundamental role on the photocatalytic activity. The results for the 0.025 M  $\text{TiO}_2$  sols, doped or undoped, did not show remarkable effect in the dyestuff bleaching. This does not mean that the 0.025M  $\text{TiO}_2$  films cannot have a photocatalytic activity, but only that it was not possible to observe significant effects for the dyestuff concentration used after 2 hours long light exposure. The bleaching rate of undoped  $\text{TiO}_2$  films seems to show an interesting linear correlation with pKa of the acid used which also depends on the concentration. The PEG addition into mineral sol-gel solution increased dramatically the rate of dye degradation under UV exposure while it was less evident under light exposure. The effect of titanium on the fabric properties was also addressed: an expected decrease in the mechanical properties (lower than 15%) was observed after 100 hours both visible and UV light exposure. Anyways further investigations are necessary to study the observed crystalline phase and the influence of polyethylene in the photocatalytic properties.

The developed textile treatments allowed to improve the fabric properties in the meanwhile maintaining the substrate mechanical properties. Moreover, water

and energy consumptions are reduced due to the use of sol-gel technique, resulting in more sustainable processes.



APPENDIX

**Figure 65. Single-step-process.**

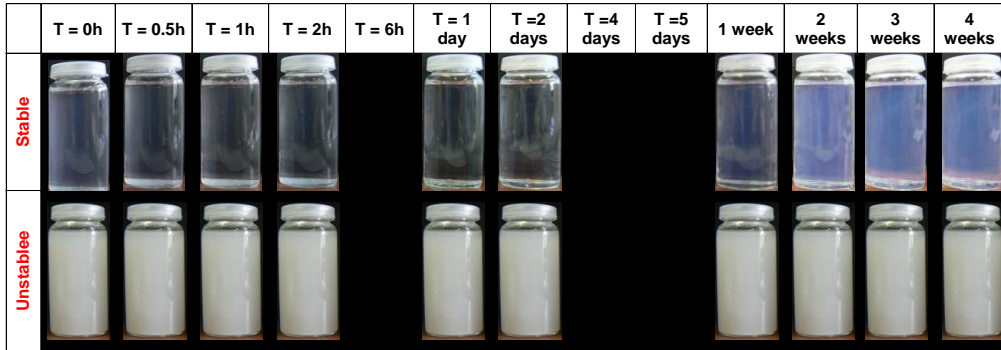


**Figure 66. Influence % Buffer (2, 6, 12, 18%).** Kost = % TiO<sub>2</sub> (1%v/v); pH 4; NO Chitosan.

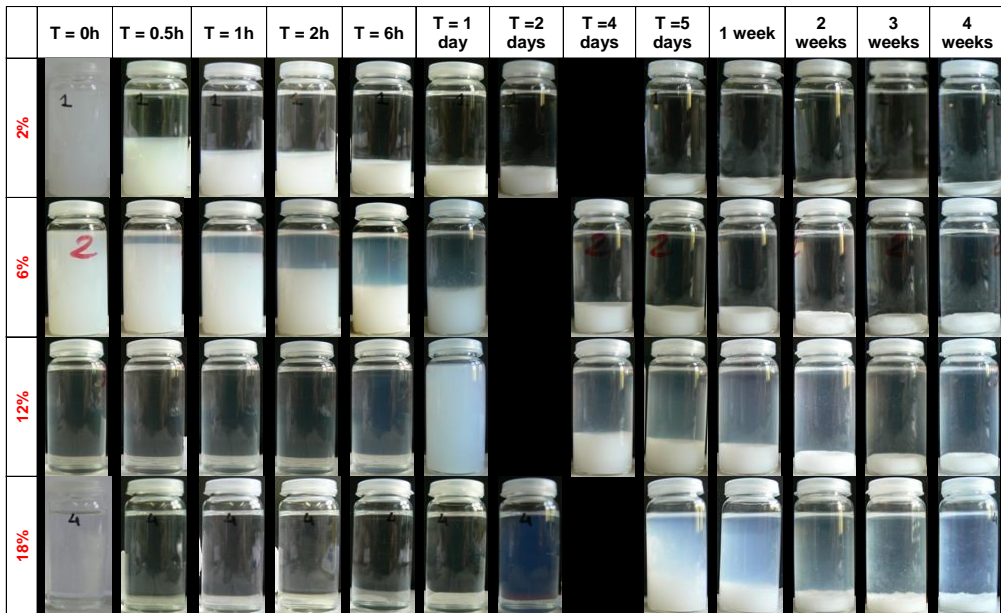


**Figure 67. Influence % Buffer (2, 6, 12, 18%).** Kost = % TiO<sub>2</sub> (1%v/v); pH 4; Chitosan (0.25%wt).

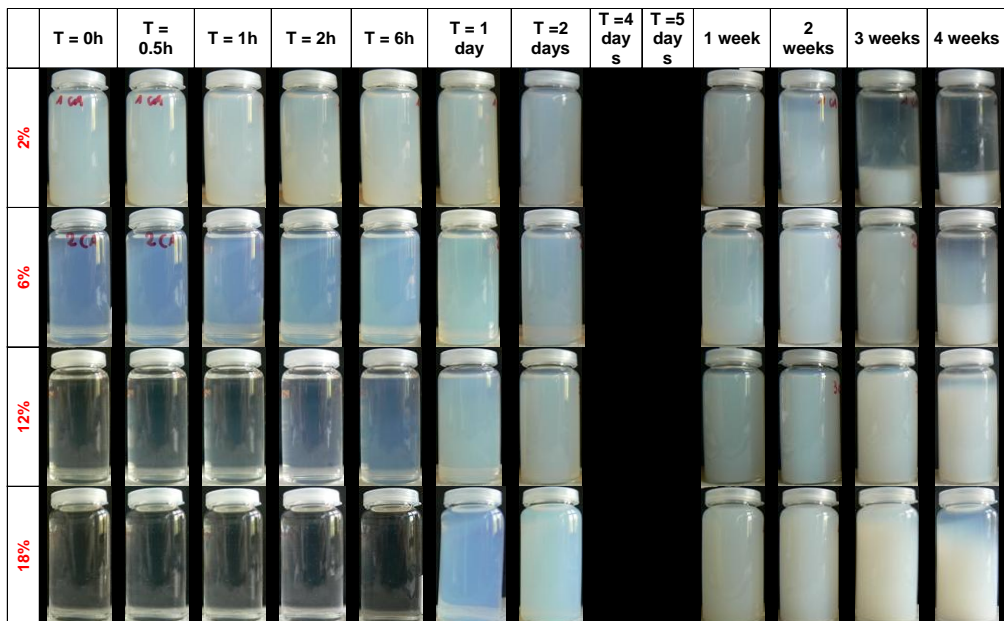


**Figure 68. Influence % TiO<sub>2</sub>.** Kost = % buffer (6%) at pH 4.

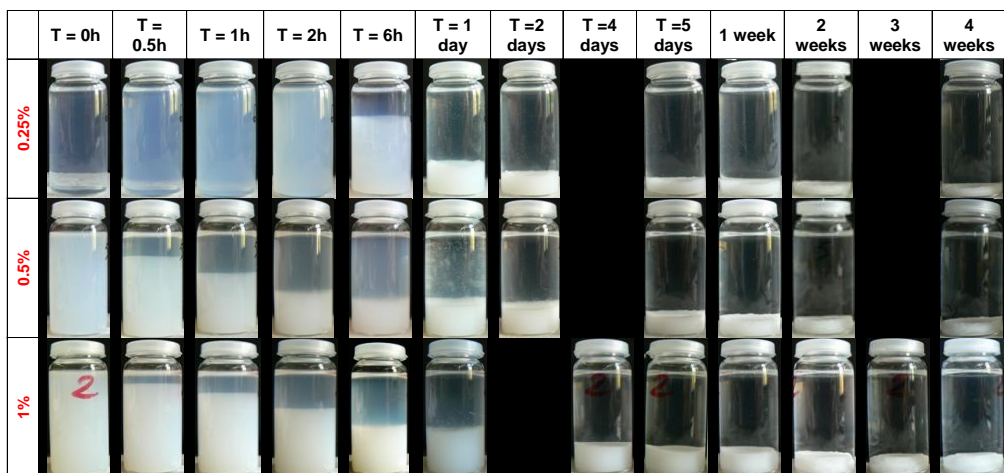


**Figure 69. Influence % TiO<sub>2</sub>.** Kost = % buffer (6%); Chitosan (0.25%wt) at pH 4.

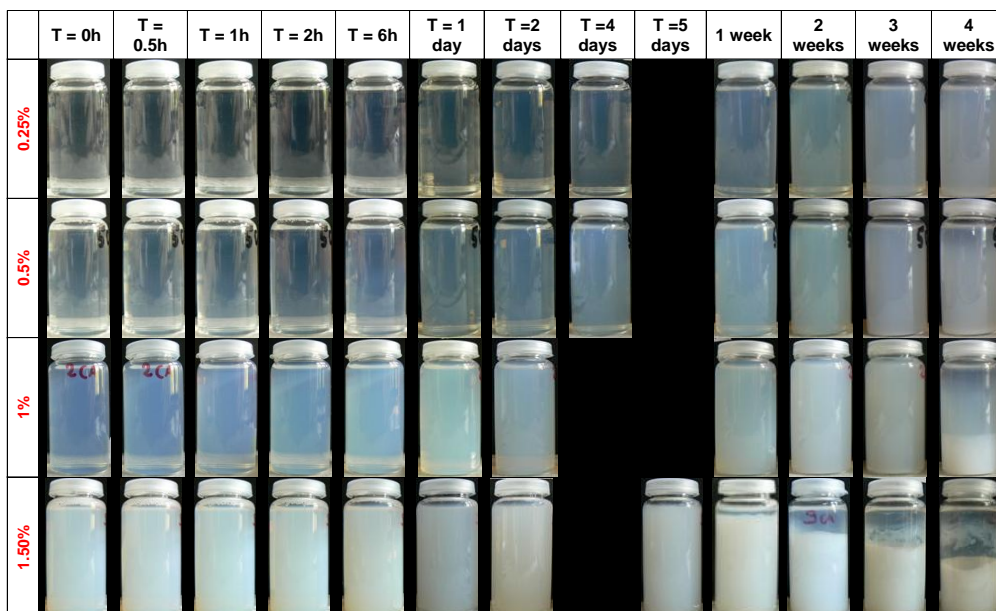


**Figure 70. Influence % TiO<sub>2</sub>.** Kost = % buffer (18%); Chitosan (0.25%wt) at pH 4.

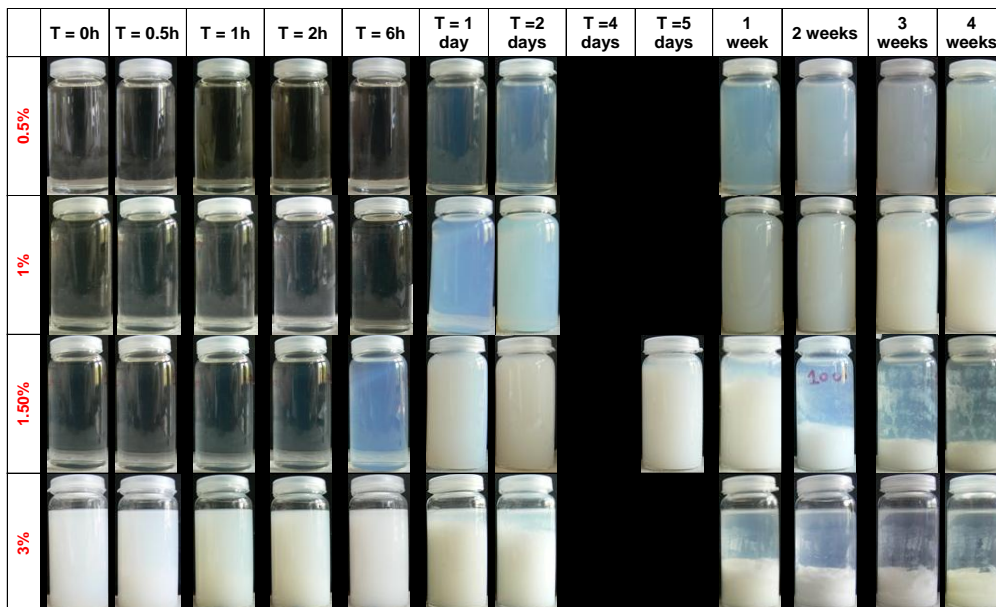


**Figure 72. Influence % chitosan.** Kost = % buffer (6%); TiO<sub>2</sub> (1%v/v) at pH 4.

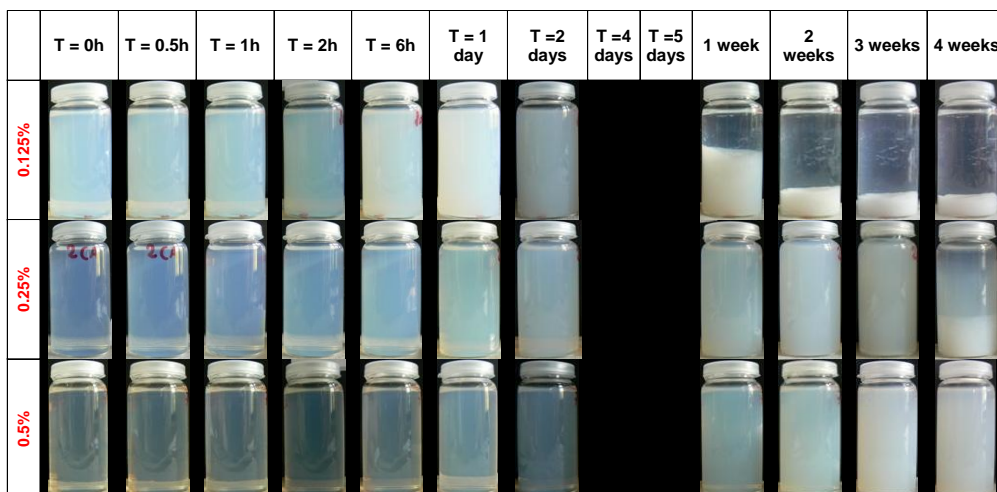


**Figure 73. Mass Ratio; %TiO<sub>2</sub>: %buffer = 1:12.** Kost = chitosan (0.25%wt) at pH 4.

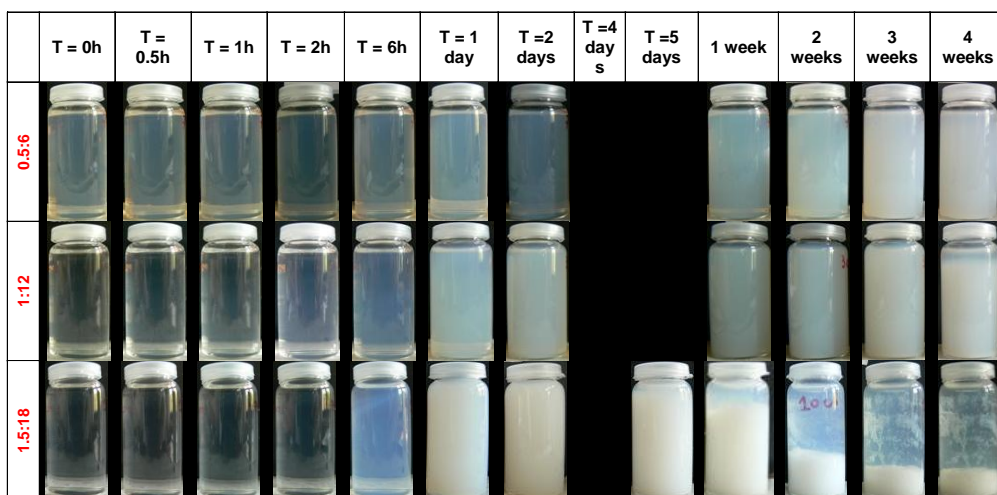


**Figure 74. Mass Ratio; % chitosan : %TiO<sub>2</sub> = 1:2.** Kost = buffer (6%) at pH 4.

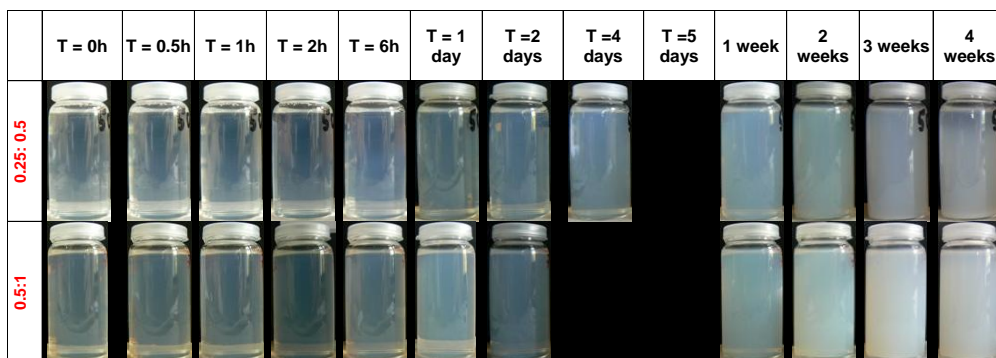


**Figure 75. Mass Ratio; % chitosan : %Buffer = 1:48.** Kost = TiO<sub>2</sub> (1%v/v) at pH 4

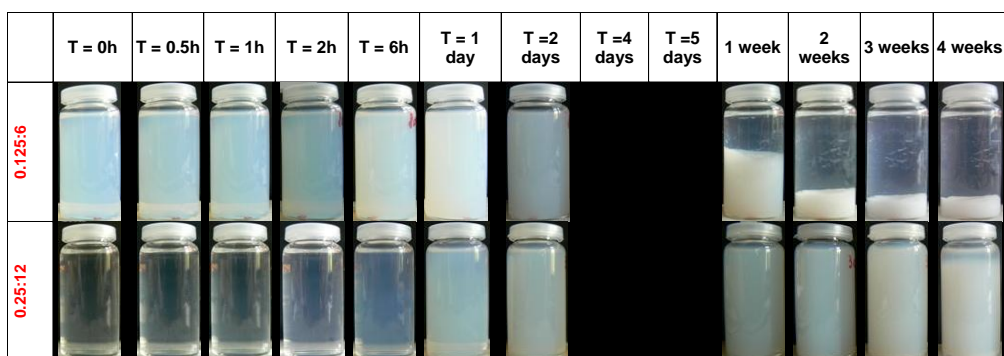


**Figure 76. Effect of temperature (room temperature and 95°C).** Kost = % TiO<sub>2</sub> (1%v/v), chitosan (0.25%wt) at pH4.

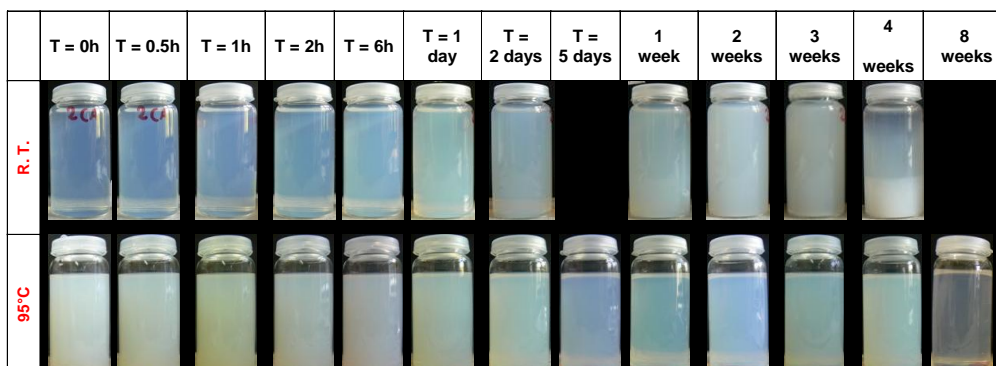




**Figure 77. Different routes.**

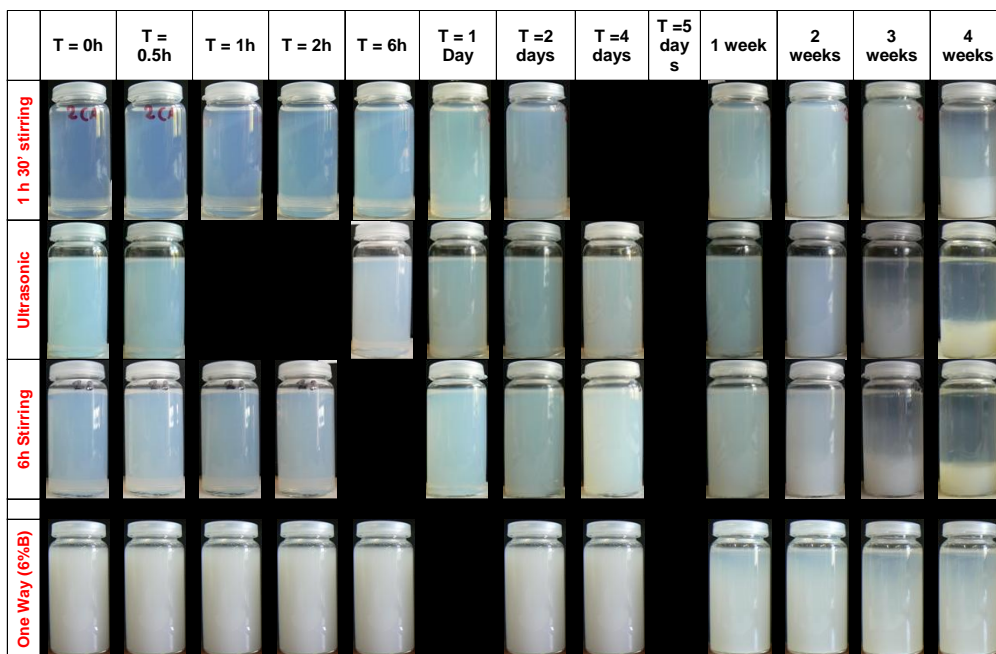


**Figure 78. Influence of pH 3 - 4 - 5.** Kost = % TiO<sub>2</sub> (1%v/v), % Chitosan (0.25%wt).

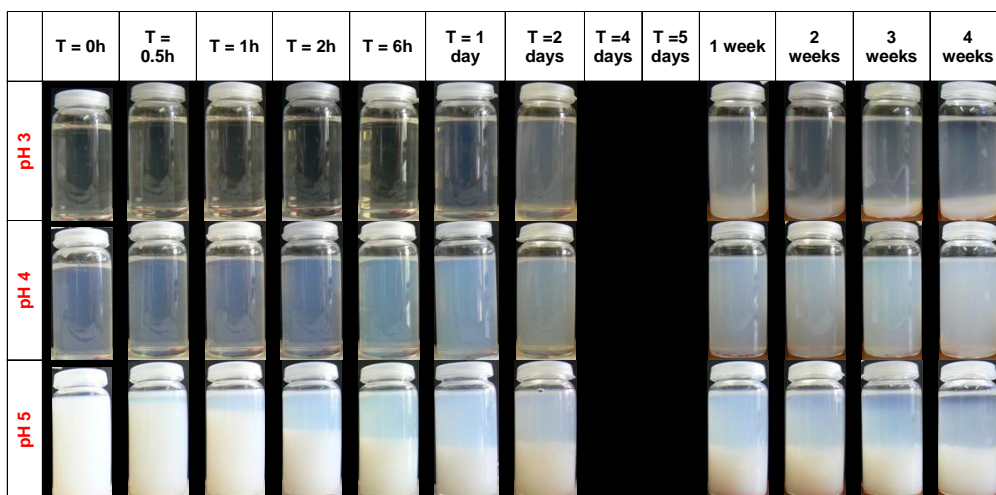
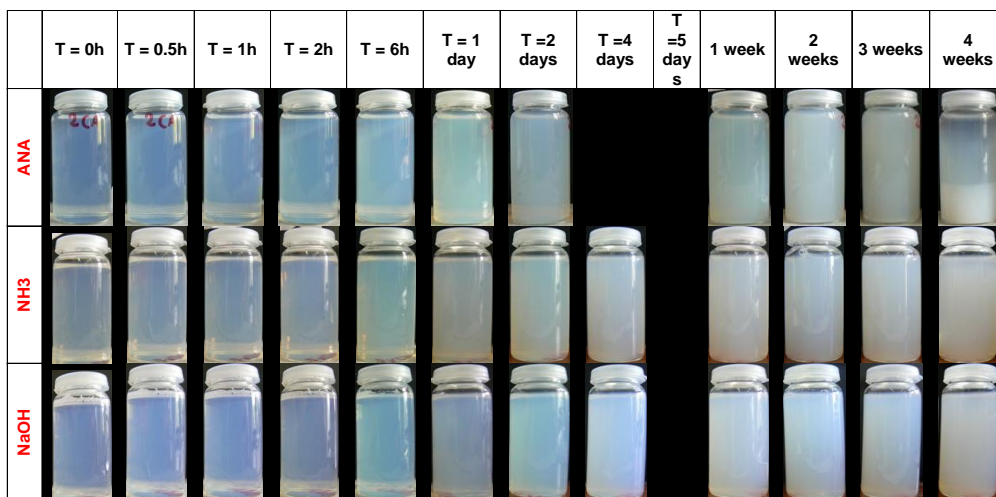


**Figure 79. pH 3.8 ANA, NH<sub>3</sub>, NaOH.** Kost = % TiO<sub>2</sub> (1%v/v), % Chitosan (0.25%wt).





## LIST OF FIGURES

Figure 1. Sol-gel process.	3
Figure 2. Different kind of network.	5
Figure 3. Hydrolisis reaction.	6
Figure 4. Alcoxolation reaction.	7
Figure 5. Oxolation reaction.	7
Figure 6. Acid catalyst reaction.	11
Figure 7. Partially hydrolysed polymer.	11
Figure 8. General products for cellulose pyrolysis.	26
Figure 9. ATR FT-IR of the synthesized hybrid organic-inorganic xerogel.	33
Figure 10. Proposed interaction between the hydrolyzed APTES and DEP.	35
Figure 11. Proposed interactions after condensation and annealing process for Si-P-C xerogel.	35
Figure 12. ATR FT-IR ATR spectra of untreated and treated cotton fabrics.	36
Figure 13. SEM micrographs and EDX spectra of cotton fabrics untreated (a), and treated with Si (b), Si-P (c) and Si-P-C (d) sols.	37
Figure 14. TGA and DTG curves of cotton fabrics in nitrogen (a, b) and air (c, d) atmosphere.	38
Figure 15. DSC curves of cotton fabrics in nitrogen (a) and air (b) atmosphere.	40
Figure 16. Samples subjected to flammability test after exposure to flame for 5 seconds.	42
Figure 17. ATR FT-IR spectra of cotton fabrics treated with Si, Si-P and Si-P-C sols pyrolyzed at 600°C.	43
Figure 18. FT-IR spectra of untreated, APTES, DPTES and MF treated cotton fabrics.	44
Figure 19. FT-IR spectra of untreated and DPTES:MF (B-MF) treated cotton fabrics. Molar ratio 1:1 (B-MF 1), 2:1 (B-MF 2), 3:1 (B-MF 3).	46
Figure 20. FT-IR spectra of untreated and APTES:DPTES (a-b) treated cotton fabrics. Molar ratio 0.5:2 (a-b 0.5), 1:2 (a-b 1), 2:2 (a-b 2).	47
Figure 21. Schematic representation of possible orientations of APTES (a), DPTES (b), APTES-DPTES (c) and DPTES-MF (d) on the cotton fabric surface.	47
Figure 22. SEM magnifications of some formulations under study.	48

Figure 23. TG and dTG curves of untreated and treated cotton fabrics in nitrogen.	49
Figure 24. TG and dTG curves of untreated and treated cotton fabrics in air.	53
Figure 25. Residues of untreated and treated cotton fabrics at the end of the flammability test.	54
Figure 26. Schematic description of wetting states of a drop placed on a surface. A. Wenzel	59
Figure 27. Fatty acid metal salts. A) hydrophobic interactions; B) polar interactions; C) fibre surface.	62
Figure 28. Stearic acid and melamine derivative.	63
Figure 29. Structure of PFOA and PFOS.	64
Figure 30. IR spectra of cotton fabric before and after washing cycles.	69
Figure 31. IR spectra of PET untreated, treated and treated after washing cycles.	70
Figure 32. Hysteresis test results of cotton samples treated at different molar ratio (MF:Si).	72
Figure 33. Hysteresis test results of cotton samples treated at different molar ratio (MF:Si).	72
Figure 34. Drop test results of cotton and PET samples treated at different molar ratio (MF:Si) for 20g/L MF.	73
Figure 35. Drop test results of cotton and PET samples treated at different molar ratio (MF:Si) for 60g/L MF.	74
Figure 36. Drop test results of cotton and PET samples treated at different molar ratio (MF:Si) for 100g/L MF.	74
Figure 37. Drop test results of cotton and PET samples treated with only melamine derivative (OMF: 20 g/L – 60 g/L - 100 g/L) and only silica precursor (OSi).	75
Figure 38. DuPont test results of PET samples treated at different molar ratio (MF:Si) compared to untreated PET.	76
Figure 39. DuPont test results of Cotton samples treated at different molar ratio (MF:Si) compared to untreated cotton.	76
Figure 40. DuPont test results of cotton and PET samples treated with only melamine derivative (OMF: 20 g/L – 60 g/L - 100 g/L) and only silica precursor (OSi).	77

Figure 41. Water uptake test results of PET samples treated at different molar ratio (MF:Si) compared to untreated PET.	78
Figure 42. Water uptake test results of cotton samples treated at different molar ratio (MF:Si) compared to untreated cotton.	79
Figure 43. Water uptake test results of cotton and PET samples treated with only melamine derivative (OMF: 20 g/L – 60 g/L - 100 g/L) and only silica precursor (OSi).	79
Figure 44. Schematic representation of possible interaction of MF and OTES on the fabric surface. Molar ratio (MF:OTES: 1:1 and 1:4).	80
Figure. 45. 3D structures of possible interaction between MF and OTES. Orientation alky chain.	81
Figure 46. Single-step process; pure TiO <sub>2</sub> sol. Titania precursor was dissolved in an acidic solution of a given pH-value. MS and US are magnetic stirring and ultrasonic treatment.	90
Figure 47. Single-step process; chitosan- TiO <sub>2</sub> . Titania precursor was dissolved in an acidic solution of a given pH-value contain a certain amount of chitosan. MS and US are magnetic stirring and ultrasonic treatment.	90
Figure 48. <i>Two-step process</i> ; pure TiO <sub>2</sub> sol were prepared adding titania precursor in acetate buffer solution. MS and US are magnetic stirring and ultrasonic treatment.	91
Figure 49. <i>Two-step process</i> ; Chitosan-TiO <sub>2</sub> sol were prepared adding titania precursor to an acetate buffer solution containing chitosan. MS and US are magnetic stirring and ultrasonic treatment.	93
Figure 50. FT-IR spectrum of pure acetic acid.	95
Figure 51. Infrared spectrum after the addition of TiO <sub>2</sub> precursor to acetic acid.	96
Figure 52. Infrared spectrum of xerogel (80°C for 10 min) derived from addition of TiO <sub>2</sub> precursor to acetic acid. Xerogel.	97
Figure 53. Characteristic Infrared spectrum of xerogel (80°C for 10 min) derived from stable TiO <sub>2</sub> sol prepared in buffer solution.	98
Figure 54. Possible reactions of the acetate anion with Titanium.	98
Figure 55. Infrared spectrum of xerogel (80°C for 10 min) derived from unstable TiO <sub>2</sub> sol (in buffer solution) synthesized at room temperature and 95°C.	100

Figure 56. FT-IR of pure chitosan.	101
Figure 57. FT-IR of chitosan acetate.	101
Figure 58. Structural formula of chitosan acetate.	102
Figure 59. FT-IR of xerogel (80°C for 10 min) derived from the Chitosan-TiO <sub>2</sub> stable sols.	102
Figure. 60. FT-IR of chitosan acetate and xerogel (80°C for 10 min) derived from Chitosan-TiO <sub>2</sub> unstable sols.	103
Figure 61. DLS analysis of Chitosan-TiO <sub>2</sub> samples (0.25%v/v TiO <sub>2</sub> ; 6% buffer). A) Intensity (%); B) Number distribution (%). h: hours; w: week.	106
Figure 62. DLS analysis of Chitosan-TiO <sub>2</sub> samples (0.5%v/v TiO <sub>2</sub> ; 6% buffer). A) Intensity (%); B) Number distribution (%). h: hours; w: week.	107
Figure 63. DLS analysis of Chitosan-TiO <sub>2</sub> samples (0.5%, 1% 1.5%, 3%v/v TiO <sub>2</sub> ; 18% buffer). A) Intensity (%); B) Number distribution (%).	108
Figure 64. DLS analysis of Chitosan-TiO <sub>2</sub> samples (0.25%, 0.5% 1.5%v/v TiO <sub>2</sub> ; 6% buffer). A) Intensity (%); B) Number distribution (%).	109
Figure 65. Turbidity measurement. Single-step process. TiO <sub>2</sub> Sol at pH 1 in HCl.	110
Figure 66. Turbidity measurement. Influence % Buffer CH <sub>3</sub> COOH/CH <sub>3</sub> COONa (2%, 6%, 12%, 18%). Kost = 1 %v/v TiO <sub>2</sub> precursor at pH 4. B) Detail.	112
Figure 67. Turbidity measurement. Influence % Buffer CH <sub>3</sub> COOH/CH <sub>3</sub> COONa (2%, 6%, 12%, 18%). Kost = % TiO <sub>2</sub> (1%v/v), chitosan (0.25%wt) at pH 4. B) detail.	114
Figure 68. Turbidity measurement. Influence %TiO <sub>2</sub> . Kost = % buffer CH <sub>3</sub> COOH/CH <sub>3</sub> COONa (6%) at pH4.	115
Figure 69. Turbidity measurement. Influence % TiO <sub>2</sub> . Kost = % buffer CH <sub>3</sub> COOH/CH <sub>3</sub> COONa (6%), 0.25%wt chitosan at pH 4.	116
Figure 70. Turbidity measurement. Influence % TiO <sub>2</sub> . Kost = % buffer CH <sub>3</sub> COOH/CH <sub>3</sub> COONa (18%), 0.25%wt chitosan at pH 4.	116
Figure 71. Turbidity measurement. Relationship % TiO <sub>2</sub> (0.5%, 1%, 1.5%v/v) and % Buffer CH <sub>3</sub> COOH/CH <sub>3</sub> COONa (6% and 18%). Kost = 0.25%wt chitosan at pH 4. B) Detail.	117

Figure 72. Turbidity measurement. Influence % Chitosan (0.125%, 0.25%, 0.5%). Kost = % buffer CH <sub>3</sub> COOH/CH <sub>3</sub> COONa (6%), %TiO <sub>2</sub> (1%v/v) at pH 4.	118
Figure 73. Turbidity measurement. Mass Ratio; % TiO <sub>2</sub> : % Buffer = 1:12. Kost = chitosan (0.25%wt) at pH 4.	119
Figure 74. Turbidity measurement. Mass Ratio; % Chitosan : % TiO <sub>2</sub> = 1:2. Kost = % buffer CH <sub>3</sub> COOH/CH <sub>3</sub> COONa (3%) at pH 4.	119
Figure 75. Turbidity measurement. Mass Ratio; % Chitosan : % Buffer = 1:48. Kost = % TiO <sub>2</sub> (1%v/v) at pH 4.	120
Figure 76. Turbidity measurement. Effect of temperature (room temperature and 95°C). Kost = % TiO <sub>2</sub> (1%v/v), chitosan (0.25%wt) at pH4.	121
Figure 77. Turbidity measurement. Effect of sol-gel route: Kost = % TiO <sub>2</sub> (1%v/v), chitosan (0.25%wt) at pH 4.	122
Figure 78. Turbidity measurement. Two-step process: influence of pH: 3, 4, 5; Kost = % TiO <sub>2</sub> (1%v/v), % Chitosan (0.25%wt).	123
Figure 79. Turbidity measurement. Influence of different alkali: CH <sub>3</sub> COONa (AcA), ammonia NH <sub>4</sub> OH (NH <sub>3</sub> ) and NaOH. Kost = % TiO <sub>2</sub> (1%v/v), Chitosan (0.25%wt).	123
Figure 80. Viscosity measurements. Influence % Buffer (2%, 6%, 12%, 18%). Kost = %TiO <sub>2</sub> (1%v/v) at pH 4.	124
Figure 81. Viscosity measurements. Influence % Buffer (2%, 6%, 12%, 18%). Kost = % TiO <sub>2</sub> (1%v/v), chitosan (0.25%wt) and pH 4.	125
Figure 82. Viscosity measurements. Relationship % TiO <sub>2</sub> (0.5%, 1%, 1.5%v/v) Vs %Buffer CH <sub>3</sub> COOH/CH <sub>3</sub> COONa (6% and 18%). Kost = 0.25%wt chitosan at pH 4.	125
Figure 83. Viscosity measurements. Influence % Chitosan (0.125%, 0.25%, 0.5%wt). Kost = % buffer CH <sub>3</sub> COOH/CH <sub>3</sub> COONa (3%), %TiO <sub>2</sub> (1%v/v), at pH 4.	126
Figure 84. Viscosity measurements. Two-step: influence of pH: 3, 4, 5. Kost: %TiO <sub>2</sub> (1%v/v), %Chitosan (0.25%wt).	126
Figure 85. Viscosity measurements. Mass Ratio; % TiO <sub>2</sub> : %Buffer = 1:12. Kost = chitosan (0.25%wt) at pH 4.	127
Figure 86. Viscosity measurements. Mass Ratio; % Chitosan : %Buffer = 1:48. Kost = %TiO <sub>2</sub> (1%v/v) at pH 4.	127



Figure 87. SEM images of cotton samples: UN) cotton fabric untreated; cotton fabric samples treated by: B) 0.025M HCl TiO <sub>2</sub> sol, C) 0.025M HCl TiO <sub>2</sub> sol doped, D) 0.25M HCl TiO <sub>2</sub> sol, E) 0.25M HCl TiO <sub>2</sub> sol doped.	129
Figure 88. EDX spectrum for untreated (A) and treated by HCl TiO <sub>2</sub> sol (B) cotton fabric surface.	130
Figure 89. Diffuse reflectance spectra of treated sample. A) doped/undoped TiO <sub>2</sub> (0.25M) samples; B) doped/undoped TiO <sub>2</sub> (0.25M) samples.	131
Figure 90. Diffuse reflectance spectra of treated sample. A) 0.025/0.25M TiO <sub>2</sub> samples; B) doped 0.025/0.25M TiO <sub>2</sub> samples.	132
Figure 91. Energy gap of H1, H2, H1P and H2P measured by Tauc plot analysis.	134
Figure 92. Schematic illustration of TiO <sub>2</sub> inorganic network (A) and a possible mechanism of cross linked titania glycolate (B).	135
Figure 93. Possible reactions of the acetate anion with Titanium [Figure 54].	136
Figure 94. Add-on % on textile fabrics.	137
Figure 95. Photocatalytic activity undoped TiO <sub>2</sub> treated samples by: 0.25M TiO <sub>2</sub> and 0.025 M TiO <sub>2</sub> sols. UV source.	139
Figure 96. Relationship between pKa and <i>k</i> (for Hydrochloric, Nitric and Acetic acids, from left to right) of undoped TiO <sub>2</sub> treated samples.	140
Figure 97. Photocatalytic activity undoped TiO <sub>2</sub> treated samples by: 0.25M TiO <sub>2</sub> and 0.025 M TiO <sub>2</sub> sols. Visible source.	141
Figure. 98. Mechanical properties of treated and untreated samples before and after visible/UV exposure for 100 hours.	143

## LIST OF TABLES

Table 1. Electronegativity ( $\chi$ ), Coordination Number (N), and Degree of Unsaturation (N-Z) for some Metals.	10
Table 2. Different water/isopropanol mixtures used for DuPont test.	19
Table 3. Currently available flame retardants for polyester.	24
Table 4. Currently available flame retardants for cotton.	25
Table 5. Name, code and chemical structures of the sol-gel precursors, the organo-phosphorus compound and the cross-linker.	29
Table 6. Molar ratios of hybrid sols.	31
Table 7. Investigated formulations.	32
Table 8. Major vibrational frequencies of the Si, Si-P and Si-P-C xerogels.	34
Table 9. Temperature maximum of weight loss rate and char yields at 600°C of cotton fabrics in nitrogen atmosphere.	39
Table 10. Combustion times of cotton fabrics (weft direction) after exposing to flame for 5 seconds.	41
Table 11. Main vibration modes of DPTES, APTES and MF thin film.	45
Table 12. TGA data of neat cotton and treated fabrics in nitrogen.	50
Table 13. TGA data of untreated cotton and treated fabrics in air.	51
Table 14. Collected data of pure cotton and treated fabrics by flammability tests.	54
Table 15. Surface energies of selected polymers and inorganic oxides.	61
Table 16. POFA and POFS properties.	65
Table 17. Name, code and chemical structures of the sol-gel precursors and the cross-linker.	67
Table 18. Investigated formulations.	68
Table 19. Contact angle (CA) measurement.	71
Table 20. Name, code and chemical structures of the precursors, dyestuff and chitosan.	88
Table 21. Experimental setup codes.	94
Table 22. Stretching vibration of acetate ligands in different Ti(IV)-acetate complex according to [134].	99
Table 23. Stretching vibration of acetate ligands in different Ti(IV)-acetate complex (TiO <sub>2</sub> -buffer; Chitosan-TiO <sub>2</sub> ) in this research.	99

Table 24. Schematic comparison of stable and unstable sols with and without chitosan.	104
Table 25. Energy gap of TiO <sub>2</sub> thin film $E_g \pm 0.01$ eV.	133

## REFERENCE

- [1] W.D. Schindler, P.J. Hauser, In Chem. Finishing of Textiles; Eds.; Woodhead Publishing: Cambridge (2004).
- [2] M. Keshmiri, T. Troczynski, M. Mohseni, J Hazard Mater B128 (2006) 130.
- [3] J.J. Ebelmen, Ann, 57 (1846) 331.
- [4] W. Geffcken and E. Berger, German Patent no. 736 411, 1939.
- [5] L. Levene, I. M. Thomas, U.S. Pat. 3,640,093, 1972.
- [6] G. Philipp, H. Schmidt, J Non-Cryst Solids, 63 (1984) 283.
- [7] G.L. Wilkes, B. Orlor, H. Huang, Polym Prepr, 26 (1985) 300.
- [8] C.J. Brinker, B.C. Bunker et al., Structure of Sol-Gel Derived Inorganic Polymers: Silicates and Borates, Am. Chem. Soc., part II 1988.
- [9] R.W. Jones, Fundamental Principles of Sol-Gel Technology, The Institute of Metals, London 1989).
- [10] C.J. Brinker, S.W. Scherer, Sol-Gel science: the physics and chemistry of sol-gel processing. Academic Press, New York, 1990.
- [11] K. Izumi, H. Tanaka, Y. Uchida, N. Tonge, T. Minami, J Mat Sci Lett, 12 (1993) 724-727.
- [12] H.D. Dislich, J Non-cryst. Sol, 57 (1983) 371-388.
- [13] H. Schmidt, , J Sol Gel Sci Tech, 8 (1997) 557-565.
- [14] M.P. Pechini (1967) US Patent No.3.330.697 July 1.
- [15] C. Sanchez, F. Ribot, New J Chem, 18 (1994) 1007.
- [16] J. Wen, G.L. Wilkes, Chem Mater 8 (1996) 1667-1681.
- [17] L.I. Hench, D.R. Ulrich, Ann. Quim. 76B (1980).
- [18] J. Livage, M. Henry, C. Sanchez, Prog Sol State Chem, 18 (1988) 259.
- [19] I. Hasegawa, S. Sakka, J Non-cryst Sol, 100 (1988) 201-205.
- [20] A. Frignani, F. Zucchi, G. Trabanelli, V. Grassi, Corrosion science, 48 (2006) 2258-2273.
- [21] H.K. Schmidt, E. Geiter, M. Mennig, H. Krug, C. Becker, R. Winkler, J Sol Gel Sci Tech, 13 (1988) 397-404.
- [22] S. Kozhukharov, G. Tsaneva, V. Kozhukharov, J. Gerwann, M. Schem, T. Schmidt, M. Veith, J Univ Chem Techol Met (Sofia), 43 (1) (2008) 73-80.

- [23] V. Kozhukharov, High temperature method of synthesis, Ed. UCTM Sofia, 2004, 72-74.
- [24] W. Stöber, A. Fink, Journal of Colloid and Interface Science, 26 (1) (1968) 62–69.
- [25] M. Genchev, Brief Chemical Encyclopedia, Ed. Technika, Sofia, 1981, 164.
- [26] L.S. Munos. J.B. Carda, Materias primas y aditivos ceramicos, Faenza editrica Iberica II-1; Castellon-2002.
- [27] M. Del Coro Serrano, S. Kozhukharov, Application of sol-gel techniques for obtaining of multifunctional materials, Development – Future Perspectives and Innovations in the science, Proc, Sofia, 2006, 84-93.
- [28] The american society for testing and materials, ASTM D 1230e1294, Reapproved 2001. Standard Test Method for Flammability of Apparel Textiles.
- [29] T. Textor, B. Mahltig, Nanosols and textiles, World Scientific Publishing Co. Pte. Ltd. 2008, ISBN-13: 978-981-283-350-1.
- [30] J. Tauc, R. Grigorovich, A. Vancu., Phys Stat Sol, 15 (1966) 627.
- [31] G. Burns, Solid State Physics, Academic, New York (1985).
- [32] P. Kubelka, F. Z. Munk, Technol Phys, 12 (1931) 593-601.
- [33] P. Kubelka, J Opt Soc Am, 38 (1947) 448-457.
- [34] R. Alcántara, J. Navas, C. Fernández-Lorenzo, J. Martín, E. Guillén, J. A. Anta, Phys Status Solidi C 8 (6) (2011) 1970–1973.
- [35] ISO 139:2005, Textiles – Standard Atmospheres for Conditioning and Testing, International Organization for Standardization 2005.
- [36] ANSI/ASTM Designation 5035-1995, The American Society for Testing and Materials, Philadelphia, PN, USA, 1995.
- [37] EN ISO 6330:2000, Textiles – Domestic Washing and Drying Procedures for Textile Testing.
- [38] N.N. Brushlinsky, S.V. Sokolov, P. Wagner, J.R. Hall, World fire statistics. Report No. 10. Centre of fire statistics, international association of fire and rescue service; 2006. [www.ctif.org](http://www.ctif.org).
- [39] M. Kobes, K. Groenewegen, Consumer fire: European statistics and potential fire safety measures. Austrian Federal Ministry Labor, Social Affairs and Consumer Protection; 2009.

- [40] H. Frantzich, A model for performance-based design of escape routes. Technical report, Department of Fire Safety Engineering, Lund Institute of Technology. Lund: Lund University; 1994.
- [41] R.G. Gann, *Fire Technol.* 40 (2) (2004) 201–207.
- [42] A.R. Horrocks, In: D. Heywood, editor. *Textile finishing*. Bradford: Society of dyers and colourists; 2003. p. 214–50.
- [43] S. Bourbigot, In: A.R. Horrocks, D. Price, editors. *Advances in fire retardant materials*. Cambridge: Woodhead Publishing; 2008. p. 9–40.
- [44] A.R. Horrocks, *Advances in fire retardant materials*. In: A.R. Horrocks, D. Price, editors. Cambridge: Woodhead Publishing; 2008, p. 159–187.
- [45] E.D. Weil, S.V. Levchik, *J Fire Sci.* 2008;26:243–281.
- [46] L. Cabrales, N. Abidi, *J Therm Anal Calorim*, 102 (2010) 485.
- [47] S. Hu, Y. Hu, L. Song, H. Lu, *J Therm Anal Calorim*. doi:10.1007/s10973-011-1732-1.
- [48] M. Levin, *Handbook of fiber science and technology*. In: Levin M, Sello SB, editors. *Chemical processing of fibers and fabrics. functional finishes, part b, vol. II*. New York: Marcel Dekker; 1984. p. 1-141.
- [49] (a) A. Broido, M. Evett, C. Hodges, *Carbohydr Res*, 44 (1975) 267.  
(b) F. Shafizadeh, R.H. Furneaux, T.T. Stevenson, T.G. Cochran, *Carbohydr Res*, 67 (1978) 433.
- [50] (a) A.R. Horrocks, In: Le Bras M, Camino G, Bourbigot S, Delobel R, editors. *Fire retardancy of polymers e The use of intumescence*. London Royal Soc. Chem.; 1998. p. 343-62;  
(b) A.R. Horrocks, S.C. Anand, D. Sanderson, *Polymer*, 37 (15) (1996) 3197-3206.  
(c) B.K. Kandola, A.R. Horrocks, *Polym Degrad Stab*, 54 (1996) 289-303.  
(d) B.K. Kandola, A.R. Horrocks, *Textile Res J*, 69 (5) (1999) 374-381.  
(e) P.J. Davies, A.R. Horrocks, M. Miraftab, *Polym Int*, 49 (2000) 1125-1132.
- [51] (a) A.R. Horrocks, *Polym Degrad Stab*, 54 (1996) 143.  
(b) A.R. Horrocks, B.K. Kandola, P.J. Davies, S. Zhang, S.A. Padbury, *Polym Degrad Stab*, 88 (2005) 3-12.
- [52] (a) E. Devaux, M. Rochery, S. Bourbigot, *Fire Mater*, 26 (2002) 149.  
(b) White LA. *J Appl Polym Sci*, 92 (2004) 2125-2131.

- [53] C. Sanchez, B. Julian, P. Belleville, M.J. Popall, *Mater Chem* 15 (2005) 3559.
- [54] C.J. Brinker, G.W. Scherer, *The physics and chemistry of sol-gel processing*. San Diego: Academic; 1990.
- [55] (a) N. Yaman, *Fibers Polym* 10 (2009) 413.  
(b) A. Cireli, N. Onar, M.F. Ebeoglugil, I. Kayatekin, B. Kutlu, O. Culha et al, *J Appl Polym Sci* 105 (2007) 3747-3756.
- [56] G. Brancatelli, C. Colleoni, M.R. Massafra, G. Rosace, *Polymer Degradation and Stability* 96 (2011) 483-490.
- [57] S. Gaan, G.J. Sun, *Anal Appl Pyrolysis* 84 (2009) 108-115.
- [58] J. Alongi, C. Colleoni, G. Malucelli, G. Rosace, *Journal of Thermal Analysis and Calorimetry*, DOI 10.1007/s 10973-011-2142-0.
- [59] Bs EN 20139:1992, *Textiles e standard atmospheres for conditioning and testing*.
- [60] (a) E.F. Vansant, P. Van der Voort, K.C. Vranken, *characterization and chemical modification of the silica surface*. Elsevier; 1995.  
(b) C.H. Chiang, H. Ishida, J.L. Koenig, *J Coll Interf Sci* 74 (1980) 396.
- [61] L.M. Johnson, T.J. Pinnavaia, *Langmuir* 7 (1991) 2636-2641.
- [62] L. Jiang, X. Mao, J. Yu, A. Lin, *Anti Corr Meth Mater* 56 (2009) 13.
- [63] G. Guerrero, P.H. Mutin, A. Vioux, *Chem Mater* 13 (11) (2001) 4367-4373.
- [64] M.B. Mitchell, V.N. Sheinker, E.A. Mintz, *J Phys Chem B*, 101 (1997) 11192-11203.
- [65] P.J. Larkin, M.P. Makowski, N.B. Colthup, L.A. Flood, *Vib Spectrosc* 17 (1998) 53.
- [66] Q. Wang, X. Fan, W. Gao, J. Chen, *Carbohydrate Research* 341 (2006) 2170-2175.
- [67] F. Shafizadeh, A.G.W. Bradbury, W.F. De Groot, T.W. Aanerud, *Ind Eng Chem Prod Res Dev* 27 (1982) 97.
- [68] D.W. Krevelen, *Polymer* 1975;16:615.
- [69] (a) B.K. Kandola, A.R. Horrocks, *Fire Mater* 24 (2000) 265.  
(b) G.H. Hsiue, Y.L. Liu, H.H.J. Liao, *Polym Sci. Part A Polym Chem* 39 (2001) 986-996.
- [70] R.K. Jain, K. Lal, H.L. Bhatnagar, *J Appl Polym Sci* 30 (1985) 897.

- [71] S. Soares, G. Camino, S. Levchik, *Polym Degrad Stab* 49 (1995) 275.
- [72] J.T. Langley, M.J. Drews, R.H. Barker, *J Appl Polym Sci*, 259 (1980) 243.
- [73] (a) B.K. Kandola, S. Horrocks, A.R. Horrocks, *Thermochim Acta* 294 (1997) 113-125.  
(b) J.B. Dahiya, S. Rana, *Polym Int*, 53 (7) (2004) 995-1002.
- [74] E.D. Weil, In: W.C. Kuryla, A.J. Papa, editors. *Flame Retardancy of Polymeric Materials*, vol. 3. New York: Marcel Dekker; 1975. p. 185.
- [75] S. Gaan, G. Sun, K. Hutches, M.H. Engelhard, *Polym Degrad Stab*, 93 (1) (2008) 99-108.
- [76] G. Rosace, M.R. Massafra, *Text Res J.*, 78 (2008) 28–36.
- [77] D. Price, A.R. Horrocks, M. Akalin, A.A. Farooq, *J Anal Appl Pyrol.* 40-41 (1997) 511–24.
- [78] E.F. Hare, E.G. Shafrin, W.A. Zisman, *J Phys Chem* 58 (1954) 236.
- [79] T. Nishino, M. Meguro, K. Nakamae, M. Matsushita, Y. Ueda, *Langmuir* 15 (1999) 4321.
- [80] R.N. Wenzel, *Ind Eng Chem*, 28 (1936) 988.
- [81] A.B.D. Cassie, S. Baxter, *Trans. Faraday Soc*, 10 (1944) 546.
- [82] (a) T. Onda, S. Shibuichi, N. Satoh, K. Tsujii, *Langmuir* 12 (1996) 2125.  
(b) A. Nakajima, A. Fujishima, K. Hashimoto, T. Watanabe, *Adv Mater* 11 (1999) 1365.  
(c) M. Ferrari, F. Ravera, L. Liggieri, *Appl Phys Lett* 88 (2006) 203125.  
(d) Y. Coffinier, S. Janel, A. Addad, R. Blossey, L. Gengembre, E. Payen, R. Boukherroub, *Langmuir* 23 (2007) 1608.  
(e) M. Callies, D. Quere, *Soft Matter* 1 (2005) 55.
- [83] D. Quere, *Physica A (Amsterdam)*, 313 (2002) 32.
- [84] J. Jopp, H. Grull, R. Yerushalmi-Rozen, *Langmuir*, 20 (2004) 10015.
- [85] R.E. Johnson Jr., R.H. Dettre, *Adv Chem Ser*, 43 (1963) 112.
- [86] B. Arkles, *Chemtech*, 7 (1977) 766-778.
- [87] C. Minoia, E. Leoni, C. Sottani, G. Biamonti, S. Signorini, M. Imbriani, *G Ital Med Lav Erg* 30 (4) (2008) 309-323.
- [88] Y. Akamatsu, K. Makita, H. Inaba, and T. Minami, *Thin Solid Films* 389 (2001) 138.
- [89] (a) S.K. Young and K.A. Mauritz, *J Polym Sci B* 39 (2001) 1282.



- (b) A.F. Thunemann, *Polym Int*, 49 (2000) 636.
- (c) Y. Wu, H. Sugimura, Y. Inoue, O. Takai, *Chem Vap Deposition* 8 (2002) 47.
- [90] ISO 139:2005, Textiles – Standard Atmospheres for Conditioning and Testing, International Organization for Standardization 2005.
- [91] G. Rosace a, R. Canton, C. Colleoni, *Applied Surface Science* 256 (2010) 2509–2516.
- [92] V. Cecen, Y. Seki, M. Sarikanat, I.H. Tavman, *Journal of Applied Polymer Science*, 108 (2008) 2163–2170.
- [93] M. Lenzen, *Energy* 23 (6) (1998) Pages 497–516.
- [94] A. Fareed, A. Ansari, *the botanical review*, 71 (4) (2005) 449-482.
- [95] A. Bozzi, T. Yuranova, I. Guasaquillo, D. Laub, J. Kiwi, *Journal of Photochemistry and Photobiology A: Chemistry*, 174 (2) (2005) 156–164.
- [96] X. Zhang, F. Shi, J. Niu, Y. Jiang, Z. Wang, *J. Mater. Chem.*, 18 (2008) 621-633.
- [97] C.-T. Hsieh, J.-M. Chen, R.-R. Kuo, T.-S. Lin, C.-F. Wu, *Applied Surface Science*, 240 (1–4) (2005) 318–326.
- [98] D. V. Bavykin, J. M. Friedrich, F. C. Walsh, *Advanced Materials*, 18 (21) (2006) 2807–2824.
- [99] M. Mrowetz, C. Pirola, E. Selli, *Ultrasonics Sonochemistry*, 10 (4–5) (2003) 247–254.
- [100] P. Pichat, *Applied Catalysis B: Environmental*, 99 (3–4) (2010) 428–434.
- [101] D. Kibanova, J. Cervini-Silva, H. Destailats, *Environ. Sci. Technol.*, 43 (5) (2009) 1500–1506.
- [102] B. Kim, D. Kim, D. Cho, S. Cho, *Chemosphere*, 52 (1) (2003) 277–281.
- [103] W.Y. Gan, S.W. Lam, K. Chiang, R. Amal, H. Zhao, M.P. Brungs, *J. Mater. Chem.*, 17 (2007) 952-954.
- [104] J. Yu, X. Zhao, Q. Zhao, G. Wang, *Materials Chemistry and Physics*, 68 (1–3) (2001) 253–259.
- [105] U. Bach, D. Lupo, P. Comte, J. E. Moser, F. Weissörtel, J. Salbeck, H. Spreitzer & M. Grätzel, *Nature* 395 (1998) 583-585.
- [106] M. Ni, M.K.H. Leung, D.Y.C. Leung, K. Sumathy, *Renewable and Sustainable Energy Reviews*, 11 (3) (2007) 401–425.

- [107] I.K. Konstantinou, T.A. Albanis, *Applied Catalysis B: Environmental* 49 (2004) 1–14.
- [108] A.I. Kontos, I.M. Arabatzis, D.S. Tsoukleris, A.G. Kontos, M.C. Bernard, D.E. Petrakis, P. Falaras, *Catal. Today*, 101 (2005) 275-281.
- [109] B. L. Diffey, *Methods* 28 (2002) 4–13.
- [110] Y. Cong, J. Zhang, F. Chen, M. Anpo, *J. Phys. Chem. C*, 111 (2007) 6976-6982.
- [111] J. Wang, D.N. Tafen, J.P. Lewis, Z. Hong, A. Manivannan, M. Zhi, M. Li, N. Wu, *J. Am. Chem. Soc.*, 131 (34) (2009) 12290–12297.
- [112] T. Ohno, M. Akiyoshi, T. Umabayashi, K. Asai, T. Mitsui, M. Matsumura, *Applied Catalysis A: General*, 265 (1) (2004) 115–121.
- [113] P. Periyat, S.C. Pillai, D.E. McCormack, J. Colreavy, S.J. Hinder, *J. Phys. Chem. C*, 112 (2008) 7644–7652.
- [114] J.H. Park, S. Kim, A.J. Bard, *nanoletters*, 6 (1) (2006) 24-28.
- [115] W. Ren, Z. Ai, F. Jia, L. Zhang, X. Fan, Z. Zou, *Applied Catalysis B: Environmental* 69 (2007) 138–14.
- [116] D. Li, H. Haneda, N.K. Labhsetwar, S. Hishita, N. Ohashi, *Chemical Physics Letters*, 401 (2005) 579–584.
- [117] M.R.T Viseu, M.I.C Ferreira, *Vacuum*, 52 (1999) 115–120.
- [118] N.R. Mathews, E.R. Morales, M.A. Cortés-Jacome, A.J.A. Toledo, *Solar Energy*, 83 (2009) 9.
- [119] C. Millon, D. Riassetto, G. Berthomé, F. Roussel, M. Langlet, *Journal of photochemistry and photobiology. A, Chemistry*, 189 (2007) 334.
- [120] M. Vishwas , K. Narasimha Rao, K.V. Arjuna Gowda, R.P.S. Chakradhar, *Materials Chemistry and Physics*, 95 (2006) 79–83.
- [121] J.I. Simionato, A.T. Paulino, J.C. Garcia and Jorge Nozaki, *Polym Int*, 55 (2006) 1243–1248.
- [122] M.N.V Ravi Kumar, *Reactive and Functional Polymers*, 46 (1) (2000) 1–27.
- [123] J. Synowiecki, N.A. Al-Khateeb, *Critical Reviews in Food Science and Nutrition*, 43 (2) (2003) 145-171.
- [124] S. Jain, R.K. Sharma, S.P. Vyas, *Journal of Pharmacy and Pharmacology*, 58 (3) (2006) 303–310.
- [125] M. Zaru, S. Mourtas, P. Klepetsanis, A.M. Fadda, S.G. Antimisiaris,

- European Journal of Pharmaceutics and Biopharmaceutics, 67 (3) (2007) 655–666.
- [126] W.S. Wan Ngah, L.C. Teong, M.A.K.M. Hanafiah, Carbohydrate Polymers Volume 83 (4) (2011) 1446–1456.
- [127] C. Huang, S. Chen, J.R. Pan, Water Research, 34 (3) (2000) 1057–1062.
- [128] G.-J. Yang, C.-J. Li, F. Han, X.-C. Huang, J. Vac. Sci. Technol. B 22 (2004) 2364.
- [129] M. Kang, S.-Y. Lee, C.-H. Chung, S.M. Cho, G. Y. Han, B.-W. Kim, K. J. Yoon, Journal of Photochemistry and Photobiology A: Chemistry, 144 (2–3) (2001) 185–191.
- [130] ISO 139:2005, Textiles – Standard Atmospheres for Conditioning and Testing, International Organization for Standardization 2005.
- [131] K. Nakamoto, Infrared and Raman spectra of inorganic and coordination compound, 3rd ed (Wiley, New York, 1978).
- [132] D.E. Edwards, R.N. Hayward, Can J Chem 46 (1968) 3443.
- [133] S. Doeuff, M. Henry, C. Sanchez, J. Livage Journal of Non-Crystalline Solids, 89 (1–2) (1987) 206–216.
- [134] K.H.Von Thiele, M. Panse, Z Anorg Allg Chem 441 (1978) 23.
- [135] H. Zuo, J. Sun, K. Deng, R. Su, F. Wei, D. Wang Chem. Eng. Technol. 30 (5) (2007) 577–582.
- [136] Y. C. Chang, D.H. Chen, Macromolecular Bioscience, 5 (2005) 254–261.
- [137] R. Marguerite, L.D. Pham, G. Claude, M. Michel, International Journal of Biological Macromolecules, 14(1992) 122–128.
- [138] Y. Li, X.G. Chen, N. Liu, C.S. Liu, C.G. Liu, X.H. Meng, L.J. Yu, J.F. Kenedy, Carbohydrate Polymers, 67 (2007) 227–232.
- [139] C.-H. Wu, K.-S. Huang, J.-M. Chern, Ind Eng Chem Res, 45 (2006) 2040-2045.
- [140] D.M. King, X. Du, A.S. Cavanagh, A.W. Weimer, Nanotechnology, 19 (2008) 44540.
- [141] L. Ge, M. Xu, J. Sol-Gel Sci. Technol., 43 (2007) 1-7.
- [142] L. Kavan, T. Stoto, M. Graetzel, D. Fitzmaurice, V. Shklover, J. Phys. Chem, 97 (1993) 9493-9498.

- [143] S. Yin, Y. Inoue, S. Uchida, Y. Fujishiro, T. Sato, *Rev. High-Pressure Sci. Technol.*, 7 (1998) 1438–1440.
- [144] C. Pighini, D. Aymes, N. Millot, L. Saviot, *J. Nanopart. Res.*, 9 (2007) 309–315.
- [145] L. Ge, M. Xu, M. Sun, H.o Fang, *J. Sol-Gel Sci. Techn.*, 38 (2006) 47–53.
- [146] D. Chu, X. Yuan, G. Qin, M. Xu, P. Zheng, J. Lu, L. Zha, *J. Nanopart. Res.*, 10 (2008) 357–363.
- [147] V.S. Smitha, K.A. Manjumol, K. V. Baiju, S. Ghosh, P. Perumal, K. G. K. Warriar, *J. Sol-Gel Sci. Techn.*, 54 (2010) 203–211.
- [148] H.K. Yu, T.H. Eun, G.R. Yi, S.M. Yang, *J. Colloid Interf. Sci.*, 316 (2007) 175–182.
- [149] S. Bu, Z. Jin, X. Liu, L. Yang, Z. Cheng, *Mater. Chem. Phys.*, 88 (2-3) (2004) 273-279.
- [150] S. Doeuff, M. Henry, C. Sanchez, J. Livage, *J. Non-Cryst. Solids*, 89 (1-2) (1987) 206-216.
- [151] K. Eufinger, D. Poelman, H. Poelman, R. De Gryse, G.B. Marin, *Appl. Surf. Sci.*, 254 (2007) 148–152.